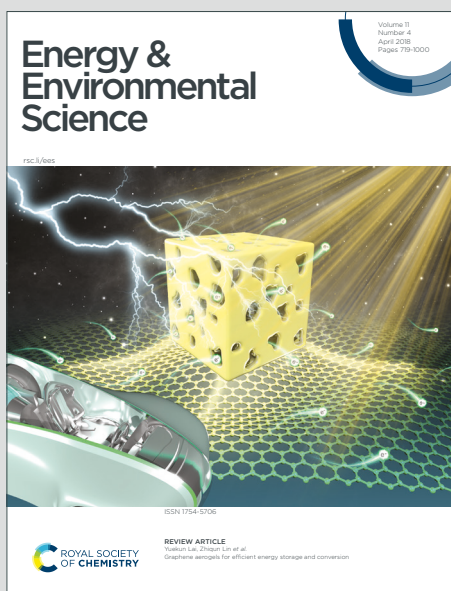


Energy & Environmental Science

Accepted Manuscript

This article can be cited before page numbers have been issued, to do this please use: X. Shi, W. Chen, T. Zhang, J. Zou and Z. Chen, *Energy Environ. Sci.*, 2021, DOI: 10.1039/D0EE03520C.



This is an Accepted Manuscript, which has been through the Royal Society of Chemistry peer review process and has been accepted for publication.

Accepted Manuscripts are published online shortly after acceptance, before technical editing, formatting and proof reading. Using this free service, authors can make their results available to the community, in citable form, before we publish the edited article. We will replace this Accepted Manuscript with the edited and formatted Advance Article as soon as it is available.

You can find more information about Accepted Manuscripts in the [Information for Authors](#).

Please note that technical editing may introduce minor changes to the text and/or graphics, which may alter content. The journal's standard [Terms & Conditions](#) and the [Ethical guidelines](#) still apply. In no event shall the Royal Society of Chemistry be held responsible for any errors or omissions in this Accepted Manuscript or any consequences arising from the use of any information it contains.

Graphical Abstract

View Article Online
DOI: 10.1039/D0EE03520C



ARTICLE

Fiber-based Thermoelectrics for Solid, Portable, and Wearable Electronics

Xiao-Lei Shi,^{a,b,†} Wen-Yi Chen,^{b,†} Ting Zhang,^c Jin Zou,^{b,d} and Zhi-Gang Chen^{a,b,*}Received 00th January 20xx,
Accepted 00th January 20xx

DOI: 10.1039/x0xx00000x

With the growing demand for solid, portable, and wearable electronics, exploring recyclable and stable charging and cooling techniques is of significance. Fiber-based thermoelectrics, enabling sustainable power generation driven by the temperature difference or refrigeration without noise and freon, exhibit great potentials for applying in advanced electronics. In this work, we review significant advances in fiber-based thermoelectrics, including inorganic fibers, organic fibers, inorganic/organic hybrid fibers, and fiber-based fabrics and devices. Fundamentals, synthesis, characterizations, property evaluation, and applications of thermoelectric fibers are comprehensively discussed with carefully selected cases, and corresponding thermoelectric devices based on these advanced fibers are introduced for both power generation and refrigeration. Further, we point out the challenges and future directions toward developments of fiber-based thermoelectrics.

1 Introduction

Since its discovery and utilization, electricity has become an indispensable energy source in human society. With the increasing demand for electricity, traditional fossil fuels, such as coal, oil, and other non-renewable resources, are considerably depleting for industrial power generations, and their consumption also causes ever-growing environmental issues.¹ Therefore, extensive efforts have been focusing on developing eco-friendly and sustainable energy resources. Portable or wearable electronics, such as mobile phones, watches, micro-computers, and health monitoring systems,² are explosively advanced in miniaturization and integration. Searching new-type portable and wearable power-supply devices with high stability and high output power are very attractive and highly urgent.

Enabling direct conversion between thermal and electrical energy, thermoelectrics exhibit great potential to overcome challenges mentioned above.¹ Thermoelectric materials and devices can recycle waste heat for power generation, and are also suitable for charging various low-energy electronic devices using the temperature difference (ΔT) between human skin and environments.³⁻⁵ To evaluate thermoelectric potentials of materials, a dimensionless figure of merit ZT is defined as $ZT = S^2\sigma T/\kappa$, where S is the Seebeck coefficient, σ is the electrical

conductivity, $S^2\sigma$ is described as the thermoelectric power factor, κ is the thermal conductivity, and T is the absolute temperature. There is $\kappa = \kappa_l + \kappa_e$, where κ_l is the lattice thermal conductivity and κ_e is the electronic thermal conductivity. Generally, to realize a high ZT , it is required to increase $S^2\sigma$ and reduce κ (especially κ_l). However, restricted by microstructures, carrier concentration (n_e for n-type materials and n_p for p-type materials), and lattice vibration mode of materials, thermal and electrical transport properties are always interrelated. Therefore, it is often challenging to obtain thermoelectric materials with large ZT values. Besides, taking a portable and wearable thermoelectric device for an example, good mechanical properties and flexibility are also needed to maximize the use of energy obtained from human body (maximizing the thermoelectric conversion efficiency),⁶ while good abrasion resistance and stability are also required for designs of materials and device.⁷

Fibers, which can be either natural or synthetic, refer to substances composed of continuous or discontinuous filaments, which have been widely used in modern society.^{8,9} Particularly in the field of thermoelectric materials and devices,¹⁰ fibers, especially nanofibers, are playing an unparalleled role in realizing high-performance, portable, and wearable thermoelectrics.¹¹ Fiber-based thermoelectric materials can be divided into three categories, namely inorganic fibers, organic fibers, and inorganic/organic hybrid fibers. **Figure 1** describes current advances in thermoelectric fibers and their various applications, including all-carbon-based fibers,¹² carbon hybrid fibers,¹³ semiconductor-based fibers,¹⁴ core-shell-structured fibers,¹⁵ oxide-based fibers,¹⁶ coated fibers,¹⁷ fibers as secondary phases in thermoelectric materials,¹⁸ fiber-reinforced thermoelectric cements,¹⁹ organic fibers,²⁰ inorganic/organic hybrid fibers,²¹ and advanced thermoelectric fabrics.²² Recently, significant breakthroughs have been made

^a Centre for Future Materials, University of Southern Queensland, Springfield Central, Queensland 4300, Australia.

^b School of Mechanical and Mining Engineering, The University of Queensland, Brisbane, Queensland 4072, Australia.

^c Institute of Engineering Thermophysics, Chinese Academy of Sciences, Beijing 100190, People's Republic of China.

^d Centre for Microscopy and Microanalysis, The University of Queensland, Brisbane, Queensland 4072, Australia.

[†] These authors contribute equally to this work.

Corresponding author: ZGC Zhang.Chen@usq.edu.au; zhigang.chen@uq.edu.au

in the theoretical research of fiber application.²³ Particularly, the lower-dimensional structure such as nanofiber can significantly improve its thermoelectric properties due to the considerable nano-size effect and unique band engineering, which provides a new direction for improving thermoelectric properties of materials. Meanwhile, considering the flexibility

of wearable thermoelectric devices, the research on organic and organic/inorganic fiber-based thermoelectric materials is also inevitable.^{6, 24, 25} Therefore, there is an urgent need for designing high-quality and high-performance thermoelectric fibers targeting various applications.²³

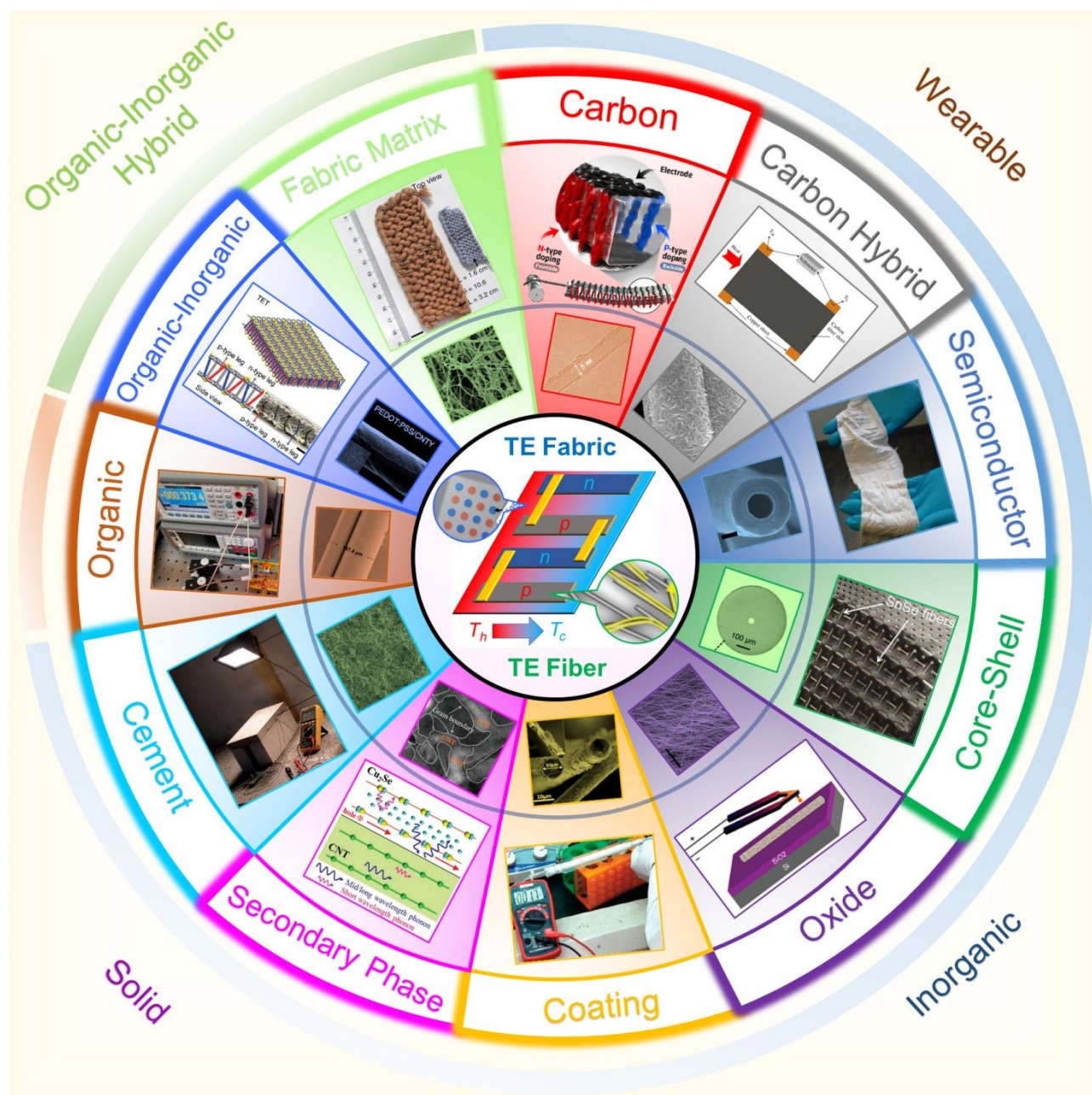


Figure 1. Classifications of fiber-based thermoelectric materials and devices for applying in advanced solid and wearable electronics. All-carbon-based fibers: reproduced with permission.¹² Copyright 2017, American Chemical Society; Carbon hybrid fibers: reproduced under a Creative Commons license.¹³ Copyright 2012, Elsevier; Semiconductor-based fibers: reproduced under a Creative Commons Attribution 4.0 International License.¹⁴ Copyright 2018, Springer Nature; Core-shell-structured fibers: reproduced with permission.¹⁵ Copyright 2020, Wiley; Oxide-based fibers: reproduced with permission.¹⁶ Copyright 2010, American Chemical Society; Coated thermoelectric fibers: reproduced with permission.¹⁷ Copyright 2012, American Chemical Society; Fibers as secondary phases in thermoelectric materials: reproduced with permission.¹⁸ Copyright 2017, Royal Society of Chemistry; Fiber-reinforced thermoelectric cement: reproduced with permission.¹⁹ Copyright 2014, Royal Society of Chemistry; Organic fibers: reproduced under the Creative Commons Attribution License.²⁰ Copyright 2020, MDPI; Inorganic/organic hybrid fibers: reproduced with permission.²¹ Copyright 2020, Royal Society of Chemistry; Thermoelectric fabric: reproduced under a

Creative Commons Attribution 4.0 International License.²² Copyright 2020, Springer Nature. In the center: Thermoelectric fiber: reproduced with permission.²⁶ Copyright 2019, Royal Society of Chemistry; Thermoelectric fabric: reproduced with permission.¹² Copyright 2014, Royal Society of Chemistry.

With the fast development of computational science and fabrication techniques, thermoelectric performance of various thermoelectric fibers has been significantly improved. **Figure 2** summarizes the reported maximum power factor $S^2\sigma_{max}$ and maximum figure-of-merit ZT_{max} of fiber-based materials,^{12-15, 19, 21, 22, 26-151} from which some advanced thermoelectric fibers have shown highly competitive performance compared to those

of bulk thermoelectric materials. For example, flexible Sb_2Te_3 /polyacrylonitrile (PAN) nanofibers exhibit an ultrahigh $S^2\sigma$ of $\sim 6500 \mu W m^{-1} K^{-2}$ with a high ZT of 0.48,⁶⁹ while single-crystal SnSe-based core fibers with a high ZT of up to ~ 2 at 862 K¹⁵ are very competitive to some inorganic bulk materials such as Bi_2Te_3 ,¹⁵²⁻¹⁶⁴ Cu_2Se ,¹⁶⁵⁻¹⁷¹ $GeTe$,¹⁷²⁻¹⁸⁰ $PbTe$,¹⁸¹⁻¹⁸⁹ $SnSe$,¹⁹⁰⁻²⁰¹ and $SnTe$.²⁰²⁻²⁰⁹

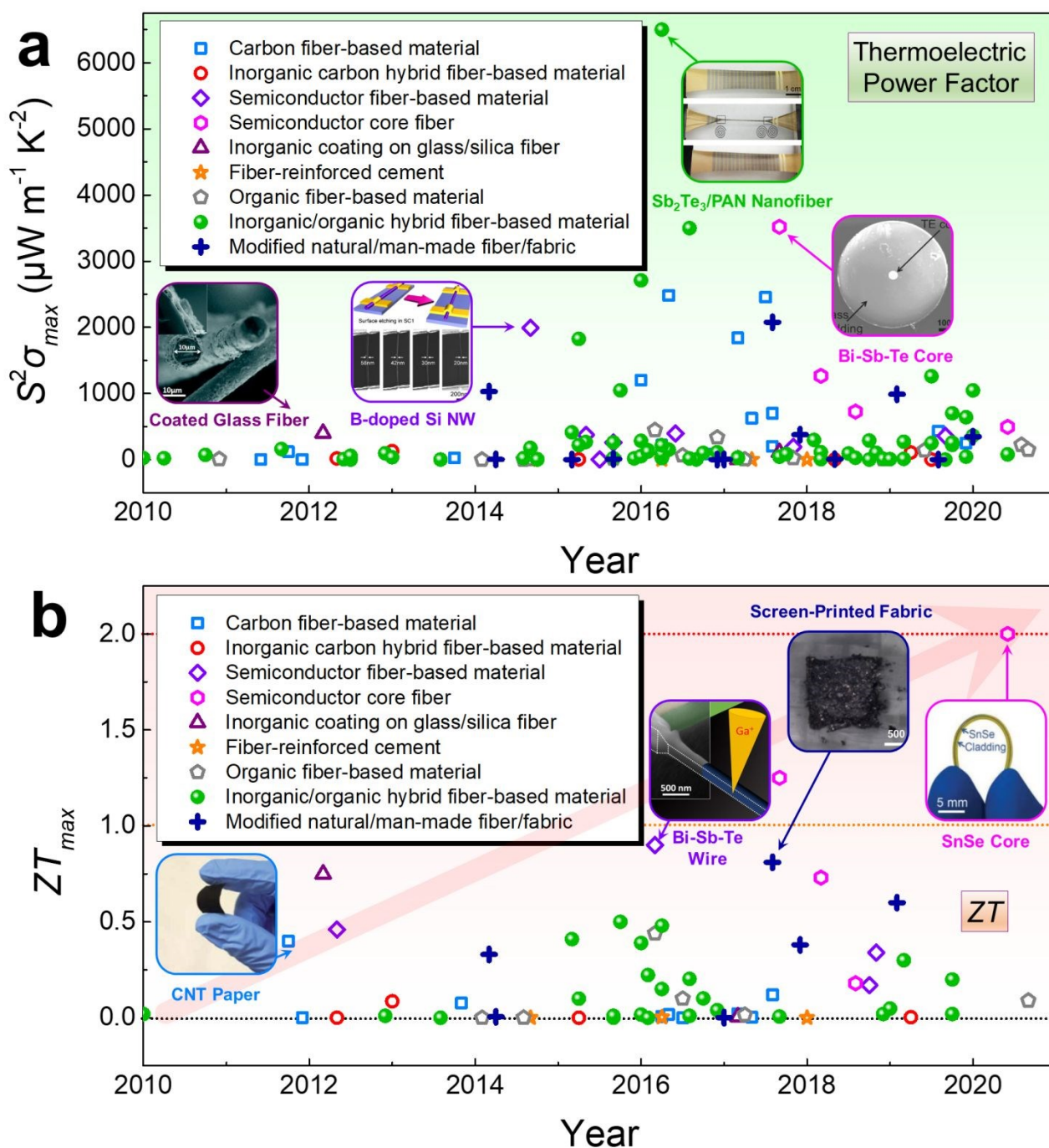


Figure 2. A summary of fiber-based thermoelectrics over the past decade: (a) Maximum power factor ($S^2\sigma_{max}$),^{12, 13, 15, 19, 21, 22, 26-144} and (b) maximum figure-of-merit (ZT_{max}).^{13-15, 19, 27, 28, 30, 31, 33, 34, 36, 38-40, 44-47, 49, 51, 65, 66, 68, 69, 73, 77, 78, 82, 83, 85, 86, 88, 90, 91, 99, 100, 104, 107, 109,}

111, 112, 114, 115, 122-124, 130, 131, 135, 137, 140, 141, 143, 145-151 Inset images: Coated glass fiber: reproduced with permission.¹⁷ Copyright 2012, American Chemical Society; B-doped Si nanowires (NWs): reproduced with permission.²¹⁰ Copyright 2014, American Chemical Society; Sb₂Te₃/polyacrylonitrile (PAN) Nanofiber: reproduced with permission.⁶⁹ Copyright 2016, Wiley; Bi-Sb-Te core: reproduced with permission.⁴⁶ Copyright 2017, Elsevier; CNT paper: reproduced with permission.²¹¹ Copyright 2012, Royal Society of Chemistry; Bi-Sb-Te wire: reproduced under a Creative Commons Attribution 4.0 International License.¹⁴⁹ Copyright 2016, Springer Nature; Screen-printed fabric: reproduced under a Creative Commons Attribution 4.0 International License.⁸³ Copyright 2017, Springer Nature; and SnSe core: reproduced with permission.¹⁵ Copyright 2020, Wiley.

Considering the demanding potentials for fiber-based thermoelectrics, in this work, we review significant advances in fiber-based thermoelectrics, including inorganic fibers, organic fibers, inorganic/organic hybrid fibers, and fiber-based fabrics and devices. The fundamentals, synthesis, characterizations, property evaluation, and applications of thermoelectric fibers are comprehensively discussed with carefully selected cases, and corresponding thermoelectric devices based on these advanced fibers are introduced for both power generation and refrigeration. Further, we discuss the challenges and future directions toward developments of fiber-based thermoelectrics.

2 Inorganic Thermoelectric Fibers

To achieve the goal of applying high-performance inorganic thermoelectric materials in wearable thermoelectric devices, high flexibility should be achieved in these inorganic materials, and lowering their dimensions from three-dimensional (3D) bulks into one-dimensional (1D) fibers is a good way, as illustrated in **Figure 3(a)**. In addition to the strengthened flexibility, computation-based theoretical results on low-dimensional materials indicate that, when an electron is confined to a structure with a scale smaller than the electron wave function space, the electron can possess special movement characteristics, which induce the quantum confinement effect and may enlarge bandgaps of materials,²¹²⁻²¹⁵ leading to potentially improved thermoelectric performance,²¹⁶ as illustrated in **Figure 3(b)**. For example, first-principles density functional theory (DFT) calculations indicated that with increasing the diameter of 1D GaAs_{1-x}P_x,²¹⁷ its bandgap can be obviously decreased due to quantum confinement effect; while with increasing x , the bandgap can be enlarged, indicating the electrical transport performance of 1D materials can be improved by rational compositional design. In terms of the predicted thermoelectric performance of 1D materials, calculations indicated that a diameter of <1 nm in Bi₂Te₃ NWs could induce an ultra-high ZT of >14,²¹⁴ while other computational-based work reported that a high ZT of >3 could be achieved in ZnO NWs when the carrier density was rationally tuned to $\sim 2 \times 10^{20}$ cm⁻³ with an ultralow κ_f of 0.12 W m⁻¹ K⁻¹.²¹⁸ Owing to the increased density of states (DOS) near the Fermi level, sufficient carriers of low-dimensional inorganic materials such as nanofibers may maintain high σ and S .²¹⁵ Besides, the low Fermi energy contributes to a high S , leading to a high $S^2\sigma$.¹ Besides, owing to the low-dimensional feature that provides more surfaces/interfaces, strengthened phonon scatterings reduce κ_f ,²¹⁹ as illustrated in **Figure 3(c)**. Therefore, low-

dimensional nanofiber-based inorganic thermoelectric materials gain significant attentions.^{220, 221}

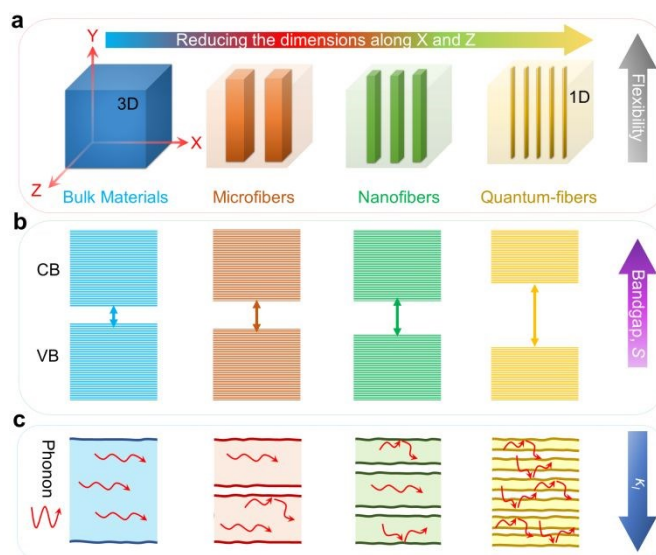


Figure 3. Illustrations of (a) improved flexibility, (b) enlarged bandgap by quantum confinement effect, and (c) reduced κ_f by strengthened phonon scattering through lowering the dimensions from three-dimensional (3D) bulk materials to one-dimensional (1D) micro/nano/quantum-fibers.

In order to realize high performance in low-dimensional thermoelectrics, one way relates to utilizing the quantum confinement effect to enlarge bandgap, resulting in an improved $S^2\sigma$,²¹² and another way is designing a large number of internal interfaces in 1D materials, which significantly strengthens phonon scatterings and ensures that the reduction of κ should be much larger than the reduction of σ .²²² Such two strategies are developing fast and dependently. Currently, it is promising that employing advanced material preparation technology to prepare low-dimensional inorganic nanofibers based on the discovered high-performance bulk thermoelectric material.²²³ Both theoretical and experimental results indicate that inorganic nanofibers possess high thermoelectric performance. However, it is still slow for the development of efficient preparation technology in synthesizing high-quality thermoelectric nanofibers, especially for the nanofibers that can work under high temperature and high flexibility.

2.1 Carbon Fibers

Carbon-based fibers such as carbon nanotubes (CNTs) and graphene fibers have been widely considered as promising thermoelectric materials, owing to their high σ and tuneable

S₃₀, S₃₂, S₃₉, S₁₄₅, S₁₄₆, S₂₂₄₋₂₄₃ Graphene and CNTs are typical carbon elements that belong to allotropes of carbon;^{244, 245} therefore, we classify these two materials as inorganic materials in this review. Calculation results indicate that graphite nanofibers could achieve a high ZT up to 8 by ¹⁴C isotope doping and effect of finite phonon mean free path.²⁴⁶ As a typical 1D inorganic nanofiber, CNTs have exhibited unique thermoelectric performance.³⁵ A high ZT of 0.4 at 673 K was reported in CNT papers treated with Ar plasma.²¹¹ In terms of their fundamentals, **Figure 4(a)** illustrates a single-walled CNT (SWCNT), which can be formed by rolling a graphene sheet from (0,0) to (n,m) along the “roll-up vector” (with respect to the zig-zag axis).²⁴⁴ A set of chiral indices (n,m) are defined by the chiral angle (α) and the magnitude of this roll-up vector, which denotes unique SWCNTs with particular electronic structures (1/3 SWCNTs are metallic and 2/3 SWCNTs are semiconducting). In **Figure 4(a)**, a cylinder formed by rolling up the shaded blue area corresponds to a segment of (9,4) SWCNT unit cell.²⁴⁴ **Figure 4(b)** illustrates structures and thermopowers of metallic (8,5) SWCNT and semiconducting (9,4) SWCNT.²⁴⁴ In the DOS of SWCNTs, the sharp singularities are produced by quantum confinement in two dimensions. It is interesting to note that slight changes in the chirality, diameter, and α result in dramatic differences in DOS and S. Rational doping is commonly employed to enhance thermoelectric properties of SWCNTs. **Figure 4(c)** summarizes thermoelectric properties (top: S, bottom: $S^2\sigma$) of p-type and n-type redox doped SWCNTs.³⁰ Both p-type and n-type SWCNTs show high $S^2\sigma$ of $>25 \mu\text{W m}^{-1} \text{K}^{-2}$ by appropriate doping with different molecules.

SWCNTs can form free-standing networks by using advanced fabrication techniques. Such free-standing networks can act as thermoelectric materials for applying into flexible thermoelectric devices. For example, **Figure 4(d)** illustrates the fabrication of semiconducting SWCNT thermoelectric thin films.²⁸ In this study, in order to better disperse the high-purity semiconducting SWCNTs, cleavable polymers based on fluorene were used, which could be removed from the deposited films by submersion in a trifluoroacetic acid (TFA) solution, leading to only-semiconducting-SWCNTs in the as-deposited films.²⁸ In terms of the mechanism of removing polymers, polymer backbones were destroyed by TFA through catalyzing hydrolytic cleavage of the imine (CQN) bonds in PFPD-based polymers or disrupting the hydrogen bonds in SMP-based polymers.²⁸ Here PFPD is the abbreviation of poly[(9,9-di-n-dodecyl-2,7-fluorendiyl-dimethine)-(1,4-phenylene-dinitrilmethine)], and SMP is the abbreviation of 1,10-(((1E,10E)-(9,9-didodecyl-9H-fluorene-2,7-diyl)bis(ethene-2,1-diyl))bis(6-methyl-4-oxo-1,4-dihydropyrimidine-5,2-diyl))bis(3-dodecylurea). **Figure 4(e)** shows an atomic force microscope (AFM) image of semiconducting SWCNT networks prepared from PT:PFPD dispersions.²⁸ Here PT is the abbreviation of the plasma-torch process. It is clearly seen that pure SWCNT networks were obtained. **Figure 4(f)** compares σ -dependent $S^2\sigma$ of

semiconducting SWCNT networks from PT:SMP and PT:PFPD dispersions,²⁸ from which a high $S^2\sigma$ up to $700 \mu\text{W m}^{-1} \text{K}^{-2}$ could be achieved at room temperature, which is competitive to that of many bulk inorganic materials such as SnSe,^{191, 192, 194} Cu₂Se,²⁴⁷ and Bi₂Te₃.¹⁵⁵ By treating with salts and crown ether, SWCNTs exhibit n-type semiconducting features with a promising ZT of 0.1 and excellent air- and heat-stability (stable at 100 °C for more than 1 month).³³ Similarly, n-type SWCNT networks could be realized by K-doping, and I₂-doping for enhancing their σ .³⁸ Such unique SWCNT networks exhibited an ultralow room-temperature κ of only $0.035 \text{ W m}^{-1} \text{K}^{-1}$.³⁸ Furthermore, by twisting SWCNT interconnected films, an ultrahigh $S^2\sigma$ up to $2482 \mu\text{W m}^{-1} \text{K}^{-2}$ can be achieved at room temperature due to the maintained high S by avoiding conventional nitric acid treatment and tedious composite technology,³⁴ and ZT values of 0.74-1.86 could be estimated if reported out-of-plane κ values of $0.4\text{-}1 \text{ W m}^{-1} \text{K}^{-1}$ are used.²¹¹

Owing to the high electrical performance and high flexibility of CNTs (especially for semiconducting SWCNTs), CNT-based yarn (CNTY) is further designed to compose highly flexible thermoelectric generators (F-TEG). **Figure 4(g)** illustrates a typical fabrication of CNTYs and F-TEG based on these CNTYs.¹² CNTYs can be continuously produced by direct spinning after synthesis. In order to form F-TEGs, synthesized CNTYs are wound onto a flexible supporting unit, and alternatively doped into n-type by polyethyleneimine (PEI) and p-types by FeCl₃ solution. Undoped materials are between the two doped regions. Such a unique design does not need any metal electrode, which eliminates the influence of the interface resistance. Both n-type and p-type CNTYs exhibit high $S^2\sigma$ up to $\sim 2375 \mu\text{W m}^{-1} \text{K}^{-2}$ at room temperature, derived from e high σ of $> 7000 \text{ S cm}^{-1}$ and improved absolute S of $>50 \mu\text{V K}^{-1}$. To fabricate these CNTYs into F-TEGs, the alternately n- and p-doped CNTY as thermoelectric “legs” with undoped regions as electrodes were carefully wound around a polydimethylsiloxane (PDMS) substrate without interconnection of the CNTY.¹² **Figure 4(h)** shows optical images of CNTY-based F-TEG with 60 p-n pairs,¹² and **Figure 4(i)** shows the obtained output voltage of CNTY-based F-TEG with 240 p-n pairs at a ΔT between atmosphere and body heat.¹² The ΔT between F-TEG and human arm was measured to $\sim 6 \text{ K}$, leading to an output voltage of $\sim 54 \text{ mV}$. In addition, the maximum power density could reach $697 \mu\text{W g}^{-1}$ at a ΔT of 40 K for a CNTY-based F-TEG with 60 p-n pairs.¹² Similarly, a high $S^2\sigma$ could be realized in wet-spun CNT fibers ($432 \mu\text{W m}^{-1} \text{K}^{-2}$) by mild annealing, and F-TEGs based on 40 pairs of p- and n-type CNT fibers show a power density of $259 \mu\text{W g}^{-1}$ at a ΔT of 20 K.²⁶ Wet environment also plays a significant role in determining thermoelectric performance of CNT fibers.³² Furthermore, by floating catalyst chemical vapor deposition (FCCVD), continuous n-type CNTs networks can be formed with a high $S^2\sigma$ of $\sim 1500 \mu\text{W m}^{-1} \text{K}^{-2}$. Fabricated F-TEGs with 3 p-n pairs exhibit an output power density of $\sim 167 \mu\text{W cm}^{-2}$ at a ΔT of 27.5 K.³⁶

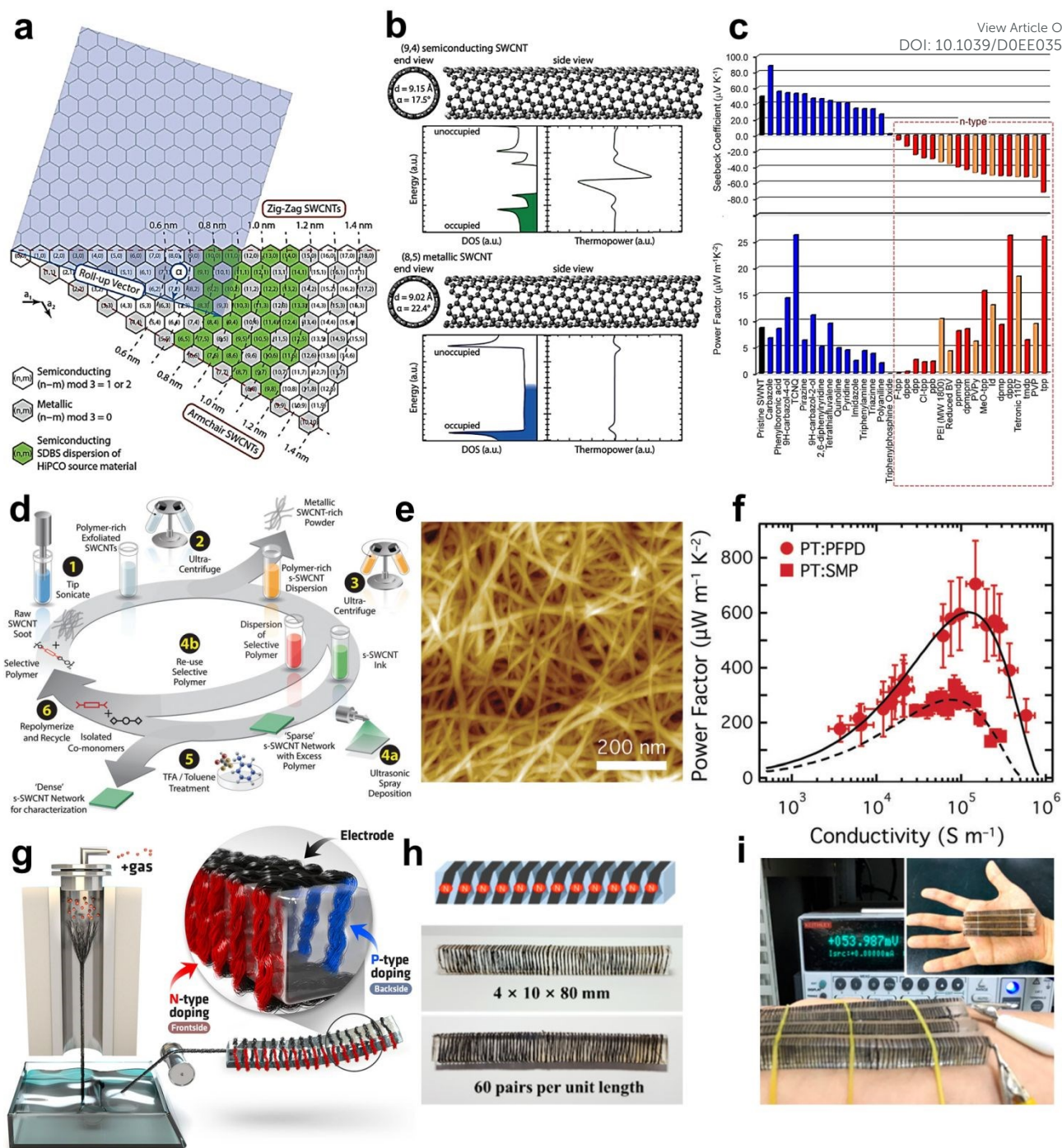


Figure 4. (a) Single-walled carbon nanotube (SWCNT) formed by rolling a graphene sheet from $(0,0)$ to (n,m) along the “roll-up vector”. Here the (n,m) are chiral indices, and a cylinder formed by rolling up the shaded blue area corresponds to a segment of the unit cell of the $(9,4)$ SWCNT. (b) Structures and corresponding electronic properties of the semiconducting $(9,4)$ SWCNT and metallic $(8,5)$ SWCNT. Reproduced with permission.²⁴⁴ Copyright 2018, Wiley. (c) A summary of thermoelectric properties of SWCNT (top: S , bottom: $S^2\sigma$). Reproduced under a Creative Commons Attribution-NonCommercial-NoDerivs 3.0 Unported License.³⁰ Copyright 2013, Springer Nature. (d) The illustration of fabricating semiconducting SWCNT thermoelectric thin films with cleavable polymers. (e) Atomic force microscope (AFM) image of semiconducting SWCNT networks prepared from PT:PFPD dispersions. (f) The σ -dependent $S^2\sigma$ of semiconducting SWCNT networks from PT:PFPD and PT:SMP dispersions. Here PT is the abbreviation of plasma-torch process, PFPD is the abbreviation of poly[(9,9-di-n-dodecyl-2,7-fluorendiyl-dimethine)-(1,4-phenylene-dinitrilomethine)], and SMP is the abbreviation of 1,10-(((1E,10E)-(9,9-didodecyl-9H-fluorene-2,7-diyl)bis(ethene-2,1-diyl))bis(6-methyl-4-oxo-1,4-dihydropyrimidine-5,2-diyl))bis(3-dodecylurea). Reproduced with permission.²⁸ Copyright 2017, Royal Society of Chemistry. (g) The illustration of fabricating carbon nanotube yarn (CNTY) and flexible thermoelectric generator (F-TEG) based on CNTY. (h) Optical image of CNTY-based F-TEG with 60 p-n pairs. (i) Output voltage of CNTY-based F-TEG obtained

from the temperature difference (ΔT) between atmosphere and body heat. Reproduced with permission.¹² Copyright 2017, American Chemical Society. DOI: 10.1039/D0EE03520C

In addition to CNT fibers, graphene fibers are also commonly studied in recent years. Graphene is a typical two-dimensional (2D) material with extraordinary electrical and thermal performance, and graphene possesses a great potential for applying to thermoelectrics.²⁴⁸ It was reported that a ZT value of 3.7×10^{-6} could be obtained in pristine graphene fibers due to high κ (from 45.8 to 149.7 $\text{W m}^{-1} \text{K}^{-1}$) and low S (from -3.9 to $0.8 \mu\text{V K}^{-1}$).¹⁴⁵ By bromine doping, the ZT of graphene fibers can be improved up to 2.76×10^{-3} , benefited from the improved $S^2\sigma$ ($624 \mu\text{W m}^{-1} \text{K}^{-2}$).³⁹ Besides, integral p-n connected graphene oxide (GO) fibers were designed for assembling F-TEGs.⁶² The GO fibers reduced with $\text{N}_2\text{H}_4 \cdot \text{H}_2\text{O}$ showed a p-type feature, while n-type GO fibers can be produced by doping polyethyleneimine ethoxylated (PEIE). Acceptable $S^2\sigma$ of ~ 1 and $\sim 0.25 \mu\text{W m}^{-1} \text{K}^{-2}$ were achieved in the p- and n-type fibers.⁶² By integrating p-n connected GO fibers into flexible PDMS substrate, a wearable F-TEG was realized, which exhibited an output voltage of 3 mV and an output power of 500 nW by a ΔT of 70 K.⁶²

Sometimes, other inorganic materials are added into carbon-based fibers to further improve their thermoelectric properties. For SWCNTs, the addition of MoS_2 flakes improved their ZT by 10 times (up to 0.003).³¹ For recycled carbon fibers,²⁴⁹ it was reported that by an electro-deposition technique, n-type thermoelectric recycled carbon fiber sheets with Bi_2Te_3 coating were fabricated, which exhibited a competitive absolute S of $54 \mu\text{V K}^{-1}$.¹³ In addition to Bi_2Te_3 , Bi_2S_3 was also added into the recycled carbon fibers to form inorganic hybrids with $S^2\sigma$ of $>1 \mu\text{W m}^{-1} \text{K}^{-2}$.^{41, 42}

2.2 Semiconductor Fibers

Semiconductors are important members of thermoelectric family. Compared with carbon-based thermoelectric materials, semiconductors exhibit much higher thermoelectric performance due to their suitable band structures and much low κ . Till now, many state-of-the-art semiconductors have shown outstanding thermoelectric performance with $ZTs > 2$, such as Cu_2Se ($ZTs > 2.6$),^{250, 251} PbTe ($ZTs > 2.5$),^{252, 253} SnSe ($ZTs > 2.6$),^{254, 255} and GeTe ($ZTs > 2.4$).²⁵⁶⁻²⁵⁸ Therefore, to further improve their thermoelectric performance or employ them in wider applications such as miniature thermoelectric devices or F-TEGs, fabrications of lower-dimensional semiconductors such as nano/microfibers are developing.

Nanowires (NWs) are a typical kind of nanofibers, which are usually epitaxially grown on a substrate.²⁵⁹ To ensure that NWs are grown along specific directions, catalyst particles are employed to control the lowest formation energy.¹ Besides, focused ion beam (FIB) technique is commonly used to "trim" NWs to achieve specific diameters.¹⁴⁹ **Figure 5(a)** shows scanning electron microscope (SEM) images of trimmed $\text{Bi}_{2-x}\text{Sb}_x\text{Te}_{3-y}$ NWs by FIB.¹⁴⁹ After trimming, the 750-nm-diameter $\text{Bi}_{0.8}\text{Sb}_{1.2}\text{Te}_{2.9}$ could exhibit a peak ZT of ~ 0.9 .¹⁴⁹ Other works indicate that Si-Ge NWs fabricated by a vapor-liquid-solid (VLS)

method show large ZT values of ~ 0.46 at 450 K experimentally and even > 2 at 800 K theoretically by rationally tuning the ratio of Si and Ge,¹⁴⁸ and 130-nm-diameter SnSe NWs using a catalyst-assisted VLS method exhibits a ZT of ~ 0.156 at 370 K.¹⁵⁰ In some occasions, NWs possess multi-phases. Ultralong Ag_xTe_y nanofibers, synthesized by galvanically displacing electro-spun Ni nanofibers,⁴³ have two types, namely Ag-rich fibers (co-existing Ag and Ag_2Te phases) and Te-rich fibers (co-existing Te and Ag_7Te_4 phases). Phase interfaces act as energy barriers to tune the thermoelectric performance of the nanofibers, and a maximum $S^2\sigma$ of $4 \mu\text{W m}^{-1} \text{K}^{-2}$ could be observed at a Te content of 30 % with an energy barrier height of 0.054 eV.⁴³ Similarly, $\text{Bi}_2\text{Te}_3/\text{Te}$ multi-segmented nanofibers with different segment lengths could be achieved by annealing super-saturated $\text{Bi}_x\text{Te}_{1-x}$ nanowires (NWs), which show a low κ of $\sim 0.65 \text{ W m}^{-1} \text{K}^{-1}$ and a high absolute S of $\sim 160 \mu\text{V K}^{-1}$ at 300 K.²⁶⁰ In addition, NWs can form dense films to better evaluate their thermoelectric performance. Flexible n-type Ag_2Te NW films on copy-paper substrates were fabricated by a novel glass-fiber-aided cold-press method.⁷⁹ A high $S^2\sigma$ could be achieved at $\sim 468 \text{ K}$ ($192 \mu\text{W m}^{-1} \text{K}^{-2}$), and a thermoelectric module containing 10 pieces of series-connected Ag_2Te films exhibits an output voltage of 60 mV at a ΔT of 80 K.⁷⁹

In addition to NWs, 1D nanotubes and nanorods are also typical kinds of nanofibers. It was reported that large-area paper-like fabrics made of Si nanotubes could exhibit a ZT of 0.34 at 823 K,¹⁴ as illustrated in **Figure 5(b)**. In terms of the fabrication, carbon fibers were first coated by poly-Si layers. After the annealing of carbon fiber cores, SiO_2 substrates remained, and finally the poly-Si layers surrounded the SiO_2 substrates to form Si nanotubes. In addition to their promising ZT values, the as-fabricated TEG based on Si nanotube fabric also exhibited an outstanding power density of $10000 \mu\text{W cm}^{-2}$ at 973 K.¹⁴ Besides, heavily Cu-doped SnSe 1D microbelts synthesized by a solvothermal method showed a σ of $\sim 4.2 \text{ S cm}^{-1}$ at room temperature, which can be further improved by applying 1 % strain ($\sim 6.0 \text{ S cm}^{-1}$).¹⁹⁶ Calculations indicated that the applied 1 % strain narrowed the bandgap of SnSe, leading such an enhancement on σ .¹⁹⁶ As a result, a $S^2\sigma$ of $> 36 \mu\text{W m}^{-1} \text{K}^{-2}$ could be evaluated,¹⁹⁶ indicating potentials for applying these microbelts in miniature thermoelectric devices.

Coating semiconductor nanocrystals on glass or silica fibers is another suitable way to realize high-performance, stable and flexible inorganic thermoelectric fibers. **Figure 5(c)** shows a transmission electron microscope (TEM) image of PbTe nanocrystals and an inset SEM image of nanocrystal-coated glass fibers.²⁶¹ PbTe nanocrystals were synthesized by an aqueous solution method, and the coating of glass fibers involved the alternative dipping of the glass fibers among PbTe nanocrystal solution, diluted hydrazine aqueous solution, and anhydrous acetonitrile.²⁶¹ Such unique composite fibers were reported to have a low κ of $\sim 0.226 \text{ W m}^{-1} \text{K}^{-1}$ and a high $S^2\sigma$ of $> 400 \mu\text{W m}^{-1} \text{K}^{-2}$ at 400 K (measured by the 3ω method),^{17, 261} giving rise to a high ZT of ~ 0.75 .¹⁷ Besides, the glass fiber yarn

coated with PbTe nanocrystals can be bent to a curvature of 84.5° , indicating certain flexibility.¹⁷ By stuffing the PbTe nanocrystal-coated glass fibers between hot and cold water flow through a coaxial design, a ΔT of 58 K can lead to an output voltage of 1.7 mV,¹⁷ indicating potential for applying to harvesting waste heat from industrial pipes for power generation. Other works indicated that by coating with ZnO and Al-doped ZnO, glass fibers showed S of -478.3 and -1057.8 μV at ΔT s of 4.5 and 4.3 K,⁴⁷ respectively. In addition, striped thin-film thermoelectric fibers made with thermal evaporation of Ni and Ag were reported, which showed a maximum power of 2 nW for 7 couples at a ΔT of 6.6 K.²⁶² CNT networks were also attempted to coat the surface of intrinsically insulating glass fiber yarns by a dip-coating deposition process, which showed a maximum $S^2\sigma$ of $\sim 109.8 \mu\text{W m}^{-1} \text{K}^{-2}$.⁴⁸

In addition to semiconductor-nanocrystal-coated glass/silica nanofibers, semiconductor core fibers are also developing fast. Different from the coated nanofibers, the crystalline semiconductor core fibers are commonly fabricated by thermally drawing hermetically sealed high-quality inorganic materials in a flexible fiber-like substrate. Single-crystal SnSe thermoelectric fibers were fabricated by a laser-induced directional crystallization based on a typical thermal drawing and CO_2 laser recrystallization technique,¹⁵ as shown in **Figure 5(d)**. The thermal drawing process made polycrystalline SnSe cores, and the following laser recrystallization process recrystallized the SnSe cores into single crystals with a rock-salt Fm-3m structure. Such unique single-crystal SnSe core fibers were reported to show a ZT up to 2 at 862 K.¹⁵ Besides, to

achieve high flexibility, the diameter of the resulting fiber was kept being 500 μm , while the diameter of the fiber core was 40 μm .¹⁵ This work also designed multi-core SnSe fibers with both high-density p- and n-type SnSe micro/nanowires,¹⁵ as illustrated in **Figure 5(e)**, which is a typical p-n flexible thermoelectric structure within a fiber. Such unique thermoelectric fibers can be used for designing large-area, light-weight, high-performance, and flexible/wearable thermoelectric devices, as illustrated in **Figure 5(f)**. By converting human body heat to electricity, a 30 mV output voltage was realized by a ΔT of ~ 10 K.¹⁵ In addition to power generation, such unique semiconductor core fibers could also be used for refrigeration. **Figure 5(g)** shows the finite element modelling (FEM) simulated and actual infrared (IR) camera captured temperature profiles for the wearable cooling fabric based on n-type Bi_2Se_3 core fibers and p-type $\text{Bi}_{0.5}\text{Sb}_{1.5}\text{Te}_3$ core fiber.⁴⁶ The ZT s of p- and n-type fibers were 1.25 and 0.23 at 300 K,⁴⁶ respectively, and a maximum cooling of 5 $^\circ\text{C}$ could be realized by wearing the 2D cooling textile, which is promising for personal temperature management.⁴⁶ Other works indicated that by a modified molten core drawing method, novel Bi_2Te_3 core fibers consist of hexagonal polycrystalline nanosheets with borosilicate glass cladding were fabricated with a high ZT of 0.73 at 300 K.⁴⁴ Similarly, a promising ZT of 0.18 at room temperature was realized in Bi_2Se_3 core thermoelectric fibers with K9 glass cladding, fabricated by a similar route.⁴⁵ In addition to Bi_2Te_3 and Bi_2Se_3 , n-type In_4Se_3 alloy core thermoelectric fibers were also fabricated by a similar molten core drawing method and show a high S of $-347 \mu\text{V K}^{-1}$.²⁶³

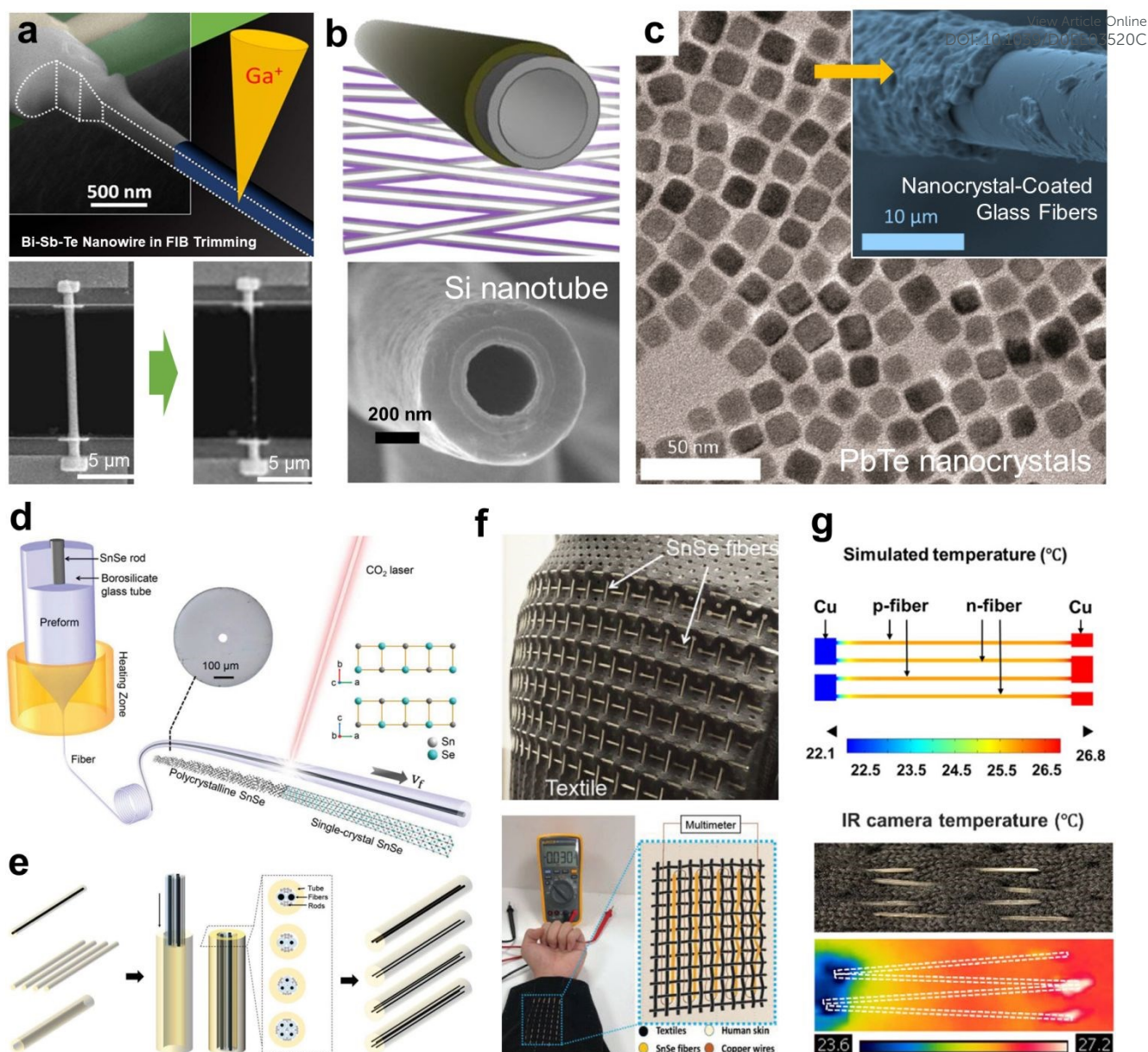


Figure 5. (a) Illustrations and scanning electron microscope (SEM) images of trimmed Bi_{2-x}Sb_xTe_{3-y} nanowires (NWs) by the focused ion beam (FIB). Reproduced under a Creative Commons Attribution 4.0 International License.¹⁴⁹ Copyright 2016, Springer Nature. (b) The illustration and SEM image of poly-silicon nanotube. Reprinted under a Creative Commons Attribution 4.0 International License.¹⁴ Copyright 2018, Springer Nature. (c) Transmission electron microscope (TEM) image of PbTe nanocrystals and inset SEM image of nanocrystal-coated glass fibers. Reproduced with permission.²⁶¹ Copyright 2013, American Chemical Society. (d) The illustration of thermal drawing SnSe fiber and post-draw laser recrystallization process. (e) The fabrication of multicore SnSe fibers. (f) The demonstration of converting human body heat to electricity by multi-dimensional SnSe fabric. Reproduced with permission.¹⁵ Copyright 2020, Wiley. (g) The finite element modelling (FEM) simulated and actual infrared (IR) camera captured temperature profiles for the wearable cooling fabric based on n-type Bi₂Se₃ fiber and p-type Bi_{0.5}Sb_{1.5}Te₃ fiber. Reproduced with permission.⁴⁶ Copyright 2017, Elsevier.

In addition to flexible thermoelectric devices, miniature thermoelectric devices based on semiconductor fibers were also developed. It was reported that by an extrusion process, flexible and continuous fibers could be achieved from a solution of mixed semiconductor powders and a thermoplastic resin dissolved in an organic solvent.⁸⁴ The polymer phases in the as-extruded fibers were then removed by sintering, leading to all-

semiconductor fibers.⁸⁴ The as-fabricated p-type Bi_{0.5}Sb_{1.5}Te₃ fibers showed a S of 179~193 $\mu\text{V K}^{-1}$ and a $S^2\sigma$ of 170~260 $\mu\text{W m}^{-1} \text{K}^{-2}$, while the n-type Bi₂Te_{2.7}Se_{0.3} fibers showed an absolute S of 207~268 $\mu\text{V K}^{-1}$ and a $S^2\sigma$ of 30~40 $\mu\text{W m}^{-1} \text{K}^{-2}$.⁸⁴ The designed miniature thermoelectric generator based on these semiconductor fibers exhibited an output voltage of 4.8 mV and an output power of 18 nW by a ΔT of 12 °C.⁸⁴ Such unique

miniature thermoelectric devices are suitable as power sources of small sensors such as heart pacemaker.²

2.3 Oxide Fibers

Different from semiconductor-based fibers, oxide-based thermoelectric fibers possess many unique advantages.^{181, 264} Most of the oxide fibers are non-toxic, indicating that they are ideal candidates for applying to wearable thermoelectrics. Meanwhile, oxide fibers can exhibit significantly high stability at high temperatures, which broaden their applications such as industrial and vehicle waste heat collections. Furthermore, the fabrications of oxide fibers are relatively mature, which can meet the requirement of industrial scale-up. Therefore, oxide-based thermoelectric fibers are especially suitable for industrial power generation.

Within the oxide thermoelectric fibers, perovskite n-type SrTiO₃ has attracted much attention in recent years due to its high thermal stability (the melting point is as high as 2080 °C), eco-friendly feature, low cost, mature fabrication technique, and promising thermoelectric properties.²⁶⁴ The bandgap of SrTiO₃ is ~3.2 eV,²⁶⁵ which ensures a suitable S of >100 $\mu\text{V K}^{-1}$ with potentially high n_e ($\sim 1 \times 10^{22} \text{ cm}^{-3}$).²⁶⁴ By rationally doping with La/Nb and structural design, significantly improved thermoelectric properties of SrTiO₃ are observed.^{266, 267} SrTiO₃ fibers could be fabricated by an *in situ* hydrothermal method using hydrated TiO₂ fibers as both reactant and template,²⁶⁸ but their thermoelectric performance still needs further investigation. In addition to SrTiO₃, thermoelectric oxide NaCo₂O₄ nanofibers were fabricated by electrospinning technique,^{16, 269} and their thermoelectric effect can be evaluated by electrostatic force microscopy (EFM) contrast mapping, which is based on the scanning probe microscopy (SPM) technique.¹⁶ It should be noted that the thermoelectric performance of oxide-based fibers still needs further improvement to meet the requirement of practical applications.

2.4 Fiber-Reinforced Bulk Thermoelectrics

Fibers, especially for nanofibers, are ideal candidates that act as positive secondary phases in bulk thermoelectric materials. Benefited from their 1D feature, introducing nanofibers can provide high-density interfaces in the matrix, acting as effective energy barriers to further improve the S of bulk thermoelectric materials based on the energy filtering effect.²⁷⁰ Besides, the dense interfaces in the matrix can also act as phonon scattering centers to effectively scatter most of the low- and medium-wavelength phonons, leading to a much low K_f .²⁷¹

Figure 6(a) illustrates the design of Cu₂Se/CNT hybrid bulk materials for the applications of nanofibers in bulk thermoelectric materials.¹⁸ Precursors including Cu, Se, and multi-walled CNTs were mixed and reacted into Cu₂Se/CNTs hybrid powders by high energy ball-milling. After a spark plasma sintering (SPS) process, the hybrid powders were sintered into high-density Cu₂Se/CNTs bulk materials. **Figure 6(b)** shows a spherical aberration-corrected scanning transmission electron microscope (Cs-corrected STEM) image of Cu₂Se with 0.75 wt% CNTs,¹⁸ from which a cross-section of CNT can be clearly seen. These CNTs can provide high-density

interfaces in the bulk material, which effectively reduce the K_f by scattering most of the low- and medium-wavelength phonons, as illustrated in **Figure 6(c)**.¹⁸ **Figure 6(d)** shows T -dependent ZT of Cu₂Se/CNT hybrid materials with different contents of CNT.¹⁸ It is interesting to see that an ultrahigh ZT of 2.4 at 1000 K could be realized by introducing 0.75 wt% CNTs. Similarly, for oxide-based bulk thermoelectric materials, by introducing 3.0 wt% SrTiO₃ fibers into Sr_{0.75}La_{0.1}Dy_{0.1}TiO₃, a ZT of 0.19 was realized at 773 K, benefited from a high $S^2\sigma$ of $\sim 700 \mu\text{W m}^{-1} \text{K}^{-2}$.²⁶⁸

In addition to improving the thermoelectric performance, the introduction of fibers can also boost the mechanical properties of bulk materials. It was reported that Bi_{0.4}Sb_{1.6}Te₃ powders were ball-milled with multi-wall CNTs, and a co-sintering of these precursors was followed.²⁷² The adhesive force between adjacent Bi_{0.4}Sb_{1.6}Te₃ grains was significantly strengthened by the embedded CNTs between the grains, contributing to a bending strength of 90 MPa for the bulk materials. Similarly, for skutterudite-based bulk thermoelectric materials, the introduction of 1 vol.% short carbon fibers significantly improved the flexural strength of bulk CeFe₄Sb₁₂ by 53%,²⁷³ while a slight improvement of ZT was simultaneously achieved from ~ 0.8 to >0.9 at 800 K. Besides, for Mg₂Si-based alloys, by introducing 0.8 at.% SiC NWs in bulk Mg_{2.16}(Si_{0.3}Sn_{0.7})_{0.98}Sb_{0.02}, the compressive strength was improved by 30% from 450 MPa to 570 MPa,²⁷⁴ while the peak ZT of ~ 1.20 at 750 K was influenced little by introducing SiC NWs.

A special case for the fiber-reinforced bulk thermoelectric materials is the steel fiber or carbon fiber reinforced cement-based composites (CFRC).²⁷⁵⁻²⁷⁷ It is well known that cement-based materials are indispensable for the construction of modern society, owing to their good durability and mechanical properties.^{278, 279} However, conventional cement-based materials have gradually failed to meet the requirements of the new technological revolutions in current life.²⁸⁰ Therefore, in order to improve the performance and realize new functions in cement-based materials, functional cement is fast developing, and one of the typical functional cement material is fiber-reinforced thermoelectric cement,²⁸¹ as shown in **Figure 6(e)**.¹⁹ By introducing carbon fibers in the cement matrix, thermoelectric cement with a certain thermoelectric effect can be achieved, as illustrated in **Figure 6(f-g)**. Such a unique thermoelectric cement has broad application prospects in structural monitoring, intelligent buildings, and other engineering fields. For example, buildings in cities are affected by strong light, automobile exhaust, and industrial exhaust emissions, which will generate excessive heat. However, if these urban waste heat can be collected and converted into electrical energy through thermoelectric cement, considerable energy could be saved. Therefore, it is of great significance to improve the thermoelectric performance of such "smart" cement-based thermoelectric materials. Besides, fiber-reinforced thermoelectric cement could be used for road snow removal and ice melting, which solve the issues of road icing caused by rain and snow in winter. However, it should be noted that both the S and σ of current thermoelectric cement are low,^{49, 275, 282, 283} leading to ZT s <0.01 , as shown in **Figure 2**. Therefore, it is of

great significance to explore the way to improve the thermoelectric properties of fiber-reinforced cement, such as by introducing mineral admixtures,²⁸³ cement interface,²⁸⁴ and CNTs.²⁸⁵ Besides, it is also important to understand the

influence of various factors in the actual environment on their thermoelectric properties, such as fiber content,²⁸⁶ moisture,²⁸⁷ and compression shear.⁵¹

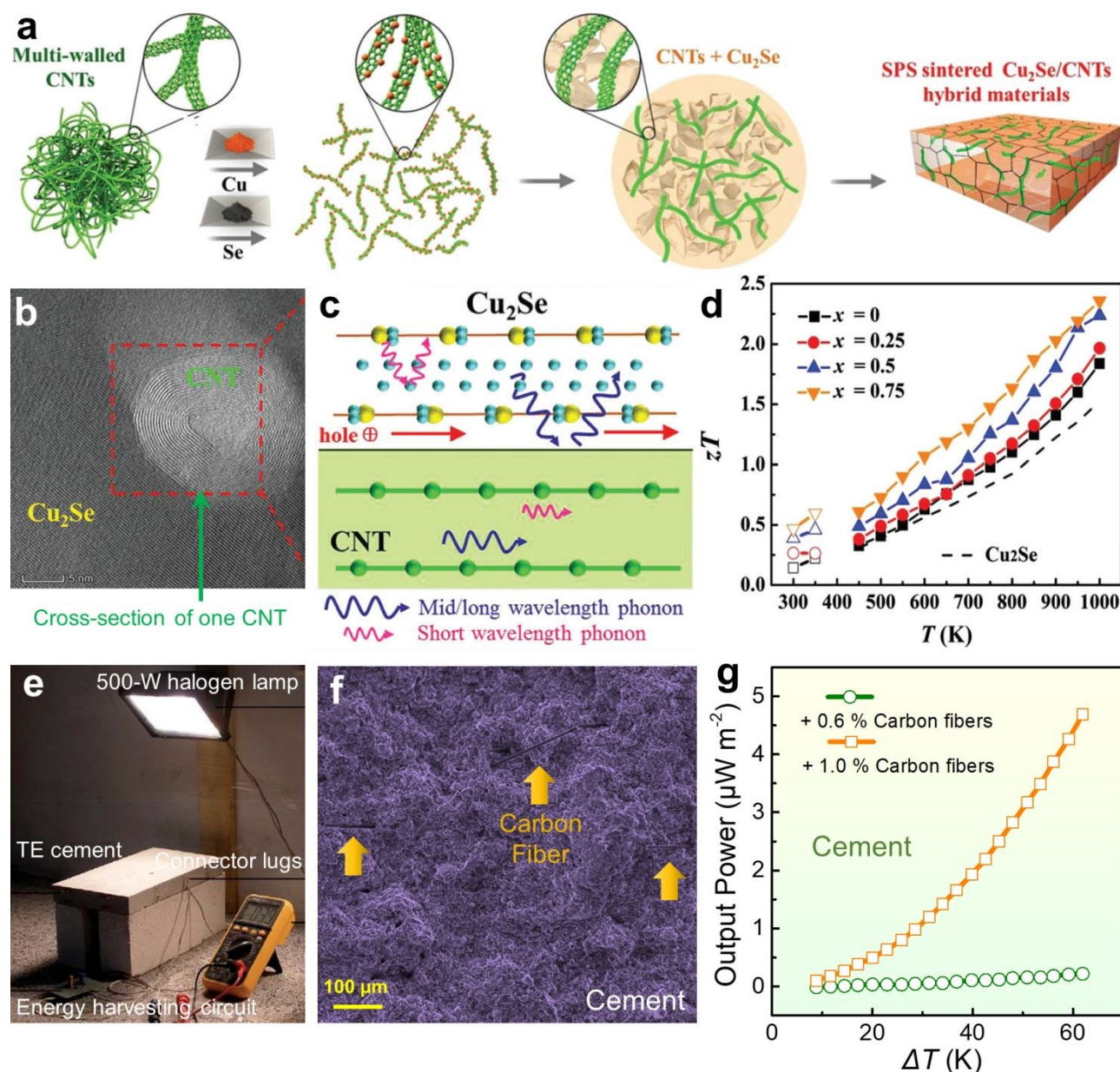


Figure 6. (a) The illustration of fabricating Cu₂Se/CNT hybrid materials. (b) Spherical aberration corrected scanning transmission electron microscope (Cs-corrected STEM) image of Cu₂Se with 0.75 wt% CNT. (c) Electrical transportation and phonon scattering in Cu₂Se/CNT hybrid materials. (d) T -dependent ZT of Cu₂Se/CNT hybrid materials. Reproduced with permission.¹⁸ Copyright 2017, Royal Society of Chemistry. (e) The investigation of the energy harvesting behavior of carbon fiber reinforced cement composites (CFRC) under solar irradiation simulated by a 500W halogen lamp. (f) SEM image of the CFRC specimens. (g) ΔT -dependent output power density of CFRC with different carbon fiber contents. Reproduced with permission.¹⁹ Copyright 2014, Royal Society of Chemistry.

3 Organic Thermoelectric Fibers

In order to realize high flexibility in inorganic-material-based thermoelectric device, one conventional method is to introduce

flexible substrate, such as fabric and polyimide.²⁸⁷⁻²⁹⁰ Although the as-fabricated thermoelectric devices possess good thermoelectric performance, there are still some considerable shortages, such as the high cost, high toxicity, complex fabrication, and poor flexibility. It was pointed out that during

the fabrication and usage of inorganic-material-based thermoelectric devices, the inorganic parts may cause serious damage to the mechanical properties and wearability of the flexible substrates. Therefore, the design of organic-material-based thermoelectric devices is developed.²⁹¹ Because organic thermoelectric materials possess much higher flexibility, they can better adhere to the skin, maximizing ΔT between human body and environment and in turn, improving the thermoelectric conversion efficiency. As a result, organic thermoelectric materials gain significant attention in recent years.²⁹²

Currently, the commonly used organic materials that target thermoelectric applications include polyacetylene (PA),²⁹³ polythiophenes (PTs),²⁹⁴ polypyrrole (PPy),¹⁰⁴ polyaniline (PANI),²⁹⁵ poly(3-hexylthiophene) (P3HT),²⁹⁶ and poly(3,4-ethylenedioxythiophene) polystyrene sulfonate (PEDOT:PSS).^{52, 297} These materials possess some common characteristics, such as low fabrication cost, light weight, good flexibility, good ductility, and intrinsic low κ .²⁹² However, it should be noted that there are still some issues in the thermoelectric applications of organic polymers. For example, PA are not stable in the air, which limits its practical application.²⁹⁸ P3HT has a high S in the undoped state, but it is easy to cause other disordered structures during the fabrication, which affects the stability of σ .²⁸⁷ Although PANI and other polymers have high stability in the environment, their σ is low, and the improvement of their ZT value is still tricky.²⁹⁹ In terms of the PEDOT:PSS, due to its water solubility, good flexibility, easy fabrication, and promising thermoelectric properties, PEDOT:PSS has attracted significant attention in recent decades.^{52, 297} At present, there are two main methods to improve the thermoelectric performance of PEDOT:PSS: one is to rationally dope it by post-treatment with acid, alkali, organic solvent, etc.,⁵² and the other is to compound it with inorganic nano-materials such as CNTs and nanosized semiconductors.⁶⁰ However, although the ZT of PEDOT:PSS has been significantly improved up to ~ 0.75 by ion accumulation on its surface,³⁰⁰ it is still not competitive enough compared to that of inorganic thermoelectric materials. Therefore, developing lower-dimensional organic thermoelectric materials such as organic thermoelectric fibers is an alternative.³⁰¹

3.1 1D Organic Thermoelectric Fibers

For conventional organic thermoelectric materials, it is recognized that increased structural order and molecular organization (such as increased chain alignment) can lead to simultaneous increase of S and σ (derived from the improved mobility μ)^{302, 303}, leading to a high $S^2\sigma$.³⁰⁴ However, ordered structures in conducting polymers may also result in high κ , due to their single-crystalline-like features, and one typical case is the ultra-drawn single-crystal polyethylene (PE) with a high κ , of $104 \text{ W m}^{-1} \text{ K}^{-1}$.³⁰⁵ In this situation, a rationally designed structure is required to balance the electrical and thermal transportation and achieve high thermoelectric performance in conventional organic thermoelectric materials, as illustrated in **Figure 7(a)**.³⁰⁶ In addition to a rationally designed structure, another promising way to achieve high thermoelectric performance is to rationally

design chain-oriented polymeric fibers, which can realize both increased chain alignment and some extents of structural disorder, as illustrated in **Figure 7(b)**.³⁰⁶ Similar to the mechanism of inorganic thermoelectric fibers, assuming that the mean free paths of phonons and charge carriers are separated in length scales, if chain lengths are shorter than the mean free path of phonons but longer than that of charge carriers, κ can be considerably reduced due to the strengthened phonon scattering at boundaries, while σ may not be influenced to a great extent,³⁰⁶ as illustrated in **Figure 7(c)**. Calculations based on molecular dynamics simulations indicated that a significant reduction of axial κ ($0.97 \text{ W m}^{-1} \text{ K}^{-1}$) could be observed in chain-orientated PEDOT fibers with a relative molecular weight of 5600 and a crystallinity of 0.49, leading to a high ZT of 0.48 at 298 K,³⁰⁶ which is much higher than that of conventional PEDOT ($ZT = 0.22$).³⁰⁷ Therefore, organic thermoelectric fiber has been treated as one of the key members in the family of organic thermoelectric materials.

Till now, fiber-based organic thermoelectric polymers are developing fast based on conventional conducting polymers, such as PANI fibers³⁰⁸ and PEDOT:PSS fibers.²⁰ **Figure 7(d)** shows a SEM image of PEDOT:PSS fibers after ethylene glycol (EG) post-treatment.⁵⁴ The width of the as-fabricated fiber is $\sim 140 \mu\text{m}$. By post-treatment with EG and dimethyl sulfoxide, the σ could be significantly improved by $\sim 200\%$ and the S was only slightly reduced by 5%, leading to a $S^2\sigma$ of $\sim 4.75 \mu\text{W m}^{-1} \text{ K}^{-2}$.⁵⁴ **Figure 7(e)** shows a schematic diagram of PEDOT:PSS-based thermoelectric device and its output voltage and power density.⁵⁴ The p-n legs consist of EG-treated p-type PEDOT:PSS fibers and n-type CNT fibers, which were connected in series and linked by Ag paste.⁵⁴ By a ΔT of $\sim 60 \text{ K}$, an output voltage of 20.7 mV and a power density of $481.2 \mu\text{W cm}^{-2}$ could be achieved.⁵⁴ Another typical case is the wet-spun PEDOT:PSS fibers, as shown in **Figure 7(f)**.⁸⁵ After the H_2SO_4 -treatment, the chain packing order of the as-fabricated PEDOT:PSS fibers was significantly improved, confirmed by their wide angle X-ray scattering (WAXS) results shown in **Figure 7(g)**.⁸⁵ As can be seen, the amorphous halo of the randomly distributed PSS with a broad peak located at $q_z = 1.16 \text{ \AA}^{-1}$ is not clearly observed in the WAXS pattern, indicating the reduction of PSS by the H_2SO_4 -treatment; instead, the π -stacking between adjacent PEDOT chains with a peak at $q_z = 1.75 \text{ \AA}^{-1}$ is widely observed, indicating the improvement of chain alignment.⁸⁵ As a result, an optimized $S^2\sigma$ of $147.8 \mu\text{W m}^{-1} \text{ K}^{-2}$ could be realized, benefited from a high σ of 4029.5 S cm^{-1} and a S of $19.2 \mu\text{V K}^{-1}$ at 300 K.⁸⁵ Besides, even at a knotted state, there is no degradation in their measured thermoelectric properties, indicating outstanding mechanical flexibility and robustness.⁸⁵ **Figure 7(h)** show earmuffs with embedded PEDOT:PSS fiber-based thermoelectric generators as a wearable device and their performance.⁸⁵ PEDOT:PSS fibers and Ni wires acted as the p- and n-legs, and 5 pairs of the p-n legs were serially connected. The joints between PEDOT:PSS fibers and Ni wires were connected using Ag paste. By a ΔT of $9.1 \text{ }^\circ\text{C}$ between the human body and the environment, an output voltage of 1.9 mV and a maximum output power density of $\sim 0.273 \mu\text{W cm}^{-2}$ were simultaneously achieved.⁸⁵ Other works reported a self-powered flexible sensor based on the

wet-spun hollow PEDOT:PSS fibers.²⁰ A ΔT of 6 °C by touching fingers on the sensors could result in an output voltage of 404 μV .²⁰

View Article Online
DOI: 10.1039/D0EE03520C

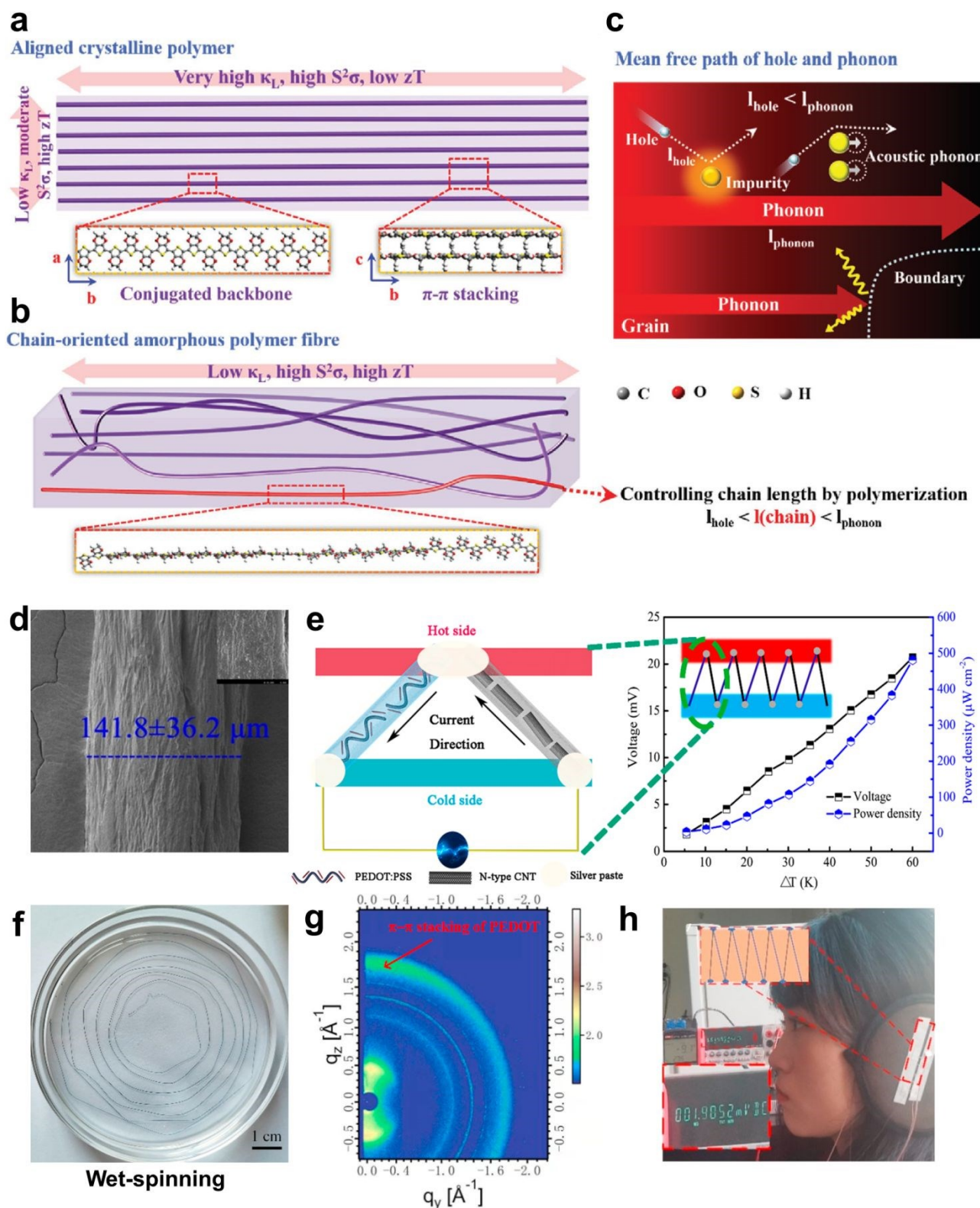


Figure 7. The illustration of thermal and electrical transportation in (a) crystalline polymers and (b) chain-oriented polymeric fibers. (c) Hole and phonon transport in chain-oriented polymeric fibers. Reproduced with permission.³⁰⁶ Copyright 2017, Wiley. (d) SEM image of poly(3,4-ethylenedioxythiophene):poly(styrenesulfonate) (PEDOT:PSS) fibers after ethylene glycol (EG) posttreatment. (e) Schematic diagram of PEDOT:PSS-based thermoelectric device and its output voltage and power density. Reproduced with

permission.⁵⁴ Copyright 2018, American Chemical Society. (f) Optical image of a continuous wet-spun PEDOT:PSS fiber in the coagulation bath. (g) Wide angle X-ray scattering (WAXS) pattern of H₂SO₄-treated PEDOT:PSS fibers. (h) Earmuffs with embedded PEDOT:PSS fiber-based thermoelectric generators as a wearable device and their performance. Reproduced with permission.⁸⁵ Copyright 2020, Elsevier.

In addition to PEDOT:PSS fibers, other organic-polymer-based thermoelectric fibers were also developed. For example, conducting PANI fibers with a submicron morphology were designed by doping with camphorsulfonic acid (CSA).³⁰⁹ Compared to the conventional PANI, the $S^2\sigma$ of as-designed PANI fibers improved by 20 times with a value of $\sim 1.1 \mu\text{W m}^{-1} \text{K}^{-2}$ at 300 K.³⁰⁹ Similarly, PANI nanotubes were fabricated by an aqueous solution method without template, doped by β -naphthalene sulfonic acid (NSA).³¹⁰ By an aniline/NSA ratio of 4:1, the as-prepared PANI nanotube showed a high S of $212.4 \mu\text{V K}^{-1}$, an improved σ of 0.0077 S cm^{-1} , and a lowered κ of $0.21 \text{ W m}^{-1} \text{K}^{-1}$ at 300 K.³¹⁰ Besides, PANI NWs, fabricated by a soft template method and doped by *p*-toluenesulfonic acid (*p*-TSA), showed a ZT of 2.75×10^{-5} at 320 K,¹⁵¹ resulted from the low κ of $0.32 \text{ W m}^{-1} \text{K}^{-1}$ at this temperature. For PEDOT, by electropolymerizing 3,4-ethylenedioxythiophene (EDOT) in aqueous LiClO₄, PEDOT NWs were fabricated based on a template method, which can be described as a lithographically patterned nanowire electrodeposition (LPNE) process.¹⁰⁵ The as-fabricated PEDOT NWs arrays with 750 NWs were reported to exhibit a high absolute S of $122 \mu\text{V K}^{-1}$ at 310 K.¹⁰⁵ Similarly, PEDOT NWs could be achieved by chemical oxidation polymerization in reverse microemulsions with sodium bis(2-ethylhexyl) sulfosuccinate (AOT) as the surfactant,¹⁰⁶ which exhibits a σ of 71.4 S cm^{-1} and a S of $48.0 \mu\text{V K}^{-1}$, leading to a competitive $S^2\sigma$ of $\sim 16.5 \mu\text{W m}^{-1} \text{K}^{-2}$ at 300 K.¹⁰⁶ Besides, freestanding PEDOT NWs can be synthesized by template-confined *in situ* polymerization.¹⁰⁷ After introducing 0.2 wt% PEDOT NWs in poly-(3,4-ethylenedioxythiophene):tosylate (PEDOT:Tos) to form nanocomposites, a high $S^2\sigma$ of $446.6 \mu\text{W m}^{-1} \text{K}^{-2}$ and a high ZT of 0.44 were obtained at room temperature.¹⁰⁷ The thermoelectric devices based on PEDOT NWs/PEDOT hybrid as *p*-type legs and nitrogen-doped graphene as *n*-type legs exhibited a normalized output power of $\sim 0.05 \mu\text{W cm}^{-2}$ under a temperature different of $10.1 \text{ }^\circ\text{C}$.¹⁰⁷ In terms of PPy, PPy nanotubes and NWs were fabricated by a chemical oxidative polymerization method.¹⁰⁸ The as-prepared PPy NWs exhibited a higher $S^2\sigma$ of $\sim 0.3 \mu\text{W m}^{-1} \text{K}^{-2}$ at 380 K, which was higher than the as-prepared PPy nanotubes ($S^2\sigma$ of $< 0.075 \mu\text{W m}^{-1} \text{K}^{-2}$ at 380 K) due to the confinement effect that simultaneously improved S and σ .¹⁰⁸

3.2 2D Organic-fiber-based Films

In order to expand the application and further improve the performance, 1D organic thermoelectric fibers can be made into two 2D organic thermoelectric films through various fabrication techniques. In terms of the design rule of organic-fiber-based films, one of the key points is to realize well-aligned chain order (strengthen the orientation or anisotropy) in the as-fabricated films to realize higher performance along specific directions, which is similar to the 1D organic thermoelectric

fibers. In fact, such a strategy that based on the anisotropy strengthening was commonly used in some polycrystalline thermoelectric materials with intrinsic anisotropy, such as SnSe,^{197-199, 311-314} Cu₂Se,^{247, 315, 316} and Bi₂Te₃.^{155, 157} **Figure 8(a)** illustrates the fabrication of small molecule 1,3,5-trichlorobenzene (TCB)-treated P3HT film.⁸⁸ The undoped P3HT film covered by TCB powder was first heated to $75 \text{ }^\circ\text{C}$, and then rapidly cooled from one side to the other to room temperature. A large temperature gradient could be achieved by the fast cooling, which solidified TCB as fiber-like crystals along the temperature gradient. At the same time, because of the strong π - π conjugated interactions between the thiophene and benzene rings, the P3HT could solidify on the TCB surface with polymer chains locking into the lattice of TCB, resulting in orientated P3HT and crystalline TCB fibers, as illustrated by **Figure 8(b)**.⁸⁸ Orientated P3HT film was achieved by removing TCB.⁸⁸ To verify the anisotropy of as-fabricated film, various characterizations were investigated. **Figure 8(c)** shows a two-dimensional-grazing incidence X-ray diffraction (2D-GIXRD) pattern of TCB-treated P3HT film,⁸⁸ and **Figure 8(d)** shows corresponding 1D diffraction profile.⁸⁸ Here q_z indicates the out-of-plane direction, and q_{xy} indicates the in-plane direction. It is clearly seen that a strong (010) π - π stacking peak at $\sim 3.8 \text{ \AA}$ and (h00) peaks along both the q_z and q_{xy} could be observed, indicating highly orientated crystallites in the film, which is ascribed to the mutual orientation of polymer backbones on both crystal surfaces along the *c* axis of TCB crystals during the crystallization process by fast cooling. Benefited from the strong anisotropy, the as-fabricated P3HT film exhibited a high room-temperature $S^2\sigma$ of $\sim 37.5 \mu\text{W m}^{-1} \text{K}^{-2}$ along the parallel direction, which was much higher than value along the parallel direction ($\sim 12.5 \mu\text{W m}^{-1} \text{K}^{-2}$) and the conventional drop-casted P3HT film with a much weaker anisotropy ($\sim 15 \mu\text{W m}^{-1} \text{K}^{-2}$), as shown in **Figure 8(e)**.⁸⁸ Such a high $S^2\sigma$ mainly resulted from the carrier hopping conduction between two ordered regions, which follows the quasi-1D hopping model as illustrated by the inset in **Figure 8(e)**.⁸⁸ Furthermore, a peak $S^2\sigma$ of $\sim 62.4 \mu\text{W m}^{-1} \text{K}^{-2}$ at 365 K could be achieved in TCB-treated P3HT film along the parallel direction,⁸⁸ indicating great potential for applying to flexible thermoelectric devices. In addition to P3HT films, other organic-fiber-based thermoelectric films were also developed. It was reported that ultrathin PEDOT NWs-based films were fabricated by filtering and drying PEDOT NWs/methanol mixture solution, which exhibited a high σ of $\sim 540 \text{ S cm}^{-1}$, an enhanced S of $\sim 28 \mu\text{V K}^{-1}$, and a high $S^2\sigma$ of $\sim 35.8 \mu\text{W m}^{-1} \text{K}^{-2}$ by a 5 min hydrazine treatment.⁸⁷ Besides, free-standing PPy nanotube films were prepared by a template method, which showed a ZT is 7.84×10^{-4} at 370 K.⁸⁶

Currently, the highly orientated organic films have been preliminarily applied in thermoelectric devices to evaluate their thermoelectric potential. **Figure 8(f)** shows an optical image of printed PEDOT:PSS film on polyimide substrate.⁵³ As shown by

the inset SEM image, the as-fabricated PEDOT:PSS film possesses a highly orientation along the in-plane direction, which was mainly derived from the treatment by EG, H₂SO₄, and tetrakis(dimethylamino)ethylene (TDAE). The pre-treatment by EG led to sufficient elimination of excess non-ionized PSS, and created a clear path for the further H₂SO₄ post-treatment, which induced a structural conformation transition of the conjugated carbon chains in PEDOT:PSS films, resulting in a highly ordered morphology.⁵² Furthermore, the post-treatment by TDAE tuned the oxidation level of the as-fabricated PEDOT:PSS films, contributing to a high $S^2\sigma$ of $\sim 224 \mu\text{W m}^{-1} \text{K}^{-2}$ at 300 K.⁵³ **Figure 8(g)** describes the F-TEGs based on these PEDOT:PSS films.⁵³ To fabricate the F-TEG, 5 free-standing EG-

H₂SO₄-TDAE-treated PEDOT:PSS films were stuck to form one thermoelectric element using conductive Ag paste, and 5 thermoelectric legs interlace through a layer of flexible polyimide substrate to keep a flexible feature of the TEG.⁵³ Each pair of legs were connected by Cu wire,⁵³ and the as-treated PEDOT:PSS films were underneath the black films, which represent the solar energy absorbers.⁵³ By a ΔT of 44.5 K induced by harvesting sunlight, a high output power density of $3 \mu\text{W cm}^{-2}$ could be achieved, as shown in **Figure 8(g)**.⁵³ These results indicate that by efficient sunlight-to-electricity conversion, the as-designed thermoelectric module can be potentially used to power microwatt electronic products.

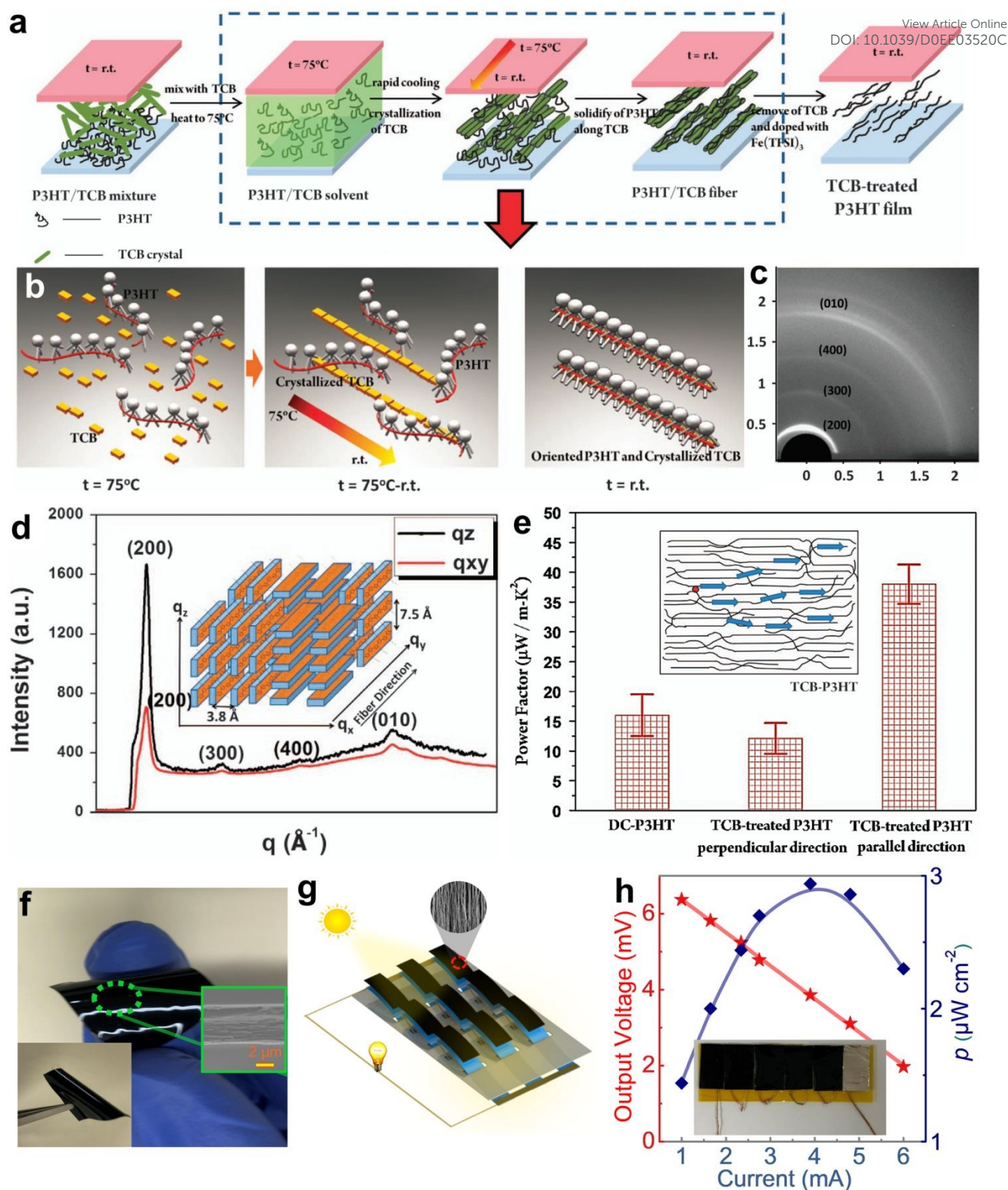


Figure 8. (a) Illustrations of fabricating small molecule 1,3,5-trichlorobenzene (TCB)-treated poly(3-hexylthiophene) (P3HT) film. (b) Realization of orientated P3HT and crystallized TCB fibers by controlling temperature. (c) Two-dimensional-grazing incidence X-ray diffraction (2D-GIXRD) pattern of TCB-treated P3HT film. (d) Corresponding 1D diffraction profile, here q_z indicates the out-of-plane direction and q_{xy} indicates the in-plane direction. (e) Comparison of $S^2\sigma$ of conventional drop-casted (DC) P3HT film and TCB-treated P3HT film along different directions. The inset illustrates the path-way of the quasi-1D model. Reproduced under a Creative Commons Attribution 4.0 International License.⁸⁸ Copyright 2016, Springer Nature. (f) Optical image of printed PEDOT:PSS

film on polyimide substrate. The inset is a corresponding SEM image. (g) F-TEGs based on PEDOT:PSS films. (h) Output power density and voltage. Reproduced with permission.⁵³ Copyright 2020, Royal Society of Chemistry. DOI: 10.1039/D0EE03520C

In addition to the orientated organic films discussed above, there were also other types of 2D organic thermoelectric materials based on 1D organic fibers, such as thermoelectric networks and mats. It was reported that P3HT nanofiber networks were fabricated by a combination of oxidative chemical polymerization (synthesize P3HT), Whisker method (form nanofibers from the bulk polymer),^{317, 318} and drop-casting on plastic substrates (form networks).⁸⁹ A ZT of ~ 0.0026 was obtained at 300 K, derived from rationally doping by silver perchlorate, which tuned the oxidation level of the networks.⁸⁹ Similarly, through building bulk interpenetrating networks of conjugated poly(3-butylthiophene)/polystyrene (P3BT/PS) polymers in insulating supporting matrix, a ZT of 0.8×10^{-4} could be achieved at room temperature when 40 wt.% P3BT was introduced, mainly derived from a reduced κ and an enhanced σ .¹⁰⁹ Besides, by a combination of aqueous solution and drop-casting method, P3HT nanofiber mat with high crystallinity was fabricated, which exhibited an ultralow κ of only $\sim 0.07 \text{ W m}^{-1} \text{ K}^{-1}$ at 300 K.⁹⁰

4 Inorganic/Organic Hybrid Fibers

Compared with rigid inorganic thermoelectric fibers, organic thermoelectric fibers and organic-fiber-based thermoelectric films have exhibited outstanding flexibility and high cost-effectiveness, making them good candidates to be employed in wearable thermoelectric devices for personal use, but their thermoelectric properties are still relatively low and need further improvement, as shown in **Figure 2**. To simultaneously achieve high performance and flexibility, one feasible solution is to design inorganic/organic hybrid fibers and hybrid-fiber-based films. Generally, such unique hybrid fibers can be fabricated by incorporating nanoscale inorganic materials into conductive polymer matrix, which exhibits a typical 1D feature; while the hybrid-fiber-based films were typical 2D materials. Currently, the mechanism of the enhancement in thermoelectric performance by combining organic and inorganic materials is still under debate, derived from the considerable difficulty in proving the underlying physics. First-principle calculations indicated that both polymer morphology and interfacial charge transfer dominate over energy-dependent scattering in organic-inorganic hybrid thermoelectrics.³¹⁹

So far, two major inorganic materials have been successfully incorporated into the polymer matrix, namely the carbon-based nanomaterials (such as CNTs and graphene fibers),^{56, 61, 110} and semiconductor-based nanomaterials (such as Te nanorods and Bi_2Te_3 NWs).^{60, 111} CNTs have been widely regarded as one of the most effective fillers in polymer matrix,^{56, 60, 110} derived from their large aspect ratio (leading to high σ) and relatively high S realized by rationally doping. In the polymer matrix, CNTs are connected by van der Waals forces. Because there are conducting polymer particles at CNT junctions, their molecular

vibration spectrum does not match that of the CNTs, which hinders the transmission of phonons at the junctions and in turn, reduce κ . In contrast, these junctions provide a continuous tunnel for electron transports without obvious obstructions, leading to high σ . Such a decoupling effect enables CNTs exhibiting high σ and S when CNTs were used as fillers in conducting polymer, while κ remains relatively stable. In terms of semiconductor-based nanomaterials such as NWs and nanotubes, because of their high $S^2\sigma$ (especially for their high S since S of conducting polymers are relatively low) and strong organic solubility at room temperature,²⁸⁷ it is effective to mix these nanomaterials with polymer matrix to improve $S^2\sigma$. Besides, κ of these composite materials is always low, which is even comparable to that of organic polymers. This is because the bonding and vibrational spectra between organic and inorganic materials are completely different. Therefore, developing inorganic/organic hybrid fibers and hybrid-fiber-based films are promising and of significance for practical application.

4.1 1D Hybrid Fibers

There are several ways to realize 1D inorganic/organic hybrid fibers.³²⁰ SWCNT/poly(vinylidene fluoride) (PVDF) composite fibers were fabricated by a wet-spinning method.⁷² By doping SWCNTs with PEI, the p-type composite fibers could be made into n-type,⁷² and $S^2\sigma$ of ~ 378 and $\sim 289 \mu\text{W m}^{-1} \text{ K}^{-2}$ were achieved in the as-fabricated p- and n-type fibers.⁷² Furthermore, a F-TEG that consisted of 12 pairs of p- and n-type composite fibers exhibited an output power of $0.61 \mu\text{W}$ by a ΔT of 10 K.⁷² In addition to doping inorganic fibers, post-treatments were also used to make the p-type composite fibers into n-type. By a conventional wet-spinning process, CNT/PEDOT:PSS composite fibers were fabricated.⁵⁶ Post-treatments including immersion in hydrazine solutions and PEI-infiltration were employed to make the p-type composite fibers into n-type, and $S^2\sigma$ of ~ 83.2 and $\sim 113 \mu\text{W m}^{-1} \text{ K}^{-2}$ were achieved in the p- and n-type fibers.⁵⁶ By assembling 12 pairs of p- and n-type fibers into a F-TEG, a ΔT of 10 K could contribute to an output power of $0.43 \mu\text{W}$.⁵⁶

In addition to fabricating simple F-TEGs discussed above, 1D inorganic/organic hybrid fibers can be further assembled into 3D wearable textiles for powering electronics by harvesting thermal energy from human body.³²⁰ **Figure 9(a)** illustrates a fabrication of thermoelectric textiles with n-type PEI/CNTY and p-type PEDOT:PSS/CNTY.²¹ The CNTY was first wrapped on a polyethylene terephthalate (PET) plate. After that, the CNTY/PET roll was soaked into PEDOT:PSS solution to form one side into p-type, and the other side is soaked into PEI/ethanol solution to become n-type. Finally, the as-fabricated p-n composite fibers were twisted with a PET filament, forming thermoelectric yarns. **Figure 9(b)** illustrates warp-knitted spacer fabric shaped thermoelectric textiles.²¹ The as-fabricated thermoelectric textiles possess 966 p-n pairs with high

flexibility and excellent air permeability, which are ideal candidates for assembling wearable F-TEGs that signify their good conformability with human skin.²¹ The as-designed F-TEGs can be bent, twisted, and compressed arbitrarily without deteriorating their thermoelectric performance.²¹ **Figure 9(c)** shows the thermoelectric output power density and output voltage of the as-designed F-TEGs, from which a high output power density of $5.15 \mu\text{W cm}^{-2}$ can be achieved at a ΔT of 47.5 K.²¹

In addition to the immersion method discussed above, deposition is another suitable way to realize thermoelectric textiles based on inorganic/organic hybrid fibers. **Figure 9(d)** illustrates a fabrication of thermoelectric yarn by depositing inorganic thermoelectric materials on an electro-spun PAN nanofiber sheet.⁶⁹ Flexible sheets composed of highly aligned PAN nanofibers were first fabricated by an extrusion process. After that, the as-fabricated nanofiber sheets were sequentially sputtered by Sb_2Te_3 -gold- Bi_2Te_3 on both sides by a stencil-mask-based method, resulting in alternating p-Au-n segments. Finally, sheets were twisted by an electric motor to form a tiger yarn with a $(\text{Au}/\text{Bi}_2\text{Te}_3/\text{Au}/\text{Sb}_2\text{Te}_3)_n$ structure, as shown in **Figure 9(e)**.⁶⁹ Based on these unique tiger yarns, plain-weave thermoelectric textiles were fabricated, as shown in **Figure**

9(f).⁶⁹ The as-designed textiles exhibit an output power density of $856 \mu\text{W cm}^{-2}$ at a ΔT of 200 K in the direction of textile thickness.⁶⁹

Similar to the deposition method, painting or printing are also feasible ways to fabricate hybrid-fiber-based thermoelectric textiles. **Figure 9(g)** illustrates the fabrication of wet-spun PEDOT:PSS/Te NW composite fibers.⁶⁴ As-fabricated fibers were first placed in a coagulation bath, and then twisted with a polymer rod that provides structural stability and mechanical support. **Figure 9(h)** illustrates the fabrication of thermoelectric fibers by periodically coating with Ag paste.⁶⁴ The coated parts act as n-type segments and the uncoated parts are p-type. The as-designed p-n fibers are woven and integrated into the fabric for wearable thermoelectric application, as shown in **Figure 9(i)**.⁶⁴ The thermoelectric fabric exhibited a high $S^2\sigma$ of $\sim 78.1 \mu\text{W m}^{-1} \text{K}^{-2}$.⁶⁴ Besides, the fibers with a Te NW content of <30 wt % exhibited good bending performance, and a measured stress value of $\sim 135 \text{ MPa}$ could be achieved at an applied strain of $\sim 7\%$, indicating good mechanical property.⁶⁴ In terms of the F-TEG based on such advanced hybrid fibers, a thermoelectric fabric was assembled by weaving the fibers into a commercial textile, which exhibited a high mass-specific power of $9.48 \mu\text{W g}^{-1}$.⁶⁴

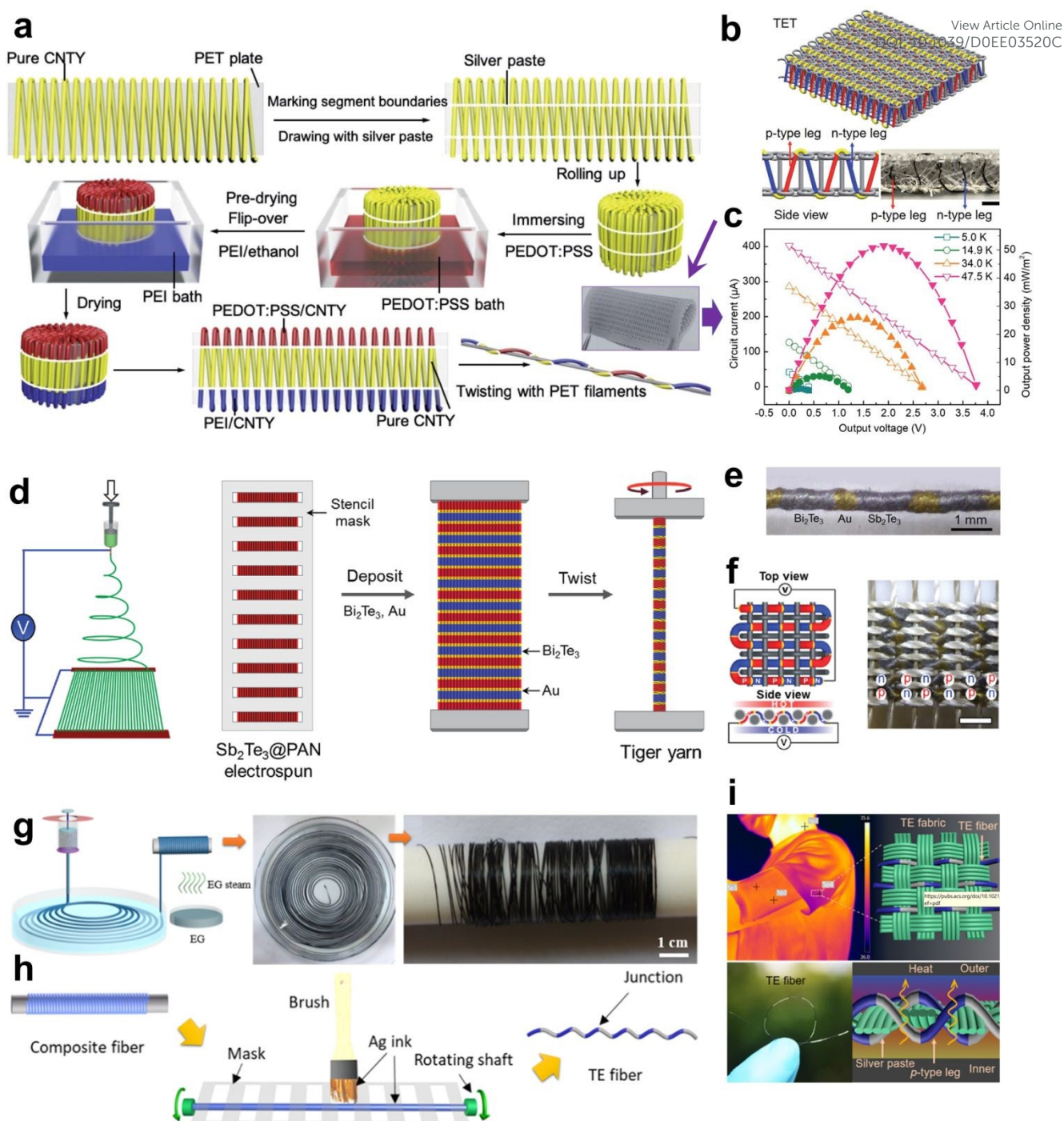


Figure 9. (a) The illustration of fabricating thermoelectric textiles with n-type PEI/CNTY and p-type PEDOT:PSS/CNTY. (b) The illustration of warp-knitted spacer fabric shaped thermoelectric textiles. (c) The thermoelectric output power density and output voltage. Reproduced with permission.²¹ Copyright 2020, Royal Society of Chemistry. (d) Schematic diagram of fabricating thermoelectric yarn by depositing inorganic thermoelectric materials on electro-spun PAN nanofiber sheets. (e) Optical image of the tiger yarn with the $(\text{Au}/\text{Bi}_2\text{Te}_3/\text{Au}/\text{Sb}_2\text{Te}_3)_n$ structure. (f) The plain-weave thermoelectric textiles. Reproduced with permission.⁶⁹ Copyright 2016, Wiley. (g) Illustration of fabricating wet-spun PEDOT:PSS/Te NWs composite fibers. (h) Illustration of fabricating thermoelectric fibers by periodically coating with Ag paste. (i) The as-designed fibers are woven and integrated into the fabric for wearable thermoelectric application. Reproduced with permission.⁶⁴ Copyright 2020, American Chemical Society.

4.2 2D Hybrid-fiber-based Films

In addition to directly apply the inorganic/organic hybrid fibers in flexible F-TEGs, hybrid fibers can also be assembled into 2D

composite films by various fabrication techniques to expand their application and further improve their performance.³²⁰ Theoretically, there are mainly two ways to achieve such composite films: one is doping and/or post-treating the

inorganic-fiber-based sheets/nets/films by organic solutions, from which the inorganic part acts as substrate and provides the flexibility; and the other is incorporating inorganic fibers as fillers into conductive polymer matrix,²⁸⁷ from which the organic part acts as substrate and provides the flexibility. However, for most of hybrid-fiber-based composite films, both organic and inorganic parts provide the flexibility and thermoelectric performance, therefore they always show high flexibility and high properties. The inorganic part includes carbon-based fibers such as CNTs,^{60, 61, 66, 67, 70, 71, 73, 75, 76, 91-94, 146, 321} graphene,^{146, 322} reduced graphene oxide (rGO),⁹⁵ semiconductor-based fibers such as Te NWs,^{68, 96} Cu_{1.75}Te NWs,⁶⁵ Bi₂Te₃ NWs,¹²⁵ and oxide-based fibers such as BaTiO₃,^{323, 324} while the organic part includes epoxy,^{40, 59, 147, 321, 325, 326} 68, 146, PPy,⁹³⁻⁹⁵ PEDOT,⁹⁶ PEDOT:PSS,^{60, 61, 68, 70, 75} PAN,³²⁷ PANI,^{66, 71, 73, 76, 92, 322} P3HT,^{66, 91} poly(3-octylthiophene) (P3OT),⁵⁷ PVDF,⁶⁵ polyurethane/poly(methyl methacrylate) (PU/PMMA),^{323, 324} waterborne polyurethane (WPU),⁶¹ and poly[2-methoxy-5-(2-ethylhexyloxy)-1,4-phenylenevinylene] (MEH-PPV).⁶⁷

Doping and/or post-treating the inorganic-fiber-based sheets/nets/films by organic solutions is a suitable way to achieve free-standing hybrid-fiber-based composite materials, from which the inorganic fibers acts as substrate and provides the flexibility. **Figure 10(a)** illustrates a fabrication of Au-doped CNT/polymer web.⁶⁶ By a direct spinning method, CNT networks with both high σ and high μ were first fabricated, and the introduction of Au nanoparticles further improved the ZT of CNT networks from 0.079 to 0.163 at room temperature. Based on such Au-doped CNT webs, the introduction of PANI enabled the webs being porous hybrids with a significantly improved flexibility, as shown in the SEM images in **Figure 10(b)**.⁶⁶ Benefited from the incorporation of PANI, the triggered energy-filtering effect significantly improved the S of the webs, and the phonon-scattering effect simultaneously reduced κ , leading to a further improved ZT of 0.203.⁶⁶ In terms of the F-TEG, the thermoelectric module was composed of Au-doped CNT/PANI webs as p-type materials and polyethyleneimine-doped CNT webs as n-type materials, and both type webs were alternatively attached on flexible plastic substrates by a wet transfer method.⁶⁶ The webs were electrically connected by Ag paste through dispensing equipment.⁶⁶ **Figure 10(c)** shows the output power and voltage of the as-fabricated F-TEG,⁶⁶ from which the F-TEG with 7 p-n couples could result in an output power of 1.74 μW at a ΔT of 20 K. Other works indicated that SWCNT/PEDOT:PSS-coated Te nanorod composite films were fabricated by using a vacuum filtration method.⁶⁰ The as-fabricated films exhibited a $S^2\sigma$ of 104 $\mu\text{W m}^{-1} \text{K}^{-2}$, derived from a high σ of 332 S cm^{-1} and a S of 56 $\mu\text{V K}^{-1}$.⁶⁰ A F-TEG based on these composite films was designed and show an output voltage of 5.6 mV and an output power of 53.6 nW at a ΔT of 44 K.⁶⁰

Incorporating inorganic fibers as fillers into conductive polymer matrix is another suitable way to achieve hybrid-fiber-based composite materials,²⁸⁷ from which the organic part acts as substrate and provides the flexibility. **Figure 10(d)** illustrates the fabrication of PEDOT:PSS/Te NW aerogel composite film by a combination of vacuum freeze drying and dimethyl sulfoxide (DMSO) vapor annealing treatment.⁶⁸ By a vacuum freeze drying method, porous 3D crosslinking PEDOT:PSS aerogel networks with hydrothermally synthesized Te NWs as fillers were first fabricated, and a followed pressing process made these networks into films. After that, a DMSO vapor annealing treatment was applied to these hybrids, which could further optimize their thermoelectric properties. In the as-fabricated aerogel films, there are two potential charge carrier-transport mechanisms that are responsible for the electrical transportation, which can be described by the series and parallel, as shown in **Figure 10(e-f)**.⁶⁸ Such unique aerogel films exhibited a ZT of 0.02 at room temperature. Besides, during the reciprocating bended process from 0 to 180°, the σ of PEDOT:PSS aerogel films did not change significantly while the S only presents a small increase during bending, indicating good flexibility and performance stability.⁶⁸ Furthermore, a F-TEG was assembled by alternately connecting p-type PEDOT:PSS-based aerogel films and n-type CNT fibers in series, and the connections were linked by the Ag paste.⁶⁸ the as-designed F-TEG based on these aerogel films showed an output power of 1.28 μW at a ΔT of 60 K, indicating potentials to be applied in wearable electronics.⁶⁸ Similar aerogels based on graphene and multi-walled carbon nanotube (MWCNT) nanocomposites were also reported with an ultralow κ of $\sim 0.056 \text{ W m}^{-1} \text{K}^{-1}$, which resulted in a ZT of ~ 0.001 at room temperature.¹⁴⁶

Sometimes, both organic fibers and inorganic fibers were rationally mixed to form composite-fiber-based films. In this situation, both the organic fibers and inorganic fibers act as substrates and provide the flexibility. **Figure 10(g)** illustrates the fabrication of PEDOT/Te NW composite film by a combination of aqueous solution and vacuum filtering.⁹⁶ The synthesis of PEDOT NWs was based on a typical aqueous solution method, from which DMSO was added into PEDOT NW solution to improve their dispersion. After that, PEDOT NW solution was mixed with Te NW solution by ultrasonication, and a typical composite film could be achieved by a combination of vacuum filtering and drying. **Figure 10(h)** shows a SEM image of the composite film with 70 wt % Te NWs, in which the two types of fibers were entangled with each other. The inset of **Figure 10(h)** shows band structures and band alignment at the interface of PEDOT NWs and Te NWs,⁹⁶ indicating that the triggered energy filtering effect is a key factor on the improvement of $S^2\sigma$ (up to $\sim 30 \mu\text{W m}^{-1} \text{K}^{-2}$) in the composites, as shown in **Figure 10(i)**.⁹⁶ Similar methods were used to fabricate PPy nanotube/rGO hybrid films, which exhibited a $S^2\sigma$ of $\sim 7.28 \mu\text{W m}^{-1} \text{K}^{-2}$ at 300 K.⁹⁵

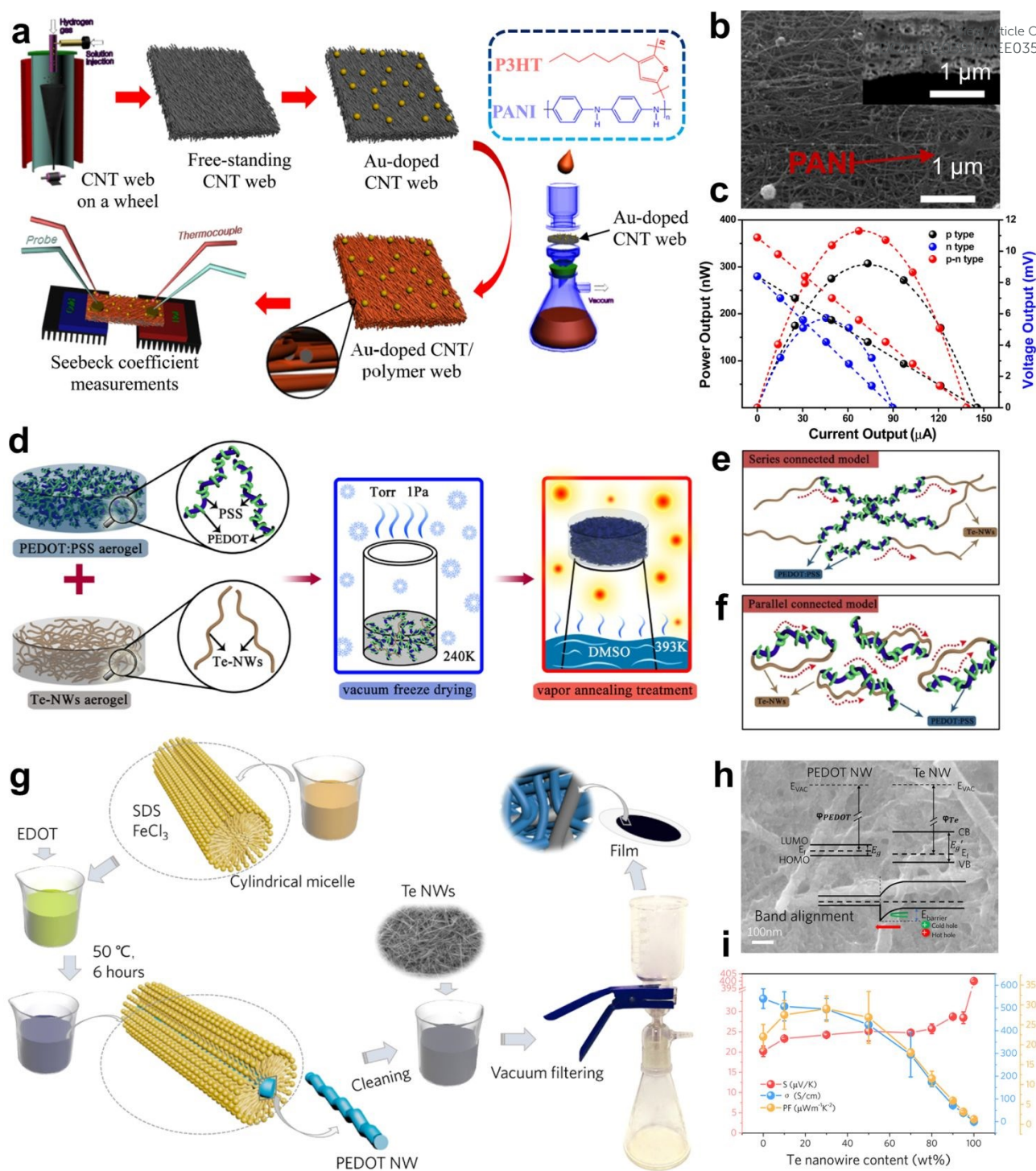


Figure 10. (a) The illustration of fabricating Au-doped CNT/polymer web using direct spinning method. (b) SEM images of Au-doped CNT/polyaniline (PANI) webs. (c) Thermoelectric power output and voltage output. Reproduced with permission.⁶⁶ Copyright 2016, American Chemical Society. (d) The illustration of fabricating PEDOT:PSS/Te NW aerogel composite film by a combination of vacuum freeze drying and dimethyl sulfoxide (DMSO) vapor annealing treatment. The illustrations of (e) series and (f) parallel models to describe the charge carrier-transport mechanisms in the composite films. Reproduced with permission.⁶⁸ Copyright 2019, American Chemical Society. (g) The illustration of fabricating PEDOT/Te NW composite film by a combination of aqueous solution and vacuum filtering. (h) SEM image of the composite film with inset band structures and band alignment at the interface of PEDOT and Te. (i) Thermoelectric performance of the composite film. Reproduced with permission.⁹⁶ Copyright 2018, American Chemical Society.

ARTICLE

5 Thermoelectric Fabric

Natural fibers, such as wool and cotton thread, are commonly used for fabricating wearable textiles due to their good moisture absorption, air permeability, and dyeability. At the same time, man-made fibers such as nylon, cellulose, acrylic, and polyester have exhibited mature manufacturing technique, high stability, and sufficient flexibility, which generally have properties similar to those of natural fibers. Considering that both natural and man-made fibers possess high flexibility, high stability, and low cost, employing these fibers as flexible substrate to fabricate thermoelectric fabrics is a promising way to realize high cost-effective and high wearability thermoelectric F-TEGs, which have been intensively studied in recent decades.^{78, 80-82, 100, 328-331}

Generally, there are several ways to fabricate thermoelectric fabrics. On the one hand, these fabrics can be used as flexible substrates for supporting inorganic thermoelectric bulks/films^{27, 83, 332} and thermoelectric yarns,⁶⁴ such as the case shown in **Figure 9(i)**. On the other hand, these fabrics can be directly modified to possess thermoelectric features, such as infiltration or depositing/coating thermoelectric materials on their surfaces.^{22, 61, 99, 101} Compared with the F-TEGs based on all-thermoelectric-fibers, the unique "composite" F-TEGs that consist of both thermoelectric materials and natural/man-made fabrics show great potential due to their potentially higher wearability and productivity.

5.1 Fabric as Pure Flexible Substrate

In the design of traditional thermoelectric devices, using flexible fabrics instead of solid ceramics as the substrates can make the thermoelectric devices have a certain degree of flexibility, thereby expanding the applications of the thermoelectric devices. n-type $\text{Bi}_2\text{Te}_{2.7}\text{Se}_{0.3}$ and p-type $\text{Bi}_{0.5}\text{Sb}_{1.5}\text{Te}_3$ were fabricated by screen-printing on flexible fiber glass fabrics.⁸³ The methyl cellulose was employed as a suitable binder additive to offer suitable viscosity for printability,⁸³ contributing to reduce the electrical resistivity. The as-printed p-type $\text{Bi}_{0.5}\text{Sb}_{1.5}\text{Te}_3$ showed a high ZT of 0.65, and the n-type $\text{Bi}_2\text{Te}_{2.7}\text{Se}_{0.3}$ exhibited a high ZT of 0.81,⁸³ respectively. In terms of the F-TEG, **Figure 11(a)** shows concept views of a F-TEG based on dispenser-printed inorganic materials on fabric.³³² The fabric acted as the substrate of the F-TEG, and the conductive thread linked the dispenser-printed n-p thermoelectric materials, both provide the flexibility. **Figure 11(b)** shows optical images of a 20-couple F-TEG printed with n-p Bi_2Te_3 100-mesh powder.³³² The as-designed F-TEG can be worn on the human body, showing good flexibility. By a ΔT of 30 K, an output voltage of ~ 25 mV

and an output power of $>2 \mu\text{W}$ could be realized.³³² Similarly, **Figure 11(c)** shows an optical image of Bi_2Te_3 and Sb_2Te_3 dots on a glass fabric.²⁷ The fabrics with n-p inorganic dots can be assembled into flexible thick films with ZT s of ~ 0.33 for the n-type Bi_2Te_3 and ~ 0.28 for the p-type Sb_2Te_3 at 300 K.²⁷ In the typical fabrication of a F-TEG, Cu electrodes were prepared on a $\text{Ni}/\text{SiO}_2/\text{Si}$ substrate to form plates. In order to reduce the contact resistance, a Ni layer was further deposited on Bi_2Te_3 and Sb_2Te_3 thick films. After that, a top plate/thick film/bottom plate structure was fabricated by bonding these components using Ag paste, and PDMS was also infiltrated into the gap between the top and bottom plates. Then, Ni peel-off in DI water was used to remove the top and bottom plates, while the remaining Ni layers were further removed by etching in a diluted mixture of hydrogen peroxide and sulfuric acid.²⁷ Such a unique light-weight and thin F-TEG exhibits a high output power density of $3800 \mu\text{W cm}^{-2}$ and $28000 \mu\text{W g}^{-1}$ at a ΔT of 50 K.²⁷ The as-designed wearable F-TEG could be applied in medical sensor systems and smart watches. In addition to the glass fabric, nanostructured Bi_2Te_3 and Sb_2Te_3 were deposited on both sides of a silk fabric to form a 12-coupled F-TEG, which showed an output voltage of ~ 10 mV and an output power of ~ 15 nW at a ΔT of 35 K.³³³

5.2 Modified Thermoelectric Fabrics

In addition to providing the flexibility for the F-TEGs, fabrics after rational modifications can exhibit thermoelectric features that act as thermoelectric materials. To achieve this goal, methods such as infiltration or depositing/coating thermoelectric materials on the surfaces of fabrics were employed.^{22, 99, 101} **Figure 11(d)** shows optical and SEM image of polyester fabric after coating by PEDOT:PSS, and the F-TEGs based on these PEDOT:PSS-coated polyester fabrics.¹⁰¹ The coating treatment was based on a solution method, and the commercial polyester fabrics after coating maintained the softness and good flexibility.¹⁰¹ A F-TEG was further fabricated by connecting the PEDOT:PSS-coated fabric strips with fine metal wires, which exhibited an output voltage of ~ 4.3 mV at a ΔT of 75.2 K.¹⁰¹ Therefore, such thermoelectric fabrics possess considerable potential for fabricating self-powered wearable electronics and power generating clothing. Similarly, PEDOT:PSS/cellulose fabric composites were fabricated by solvent evaporation of the PEDOT:PSS solution, and the F-TEG based on such composites showed an output power density of $\sim 4500 \mu\text{W cm}^{-2} \text{ mg}^{-1}$ at a ΔT of 50 K.⁷⁷ Other work indicates that a F-TEG based on p-type PEDOT:PSS-coated cotton fabrics and n-type CNT fibers treated by PEI exhibits an output power of 375 μW at a ΔT of 60 K.⁹⁷

In addition to conducting polymers, inorganic nanomaterials were also used to coat organic thermoelectric fabrics. It was reported that by an unbalanced magnetron sputtering method, commercial ubiquitous cellulose-fiber-based papers were deposited by both n- and p-type Bi_2Te_3 alloys.⁹⁹ The papers were cheap and abundant, which consisted of randomly oriented cellulose fibers. **Figure 11(e)** illustrates the carrier transport in the composite film consisting of Bi_2Te_3 /cellulose fibers,⁹⁹ in which potential energy barrier scattering effect occurred at the Bi_2Te_3 /cellulose interfaces, which was mainly caused by the thin oxide layers.⁹⁹ As a result, a promising ZT of ~ 0.38 could be achieved at 473 K in Bi_2Te_3 /cellulose fibers composite films.⁹⁹ **Figure 11(f)** shows a designed F-TEG based on these composite films and its application in harvesting heat from a hemispherical light-bulb.⁹⁹ The as-designed F-TEG with 12 pairs of n-p couples could show a high output voltage of ~ 0.144 V at a ΔT of 50 K.⁹⁹ In addition to Bi_2Te_3 , n-type Ag_2Te nanocrystals and p-type PEDOT:PSS were separately coated onto nylon fibers, and the as-designed F-TEG showed an output power of ~ 5 nW at a ΔT of 20 K.³³⁴ Besides, by a typical infiltration method, p- and n-type SWCNT networks were incorporated into cellulose fibers to

fabricate F-TEGs, which showed an output voltage of ~ 16.8 mV and an output power of ~ 75.5 nW at a ΔT of 50 K.⁹⁹

3D woven thermoelectric textiles have exhibited great potential for applying in wearable F-TEGs, as shown in **Figure 9**. To further improve their stability and wearability, modified 3D thermoelectric textiles were designed. **Figure 11(g)** illustrates the fabrication of alternately doped CNTs wrapped with acrylic fibers.²² The p-type sections of CNTs were realized by hybridizing with PEDOT:PSS, while the n-type sections of CNTs were achieved by doping with oleamine using an electrospray method. The as-fabricated p-n CNTs were then wrapped with acrylic fiber to improve their stability. Through weaving these wrapped CNT fibers into π -type thermoelectric modules, a free-standing and stretchable 3D F-TEG was realized, as shown in **Figure 11(h)**. **Figure 11(i)** shows the output power/voltage of woven fabric F-TEG.²² The as-designed woven-fiber-based F-TEG exhibits a high output power density of $7 \mu\text{W cm}^{-2}$ at a ΔT of 44 K.²² Furthermore, an excellent stretchability of $\sim 80\%$ strain can be achieved in the as-designed F-TEG without sacrificing the thermoelectric performance,²² indicating that such unique F-TEG possessed great potential for charging wearable/portable electronics.

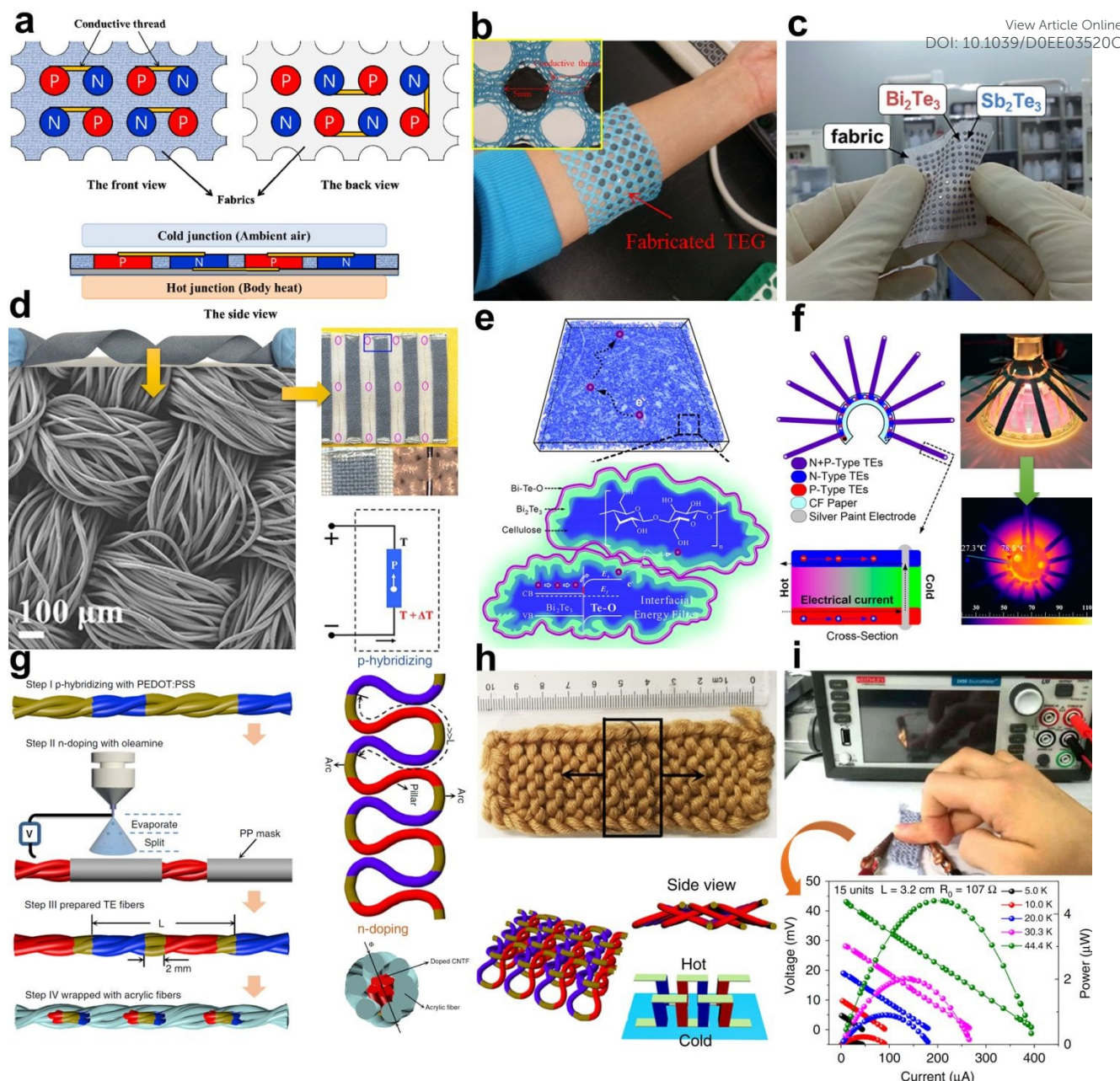


Figure 11. (a) The concept views of a F-TEG based on dispenser-printed inorganic materials on fabric. (b) Optical images of printed 20-couple F-TEG. Reproduced with permission.³³² Copyright 2013, IEEE. (c) Optical image of Bi₂Te₃ and Sb₂Te₃ dots on a glass fabric. Reproduced with permission.²⁷ Copyright 2014, Royal Society of Chemistry. (d) Optical and SEM image of polyester fabric after coating by PEDOT:PSS, and the F-TEGs based on these PEDOT:PSS-coated polyester fabrics. Reproduced under a Creative Commons Attribution-NonCommercial-ShareAlike 4.0 International License.¹⁰¹ Copyright 2015, Springer Nature. (e) Carrier transport in the composite film consisting of Bi₂Te₃/cellulose fibers (top) and the energy barrier scattering effect at the Bi₂Te₃/cellulose interfaces caused by the thin oxide layers. (f) As-designed F-TEG and its application in harvesting heat from a hemispherical light-bulb. Reproduced with permission.⁹⁹ Copyright 2018, American Chemical Society. (g) The illustration of fabricating alternately doped CNT fibers wrapped with acrylic fibers. (h) The top view and the schematic illustration of woven thermoelectric fibers. (i) The evaluation and output power/voltage of woven fabric F-TEG. Reproduced under a Creative Commons Attribution 4.0 International License.²² Copyright 2020, Springer Nature.

6 Challenge and Outlook

Owing to the unique characteristics such as lightness, softness, good comfort, excellent energy conversion performance, and high integration, thermoelectric fibers/fabrics and related TEGs have shown considerable possibilities and huge application potentials in various fields for different consumer groups, which

are definitely changing the world. With the fast development of computational science and fabrication techniques, the thermoelectric properties of thermoelectric fibers and related materials have been significantly improved, as summarized in **Table 1**. An ultrahigh $S^2\sigma$ of $\sim 6500 \mu\text{W m}^{-1} \text{K}^{-2}$ was reported in flexible $\text{Sb}_2\text{Te}_3/\text{PAN}$ nanofibers,⁶⁹ while an outstanding ZT up to ~ 2 at 862 K was reported in single-crystal SnSe-based core fibers,¹⁵ which are competitive to many high-performance

inorganic bulk materials.^{1, 5, 179, 191, 247, 271, 335-339} The development of such thermoelectric fiber/fabric with related TEGs benefits the development of multiple industries such as military industry, medical care, leisure and entertainment, and decoration, and is related to the national economy and human livelihood.

Table 1. A summary of thermoelectric performance of fiber-based thermoelectrics. Here 1,3-bis(diphenylphosphino)propane is abbreviated as DPPP; triphenylphosphine is abbreviated as TPP; tetracyanoquinodimethane is abbreviated as TCNQ; camphorsulfonic acid is abbreviated as CSA; polyvinyl acetate is abbreviated as PVAC; para toluene sulfonic acid is abbreviated as *p*TSA; reduced graphene oxide is abbreviated as rGO; poly(3-butylthiophene) is abbreviated as P3BT; polystyrene is abbreviated as PS; zeolitic imidazolate framework 67 is abbreviated as ZIF-67; polyethylene glycol is abbreviated as PEG; 1-butyl-3-methylimidazolium hexafluorophosphate is abbreviated as [BMIM]PF₆; and double walled-carbon nanotubes is abbreviated as DWCNT.

Material	Material Performance							Device Performance (Power Generation)					Year	Reference	
	Type	<i>T</i> (K)	σ (S cm ⁻¹)	<i>S</i> ($\mu\text{V K}^{-1}$)	$S^2\sigma$ ($\mu\text{W m}^{-1} \text{K}^{-2}$)	κ (W m ⁻¹ K ⁻¹)	<i>ZT</i>	Coupled Material	Couple Number	ΔT (K)	Output Voltage (mV)	Output Power (μW)			Output Power Density
Carbon Fiber-based Materials															
CNT layers	p	-	-	-	-	-	-	CNT layers	72	50	13	0.137	-	2012	331
Highly aligned CNT sheets doped by FeCl ₃	p	300	813	55	250	-	-	CNT sheets doped by PEI	9	50	23	8	-	2020	144
CNT papers treated with Ar plasma	p	673	9.1	351.3	120.5	0.25	0.4	-	-	-	-	-	-	2012	211
CNT fibers by mild annealing	p	300	1367.8	56.2	432.0	-	-	CNT fibers doped by DPPP	40	20	56.5	2.0	259 $\mu\text{W g}^{-1}$	2019	26
CNT yarns doped by PEI	n	300	7759.3	-56.4	2468.2	51	0.014	CNT yarns doped by FeCl ₃	240	40	46.7	4.1	697 $\mu\text{W g}^{-1}$	2017	12
CNT films doped by PEI	n	300	3614.5	-63.8	~ 150 0	-	-	CNT films	3	27.5	11.3	2.51	167 $\mu\text{W cm}^{-2}$	2017	36
SWCNT films	p	300	3176.5	88.4	2482	-	0.015	-	-	-	-	-	-	2016	34
SWCNT thin films	p	300	1201.5	68.6	564.8	~ 1.39	~ 0.12	-	-	-	-	-	-	2017	28
SWCNT films doped by HNO ₃	p	300	735.0	35.0	85.0	-	-	-	-	-	-	-	-	2016	35

SWCNT films doped by TPP	n	3 1 0	50.7	-70.8	25.4	0.103	0.078	SWCNT films doped by TCNQ	3	20	6	0.11	-	2013	30
SWCNTs treated with salts	n	3 1 0	69	-63	27	0.12	0.07	-	-	-	-	-	-	2016	33
Graphene fibers	n	2 9 0	1183.5	-3.9	1.9	140.7	0.00000374	-	-	-	-	-	-	2016	145
Graphene fibers doped by Br	p	3 5 0	4864.0	38.2	624	86.6	0.00276	-	-	-	-	-	-	2018	39
Graphene oxide fibers	p	3 0 0	18.5	23	0.98	-	-	Graphene oxide fibers treated with PEIE	4	70	3	0.5	-	2019	62
Inorganic Carbon Hybrid Fiber-based Materials															
Recycled carbon fiber sheets deposited by Bi ₂ Te ₃	n	3 0 0	112.4	-53.56	32.2	-	0.000966	-	-	-	-	-	-	2012	13
Recycled carbon fiber + Bi ₂ Te ₃ composites doped by CNT	n	3 0 0	2	-72.2	1.044	-	-	-	-	-	-	-	-	2019	42
SWCNT/ MoS ₂ buckypapers	p	3 5 0	146	59.7	52.0	6.8	0.0028	-	-	-	-	-	-	2015	31
rGO + Bi ₂ Te ₃ films	n	3 0 0	50	-150	108	-	0.0035	SWCNTs + Sb ₂ Te ₃ films	10	70	67.5	23.6	-	2019	143
Semiconductor Fiber-based Materials															
Ag _x Te _y nanofibers	n	3 0 0	6.8	-76.7	4	-	-	-	-	-	-	-	-	2015	43
Ag ₂ Te NW films	n	4 6 8	95.2	-142	192	-	-	-	10	80	60	-	-	2017	79
Ag ₂ Te NW films	n	4 2 0	149.8	-154.96	359.76	-	-	-	4	40	3.6	-	-	2019	142
Bi ₂ Se ₃ NWs	n	3 0 0	427	-96.3	396	-	-	-	-	-	-	-	-	2016	103
(Bi _{1-x} Sb _x) ₂ Te ₃ NWs	p	3 0 0	204.7	135.3	374.7	-	-	-	-	-	-	-	-	2015	102
Bi _{0.8} Sb _{1.2} Te _{2.9} NWs	p	3 0 0	759	166.1	2094	0.69	0.89	-	-	-	-	-	-	2016	149

Bi_{0.5}Sb_{1.5}Te₃ fibers	p	300	53.1 to 69.8	179 to 193	170 to 260	-	-	Bi ₂ Te _{2.7} S _{e_{0.3}} fibers	2	12	4.8	0.018	-	2016	84 View Article Online DOI: 10.1039/C5EE03520C
Si NWs	-	-	-	-	-	-	-	Si NWs	162	70	27.9	0.47	-	2012	289
Si NWs doped with B	p	300	418.1	218.4	1993.5	-	-	-	-	-	-	-	-	2014	210
Si nanotube fabrics	p	823	-	320	-	-	0.34	-	-	70	22	-	11000 μW cm ⁻²	2018	14
Si_{0.73}Ge_{0.27}NWs	n	450	616.2	-140.3	1212.9	1.2	0.46	-	-	-	-	-	-	2012	148
SnSe NWs	p	370	24.7	321.8	255.8	0.55	0.156	-	-	-	-	-	-	2018	150
Semiconductor Core Fiber															
Bi₂Se₃ core fibers	n	300	319	-150.85	725.9	1.25	0.18	-	-	-	-	-	-	2018	45
Bi_{0.5}Sb_{1.5}Te₃ core fibers	p	300	1568	150	3529	0.844	1.25	Bi ₂ Se ₃ core fibers	7	60	97	-	2340 μW cm ⁻²	2017	46
Bi₂Te₃ core fibers	p	300	744	130.5	1267	0.52	0.73	-	-	-	-	-	-	2018	44
SnSe core fibers	p	862	56.4	306.9	531.2	0.25	2	-	-	-	-	-	-	2020	15
Inorganic Coating on Glass/Silica Fiber															
SWCNT-coated glass fibers	p	300	1800	24.7	~109.8	-	-	-	-	-	-	-	-	2017	48
Ni-Ag-coated silica fibers	p	300	-	19.6	-	-	-	-	7	6.6	0.9	0.002	-	2008	262
PbTe nanocrystal-coated glass fibers	p	400	1.7	1545.3	406	0.226	0.75	-	-	-	-	-	-	2012	17
Fiber-reinforced Cement															
Carbon fiber-reinforced cement	p	300	0.002	19.73	0.0008	0.22	0.000001334	-	-	60	-	4 to 5	-	2014	19
Carbon fiber-reinforced cement with pyrolytic carbon layer	p	328	-	-	2.08	-	0.00311	-	-	-	-	-	-	2016	49
Graphite/carbon fiber	n	306	0.78	-11.59	0.000785	-	-	-	-	-	-	-	-	2017	50

															View Article Online DOI: 10.1039/D0EE03520C	
cement composites																
CNT-reinforced cement	p	-	0.818	57.98	0.275	0.734 to 0.947	0.0000933	-	-	-	-	-	-	-	2018	51
Organic Fiber-based Materials																
Highly anisotropic P3HT films	p	365	221.5	53.1	62.4	-	0.1	-	-	-	-	-	-	-	2016	88
P3HT nanofiber networks	p	300	-	-	6.75	-	0.0026	-	-	-	-	-	-	-	2014	89
P3HT nanofiber mats	p	300	14.8	50	3.7	0.0708	0.016	-	-	-	-	-	-	-	2017	90
P3BT + PS interpenetration networks	p	300	0.0018	616	0.0675	0.24	0.000083	-	-	-	-	-	-	-	2014	109
PANI NWs doped by pTSA	p	320	-	15	-	0.32	0.0000275	-	-	-	-	-	-	-	2014	151
PEDOT nanofibers	p	300	71.4	48.0	16.4	-	-	-	-	-	-	-	-	-	2015	106
PEDOT NWs	n	310	16.8	-74	9.2	-	-	-	-	-	-	-	-	-	2011	105
PEDOT NWs assembly	p	300	~541	~20.78	~23.4	-	-	-	-	-	-	-	-	-	2018	87
PEDOT NWs + PEDOT:Tos hybrids	p	300	1270	59.3	446.6	0.286	0.44	Nitrogen-doped graphene	1	10.1	-	-	~0.05 $\mu\text{W cm}^{-2}$	2016	107	
PEDOT:PSS fibers treated with H₂SO₄	p	300	4029.5	19.2	147.8	0.5 to 1	0.05 to 0.09	Ni wires	5	9.1	1.9	-	~0.273 $\mu\text{W cm}^{-2}$	2020	85	
PEDOT:PSS fibers treated with EG-DMSO	p	300	175.2	16.4	4.7	-	-	CNT fibers	5	60	20.7	-	481.2 $\mu\text{W cm}^{-2}$	2018	54	
Hollow PEDOT:PSS fibers treated with EG	p	300	-	24	-	-	-	-	5	6	0.404	-	-	2020	20	
Lamellar-structured PEDOT:PSS films treated with CH₃NO-H₂SO₄-NaBH₄	p	298	1786	28.1	141	-	-	-	14	12	2.9	-	~1 $\mu\text{W cm}^{-2}$	2019	52	

Lamellar-structured PEDOT:PSS films treated with EG-H ₂ SO ₄ -TDAE	p	300	1975	33.4	224	-	-	-	5	44.5	6	-	~3 $\mu\text{W cm}^{-2}$	2020	53 View Article Online DOI: 10.1039/D0EE03520C
PEDOT:PSS films treated with H ₂ SO ₄ -NaOH	p	300	2170	39.2	334	0.2 to 0.34	0.29 to 0.49	-	-	-	-	-	-	2017	55
PPy nanotube films	p	310	9.81	17.68	0.31	0.17	0.000571	-	-	-	-	-	-	2014	86
Inorganic/Organic Hybrid Fiber-based Materials															
Carbon fibers + epoxy mixed by Te/Bi ₂ Te ₃ /carb on black	p	343	47.6	163.3	126.9	0.511	0.086	-	-	-	-	-	-	2013	40
Carbon fibers + epoxy	p	300	1630	33.85	245	-	-	-	-	75	19.56	0.87	-	2019	59
Carbon fiber sheets + P3OT	p	300	3.9	134.5	7.05	-	-	-	-	-	-	-	-	2015	57
CNTs + P3HT	p	300	1553.2	24.7	95	0.19	0.01	-	-	-	-	-	-	2013	340
CNTs grafted by P3HT	p	300	33.8	113.8	43.8	2	0.0065	-	15	20	33.5	0.0145	-	2017	91
CNT nanotube networks + PANI	p	300	40.35	23.3	2.2	0.29	0.0022	-	-	-	-	-	-	2012	38
CNTs + PANI	p	300	530	33	57.7	-	-	-	-	-	-	-	-	2012	92
CNT webs doped by Au + PANI	p	300	1070.3	150.8	2433.9	3.5	0.203	CNT webs doped by PEI	7	20	-	1.74	0.4 $\mu\text{W cm}^{-2}$	2016	66
CNT networks + PDMS	p	300	60	42.6	10.9	0.84	0.004	-	-	-	-	-	-	2019	139
CNTs + PEDOT:PSS	p	300	400	25	25	0.2 to 0.4	0.02	-	-	-	-	-	-	2010	140
CNTs + PEDOT:PSS films treated with EG	p	300	800	43	151	-	-	-	-	10	5	0.03	-	2016	110
CNTs forest + PEDOT:PSS	p	410	275	60	92	-	-	-	-	-	-	-	-	2018	138

CNTs + PEDOT:PSS composite fibers treated with PEI	n	300	541.4	-45.7	~113	-	-	CNTs + PEDOT:PSS composite fibers treated with hydrazine	12	10	8	0.43	-	2018	56
CNTs + PEDOT:PSS + PVAC	p	300	960	40.8	~160	0.38	-	-	-	-	-	-	-	2011	75
CNTs + PEDOT:PSS treated with TDAE	n	300	6.34	-120.5	1047.3	0.67	0.5	-	-	-	-	-	-	2015	141
CNT/PEG composite threads	p	300	~477.7	~47.3	~107.2	-	-	Doped with [BMIM]PF ₆	-	25	-	0.008	-	2017	341
CNT yarns + PEI	n	300	1408.3	-68.7	667.8	-	-	CNT yarns + PEDOT:PSS	966	47.5	-	382.8	5.15 $\mu\text{W cm}^{-2}$	2020	21
CNTs + PS	p	300	1250	60	413	-	0.41	-	-	-	-	-	-	2015	137
CNTs + PANI-coated SnSe _{0.8} S _{0.2} nanosheets + PVDF	p	400	29.4	317.8	297	-	-	-	-	-	-	-	-	2018	116
CNTs + ZIF-67 composites	p	300	825.7	55.6	255.6	4.1	~0.02	-	-	-	-	-	-	2020	112
SWCNTs + MEH-PPV doped by I ₂	p	300	415	29	32.8	-	-	-	-	-	-	-	-	2017	67
SWCNTs + P3HT films	p	300	2750	31.2	267	-	-	-	-	-	-	-	-	2015	133
SWCNTs + PANI films	p	300	769	65	176	-	0.12	-	-	-	-	-	-	2014	342
SWCNTs + PANI	p	300	29.57	39.0	4.5	0.15	0.01	-	-	-	-	-	-	2016	73
SWCNTs + PANI	p	300	125	40	20	-	-	-	-	-	-	-	-	2010	76
SWCNTs + PANI	p	300	2380	39	362	-	-	-	8	50	14	2.86	745 $\mu\text{W cm}^{-2}$	2020	134
SWCNTs + PANI	p	300	1440	38.8	217	0.44	0.15	-	4	60	8	~4	-	2016	135

View Article Online
DOI: 10.1039/C0EE03520C

Journal Name

ARTICLE

SWCNTs + PEDOT:PSS	p	300	900	30.5	83.9	-	-	SWCNTs doped by PEI	6	50	28	0.22	-	2017	132 DOI: 10.1039/C6EE03520C
SWCNTs + PEDOT:PSS + PPy	p	300	900	22.5	45.3	-	-	-	-	-	-	-	-	2020	136
SWCNTs sandwiched by PPy	p	300	303.2	26.5	21.7	-	-	-	-	-	-	-	-	2016	93
SWCNTs + PPy	p	300	381	21.4	17.4	-	-	-	-	-	-	-	-	2016	94
SWCNTs + PVDF pastes	p	300	1950	39.6	~378	-	-	SWCNTs + PVDF pastes doped by PEI	12	10	16	0.8	-	2018	72
DWCNTs + PANI doped by CSA	p	300	610	61	220	0.7 to 15	~0.1	-	-	-	-	-	-	2015	130
Graphene + CNTs aerogels	p	300	51.9	57.9	1717	~0.056	~0.001	-	-	-	-	-	-	2015	146
Graphene + DWCNTs PANI	p	300	1080	130	1825	-	-	-	-	-	-	-	-	2015	128
PANI/graphene - PEDOT:PSS/PANI/DWCNT - PEDOT:PSS repeating sequences	p	300	1900	120	2710	0.4 to 24.6	0.03 to 2	Ag wires	5	9.7	5.1	-	-	2016	129
Graphene-iron oxide nanocomposite + PVAC + PEDOT:PSS	p	300	800	25.42	51.93	0.9	0.017	-	-	-	-	-	-	2016	78
rGO-DWCNT + PANI	p	300	950	115	1260	-	-	-	-	-	-	-	-	2019	127
rGO + PEDOT:PSS + Te NWs	p	300	34.96	202	143	-	-	SWCNTs doped by PEI	5	50	58	-	0.65 $\mu\text{W cm}^{-2}$	2016	126
rGO + PPy nanotubes hybrid films	p	300	81	30	7.28	-	-	-	-	-	-	-	-	2018	95
Bi ₂ Te ₃ NWs + P3HT films	p	300	450	118	6.3	0.85	-	-	-	-	-	-	-	2012	125
Bi ₂ Te ₃ NWs + PEDOT:PSS films	p	300	1026	47	223	0.29	0.2	-	-	-	-	-	-	2020	111
Bi ₂ Te ₃ NWs + PEDOT:PSS	p	300	123.72	24.5	7.45	0.047	0.048	-	-	80	-	130	-	2019	124

nanofilm networks															View Article Online DOI: 10.1039/D0EE03520C	
Cu_{2-x}Se NWs + PVDF	p	303	5578.2	14.16	111.84	0.79	0.04	-	-	-	-	-	-	-	2017	114
Cu₂Se NWs + PEDOT:PSS	p	300	1047	50.8	270.3	0.25 to 0.3	0.3	-	9	30	15	0.32	-	-	2019	115
Cu_{1.75}Te NWs + PVDF	p	300	2490	9.6	23	0.85	0.01	-	-	-	-	-	-	-	2015	65
Sb₂Te₃ + PAN yarns	p	300	750	178	2376.3	3	0.24	Bi ₂ Te ₃ + PAN yarns	-	200	-	14.2	858.5 μW cm ⁻²	2016	69	
Ta₄SiTe₄ whiskers + PVDF	n	220	99	-325	1045.7	-	-	-	-	35.5	35	1.7	13 μW cm ⁻²	2020	113	
Te nanorods + PANI films	p	300	95.5	111.9	119.6	0.2	0.223	-	10	40	29.9	0.73	-	2016	123	
Te-Cu_{1.75}Te/PEDOT:PSS NWs	p	300	19.8	206.1	84	-	-	-	-	-	-	-	-	2016	117	
Te NWs + PEDOT:PSS films	p	300	11	180	35.6	0.16	-	-	-	-	-	-	-	2013	120	
Te NWs/PEDOT:PSS microribbon	p	400	4	230	21	-	-	-	-	-	-	-	-	2014	118	
Te NWs + PEDOT:PSS fibers	p	300	250.8	55.8	78.1	-	-	Te NWs + PEDOT:PSS fibers coated by Ag	28	40	25.9	0.2	9.48 μW g ⁻¹	2020	64	
Te NWs + PEDOT:PSS films	p	300	104.6	48	24.1	-	-	Bi ₂ Te ₃ NWs	6	60	56	-	32 μW cm ⁻²	2017	119	
Te NWs + PEDOT:PSS NWs	p	300	488	24.1	28.3	-	-	-	-	-	-	-	-	2018	96	
Te NWs + PEDOT:PSS aerogel films	p	298	110	32	11.3	0.266	0.02	CNT fibers	6	60	31.2	1.28	-	2019	68	
Te nanorods + SWCNTs + PANI	p	300	345	54	101	0.3	0.101	-	-	40	8	1	62.4 μW cm ⁻²	2017	131	
Te nanorods + PEDOT:PSS films	p	300	19.3	163	70.9	0.22 to 0.30	0.1	-	-	8	1.25	-	-	2010	121	
Te nanorods + PEDOT:PSS films	p	300	114.97	214.86	284	0.22	0.39	-	16	5	12.75	~0.01	-	2016	122	

Te nanorods coated by SWCNT/PEDOT:PSS treated with H ₂ SO ₄	p	300	332	56	104	-	-	-	6	44	5.6	0.0536	-	2019	60
Modified Natural and Man-made Fiber/Fabric															
Acrylic fiber-wrapped CNT yarns with PEDOT:PSS	p	300	949	60.4	346.2	-	-	Acrylic fiber-wrapped CNT yarns doped by oleamine	15	44	43.5	4.38	7 μW cm ⁻²	2020	22
Commercial textiles coated by PEDOT	p	260	-	~15	-	-	-	CNTs	5	100	21	-	~0.04 μW cm ⁻²	2019	329
Cotton fabric soaked by PEDOT:PSS solution	p	300	18.8	16.2	0.5	-	-	CNT fibers	8	60	45	375	-	2019	97
Cotton thread + P3HT	p	300	-	-	-	-	-	Cotton thread + Ag paste	13	50	12	1.15	-	2018	343
Cellulose fibers coated by PEDOT:PSS	p	295	31	22	1.5	0.1	0.0013	Ni foils	6	48.5	6	2.4	-	2017	77
Cellulose fibers + SWCNT networks	p	300	29	53	8.1	-	-	Cellulose fibers + SWCNT networks treated with PEI	5	50	~16.8	0.0755	-	2015	98
Cellulose fibers + Bi ₂ Te ₃	n	473	209.6	-134.2	377.5	0.47	0.38	Cellulose fibers + (Bi,Sb) ₂ Te ₃	12	50	144	-	-	2018	99
Glass fiber coated by PEDOT:pTSA	p	300	31.84	48.5	6.74	-	-	-	-	-	-	-	-	2018	81
Glass fabric printed by Bi ₂ Te ₃	n	300	549.2	-136.9	1029.3	0.93	0.33	Glass fabric printed by Sb ₂ Te ₃	8	50	90	-	3800 μW cm ⁻²	2014	27
Glass fabric screen-printed by Bi ₂ Te _{2.7} Se _{0.3}	n	300	763	-165	2077.3	0.37	0.81	Glass fabric screen-printed by Bi _{0.5} Sb _{1.5} Te ₃	-	-	-	-	-	2017	83

Nylon membrane with Ag ₂ Se films	n	300	497	-140	~987.4	0.478	~0.6	-	4	30	18	0.46	-	2019	⁸² DOI: 10.1039/C9EE03520C
Nylon fibers coated by Ag ₂ Te nanocrystals	n	-	-	-	-	-	-	Nylon fibers coated by PEDOT:PSS	-	20	-	~0.005	0.6 μW cm ⁻²	2015	³³⁴
Paper with PEDOT:PSS	p	300	53.9	23.6	3	0.16	0.0055	-	-	-	-	-	-	2014	¹⁰⁰
Polyester fabrics printed by Bi ₂ Te ₃	n	-	-	-	-	-	-	-	20	30	25	2.1	-	2013	³³²
Polyester fabrics coated by PEDOT:PSS	p	300	1.5	16.3	0.04	-	-	Ag wires	5	75.2	4.3	0.0125	-	2015	¹⁰¹
Polymer fabrics printed by Bi _{0.5} Sb _{1.5} Te ₃	p	300	-	530	-	-	-	Polymer fabrics printed by Bi ₂ Se _{0.3} Te _{2.7}	12	15	25	0.224	-	2014	³³⁰
Silk fabric deposited by nanostructured Sb ₂ Te ₃	p	310	-	110.8	-	-	-	Silk fabric deposited by nanostructured Bi ₂ Te ₃	12	35	~10	~0.015	-	2016	³³³

Despite the rapid development of thermoelectric fibers and related materials in recent years, they still face significant challenges in both their performance and application. For inorganic fibers, their weak flexibility considerably limits applications in wearable thermoelectric devices, and the issues such as high toxicity and high cost still need significant attention during the design and application. For organic fibers, their thermoelectric properties are noticeably lower than that of the inorganic fibers, and the mechanism of further improving their performance is not mature enough with a certain limitation. For hybrid fibers, to achieve a balance between flexibility and performance is still tricky. Besides, many strategies can lead high ZTs in a narrow temperature range, which limit the overall energy conversion. It is of significance to find or develop materials with wider operating temperature ranges.⁴ In terms of the TEGs based on thermoelectric fiber/fabric, at present, there is an urgent need to realize highly integrated, multi-functional, low-cost, safe, and durable TEGs to make it more humane during the usage, therefore the design of fiber/fabric-based TEGs should focus on the balance between performance, stability, and flexibility, which is a tough work that needs intensive studies in the future. Generally, there is still a long way to go before the commercialization of fiber/fabric-based TEGs.

In terms of the outlook of future development of thermoelectric fibers and fabrics, as illustrated in **Figure 12**, the following topics should be significantly improved:

1. Performance improvement. For fiber-based thermoelectrics, with the aim to achieve a high energy conversion efficiency, the fundamental mechanisms including boosting the carrier transport and strengthening the phonon scattering need further exploring, and the adaptability between difference components in hybrids should be carefully evaluated. For TEGs based on fibers or fabrics, to realize a high output power, a rational design is needed, which should simultaneously consider the factors including device topology, integration, working mode, boundary condition, and influencing factor.¹ Computational assistance such as finite element numerical simulation is helpful for rationally designing the as-required TEGs. In addition, it is needed to improve the various physical properties of the fibers and fabrics to keep a stable thermoelectric performance, especially the tensile flexibility and spinnability. There are several ways to achieve this goal, such as designing/optimizing fabrication techniques and rational doping or modification treatments.

2. Personal thermal management. Currently, increasing researchers are beginning to pay attention to the research of

human body thermal management materials and clothing, hoping to realize the automatic regulation of human body surface temperature and effective use of body surface waste heat, and finally realize a clothing system with intelligent personal thermal management (PTM).³⁴⁴⁻³⁴⁶ To achieve this goal, wearable F-TEGs based on 1D thermoelectric fibers, 2D fiber-based films, and 3D woven thermoelectric yarns and textiles are good candidates as key components to realize the body heat harvesting for power generation or refrigeration to keep a safe temperature for human body. However, the currently known PTM-based thermoelectric materials and devices still face the problem of single function in temperature adjustment, and it is difficult to cope with the complicated and changeable external environment; in terms of heat capture, they face the problems of low conversion efficiency and difficulty in practical application.

3. Biofiber-based thermoelectrics. Biofibers such as spider silks possess many unique features that cannot be realized by current technique, therefore exploring the potential combination between biofibers and thermoelectrics is interesting and of significance. Preliminary study indicated that spider silk fibers possess complex components such as crystalline β -sheets and amorphous structural regions, providing opportunities for thermoelectric modification.³⁴⁷ It was reported that pyrolyzed spider silk could exhibit a S of $>20 \mu\text{V K}^{-1}$ at 300 K,³⁴⁷ indicating potential for further studies on thermoelectrically functionalized natural and synthetic protein polymers for unconventional applications.

4. Standardization and productivity. Thermoelectric fiber/fabric-based TEG is still a relatively new type of product. Although there are some company products on the market, there is still no standard that is generally recognized in the industry. In addition to formulating basic safety requirements for wearable products, it is also necessary to formulate relevant standards for some technical issues (such as the scope of material use). A determination of industry specifications is conducive to the development of thermoelectric fiber/fabric-based TEGs. In addition to the standardization, the productivity of thermoelectric fiber/fabric and related TEGs still needs improvement. Using natural and/or man-made fibers as raw materials is a suitable way to realize a boosting in productivity of thermoelectric fibers and fabrics.

5. Broadening the application such as 5G. The development of new technologies, such as the 5G, provides more opportunities for the application of fiber-based thermoelectrics. It was pointed out that one of the key components in 5G operation is the optical module, which can realize the optical and electrical conversion. However, one significant issue for the optical module is that the optical chip is sensitive to the heat, and the high temperature can reduce optical output power as well as the service life of the optical chip. To solve this issue, developing stable and high-performance thermoelectric coolers is of significance, and fiber-based thermoelectrics have exhibited great potential to fulfill the requirement due to their unique features such as good thermoelectric performance at low temperatures and high flexibility to target different application environments. In addition to 5G, fiber-based thermoelectrics

show considerable potential for applying in other applications, such as medical, military, aerospace, and the ocean.



Figure 12. The outlook of future development of thermoelectric fiber. TE fiber: reproduced with permission.¹⁰ Copyright 2018, Wiley. Performance improvement: reproduced with permission.²⁸⁷ Copyright 2019, Wiley. Wearable textile for personal thermal management: reproduced with permission.³⁴⁹ Copyright 2017, American Chemical Society. Biofiber for bionic thermoelectric application: reproduced under the terms of the Creative Commons Attribution License.³⁵⁰ Copyright 2018, Oxford University Press. Application on waste heat harvesting for 5G: reproduced with permission.³⁵¹ Copyright 2020, Australasian College of Nutritional and Environmental Medicine.

Conflicts of interest

There are no conflicts to declare.

Acknowledgements

This work was financially supported by the Australian Research Council, Innovation Centre for Sustainable Steel (ICSS) Project, and USQ strategic research grant.

References

1. X.-L. Shi, J. Zou and Z.-G. Chen, *Chem. Rev.*, 2020, **120**, 7399-7515.
2. M. Dargusch, W.-D. Liu and Z.-G. Chen, *Adv. Sci.*, 2020, **7**, 2001362.
3. S. M. Pourkiaei, M. H. Ahmadi, M. Sadeghzadeh, S. Moosavi, F. Pourfayaz, L. Chen, M. A. Pour Yazdi and R. Kumar, *Energy*, 2019, **186**, 115849.

4. Y. Xiao and L.-D. Zhao, *Science*, 2020, **367**, 1196.
5. X. Shi and L. Chen, *Nat. Mater.*, 2016, **15**, 691-692.
6. A. Nozariasbmarz, H. Collins, K. Dsouza, M. H. Polash, M. Hosseini, M. Hyland, J. Liu, A. Malhotra, F. M. Ortiz, F. Mohaddes, V. P. Ramesh, Y. Sargolzaeiaval, N. Snouwaert, M. C. Özturk and D. Vashaee, *Appl. Energ.*, 2020, **258**, 114069.
7. C. Li, F. Jiang, C. Liu, P. Liu and J. Xu, *Appl. Mater. Today*, 2019, **15**, 543-557.
8. W. Yan, C. Dong, Y. Xiang, S. Jiang, A. Leber, G. Loke, W. Xu, C. Hou, S. Zhou, M. Chen, R. Hu, P. P. Shum, L. Wei, X. Jia, F. Sorin, X. Tao and G. Tao, *Mater. Today*, 2020, **35**, 168-194.
9. K. Dong, X. Peng and Z. L. Wang, *Adv. Mater.*, 2020, **32**, 1902549.
10. L. Zhang, S. Lin, T. Hua, B. Huang, S. Liu and X. Tao, *Adv. Energy Mater.*, 2018, **8**, 1700524.
11. W. Zeng, L. Shu, Q. Li, S. Chen, F. Wang and X.-M. Tao, *Adv. Mater.*, 2014, **26**, 5310-5336.
12. J. Choi, Y. Jung, S. J. Yang, J. Y. Oh, J. Oh, K. Jo, J. G. Son, S. E. Moon, C. R. Park and H. Kim, *ACS Nano*, 2017, **11**, 7608-7614.
13. E. J. X. Pang, S. J. Pickering, A. Chan, K. H. Wong and P. L. Lau, *J. Solid State Chem.*, 2012, **193**, 147-153.
14. A. Morata, M. Pacios, G. Gadea, C. Flox, D. Cadavid, A. Cabot and A. Tarancón, *Nat. Commun.*, 2018, **9**, 4759.
15. J. Zhang, T. Zhang, H. Zhang, Z. Wang, C. Li, Z. Wang, K. Li, X. Huang, M. Chen, Z. Chen, Z. Tian, H. Chen, L.-D. Zhao and L. Wei, *Adv. Mater.*, 2020, **32**, 2002702.
16. F. Ma, Y. Ou, Y. Yang, Y. Liu, S. Xie, J.-F. Li, G. Cao, R. Proksch and J. Li, *J. Phys. Chem. C*, 2010, **114**, 22038-22043.
17. D. Liang, H. Yang, S. W. Finefrock and Y. Wu, *Nano Lett.*, 2012, **12**, 2140-2145.
18. R. Nunna, P. Qiu, M. Yin, H. Chen, R. Hanus, Q. Song, T. Zhang, M.-Y. Chou, M. T. Agne and J. He, *Energy Environ. Sci.*, 2017, **10**, 1928-1935.
19. J. Wei, Z. Nie, G. He, L. Hao, L. Zhao and Q. Zhang, *RSC Adv.*, 2014, **4**, 48128-48134.
20. L. Ruan, Y. Zhao, Z. Chen, W. Zeng, S. Wang, D. Liang and J. Zhao, *Polymers*, 2020, **12**, 553.
21. Y. Zheng, Q. Zhang, W. Jin, Y. Jing, X. Chen, X. Han, Q. Bao, Y. Liu, X. Wang, S. Wang, Y. Qiu, C.-a. Di and K. Zhang, *J. Mater. Chem. A*, 2020, **8**, 2984-2994.
22. T. Sun, B. Zhou, Q. Zheng, L. Wang, W. Jiang and G. J. Snyder, *Nat. Commun.*, 2020, **11**, 572.
23. L. Huang, S. Lin, Z. Xu, H. Zhou, J. Duan, B. Hu and J. Zhou, *Adv. Mater.*, 2020, **32**, 1902034.
24. H. Wu, Y. Huang, F. Xu, Y. Duan and Z. Yin, *Adv. Mater.*, 2016, **28**, 9881-9919.
25. J. Shi, S. Liu, L. Zhang, B. Yang, L. Shu, Y. Yang, M. Ren, Y. Wang, J. Chen, W. Chen, Y. Chai and X. Tao, *Adv. Mater.*, 2020, **32**, 1901958.
26. T. Lee, K. T. Park, B.-C. Ku and H. Kim, *Nanoscale*, 2019, **11**, 16919-16927.
27. S. J. Kim, J. H. We and B. J. Cho, *Energy Environ. Sci.*, 2014, **7**, 1959-1965.
28. B. A. MacLeod, N. J. Stanton, I. E. Gould, D. Wesenberg, R. Ihly, Z. R. Owczarczyk, K. E. Hurst, C. S. Fewox, C. N. Folmar, K. Holman Hughes, B. L. Zink, J. L. Blackburn and A. J. Ferguson, *Energy Environ. Sci.*, 2017, **10**, 2168-2179.
29. E. J. X. Pang, A. Chan and S. J. Pickering, *Compos. Part A-appl. S.*, 2011, **42**, 1406-1411.
30. Y. Nonoguchi, K. Ohashi, R. Kanazawa, K. Ashiba, K. Hata, T. Nakagawa, C. Adachi, T. Tanase and T. Kawai, *Sci Rep*, 2013, **3**, 3344.
31. Y. Nonoguchi, K. Hata and T. Kawai, *ChemPlusChem*, 2015, **80**, 1158-1163.
32. D. Hayashi, T. Ueda, Y. Nakai, H. Kyakuno, Y. Miyata, T. Yamamoto, T. Saito, K. Hata and Y. Maniwa, *Appl. Phys. Express*, 2016, **9**, 025102.
33. Y. Nonoguchi, M. Nakano, T. Murayama, H. Hagino, S. Hama, K. Miyazaki, R. Matsubara, M. Nakamura and T. Kawai, *Adv. Funct. Mater.*, 2016, **26**, 3021-3028.
34. W. Zhou, Q. Fan, Q. Zhang, K. Li, L. Cai, X. Gu, F. Yang, N. Zhang, Z. Xiao, H. Chen, S. Xiao, Y. Wang, H. Liu, W. Zhou and S. Xie, *Small*, 2016, **12**, 3407-3414.
35. D. Hayashi, Y. Nakai, H. Kyakuno, T. Yamamoto, Y. Miyata, K. Yanagi and Y. Maniwa, *Appl. Phys. Express*, 2016, **9**, 125103.
36. W. Zhou, Q. Fan, Q. Zhang, L. Cai, K. Li, X. Gu, F. Yang, N. Zhang, Y. Wang and H. Liu, *Nat. Commun.*, 2017, **8**, 14886.
37. Y. Nonoguchi, S. Sudo, A. Tani, T. Murayama, Y. Nishiyama, R. M. Uda and T. Kawai, *Chem. Commun.*, 2017, **53**, 10259-10262.
38. J. Chen, X. Gui, Z. Wang, Z. Li, R. Xiang, K. Wang, D. Wu, X. Xia, Y. Zhou, Q. Wang, Z. Tang and L. Chen, *ACS Appl. Mater. Interfaces*, 2012, **4**, 81-86.
39. W. Ma, Y. Liu, S. Yan, T. Miao, S. Shi, Z. Xu, X. Zhang and C. Gao, *Nano Res.*, 2018, **11**, 741-750.
40. S. Han and D. D. L. Chung, *Compos. Part A-appl. S.*, 2013, **48**, 162-170.
41. P. R. Jagadish, M. Khalid, L. P. Li, M. T. Hajibeigy, N. Amin, R. Walvekar and A. Chan, *J. Clean. Prod.*, 2018, **195**, 1015-1025.
42. P. Jagadish, M. Khalid, N. Amin, M. T. Hajibeigy, L. P. Li, A. Numan, N. M. Mubarak, R. Walvekar and A. Chan, *Compos. Part B-eng.*, 2019, **175**, 107085.
43. M. Zhang, H. Park, J. Kim, H. Park, T. Wu, S. Kim, S.-D. Park, Y. Choa and N. V. Myung, *Chem. Mater.*, 2015, **27**, 5189-5197.
44. M. Sun, Q. Qian, G. Tang, W. Liu, G. Qian, Z. Shi, K. Huang, D. Chen, S. Xu and Z. Yang, *APL Mater.*, 2018, **6**, 036103.
45. G. Qian, M. Sun, G. Tang, W. Liu, Z. Shi, Q. Qian, Q. Zhang and Z. Yang, *Mater. Lett.*, 2018, **233**, 63-66.
46. T. Zhang, K. Li, J. Zhang, M. Chen, Z. Wang, S. Ma, N. Zhang and L. Wei, *Nano Energy*, 2017, **41**, 35-42.
47. Y. Park, K. Cho and S. Kim, *Mater. Res. Bull.*, 2017, **96**, 246-249.
48. L. Tzounis, C. Gravalidis, S. Vassiliadou and S. Logothetidis, *Mater. Today P.*, 2017, **4**, 7070-7075.
49. J. Wei, Q. Zhang, L. Zhao, L. Hao and C. Yang, *Ceram. Int.*, 2016, **42**, 11568-11573.
50. J. Wei, Q. Zhang, L. Zhao, L. Hao and Z. Nie, *Ceram. Int.*, 2017, **43**, 10763-10769.
51. J. Wei, Y. Fan, L. Zhao, F. Xue, L. Hao and Q. Zhang, *Ceram. Int.*, 2018, **44**, 5829-5833.
52. S. Xu, M. Hong, X.-L. Shi, Y. Wang, L. Ge, Y. Bai, L. Wang, M. Dargusch, J. Zou and Z.-G. Chen, *Chem. Mater.*, 2019, **31**, 5238-5244.
53. S. Xu, M. Hong, X.-L. Shi, M. Li, Q. Sun, Q. Chen, M. Dargusch, J. Zou and Z.-G. Chen, *Energy Environ. Sci.*, 2020, **13**, 3480-3488.
54. J. Liu, Y. Jia, Q. Jiang, F. Jiang, C. Li, X. Wang, P. Liu, P. Liu, F.

- Hu, Y. Du and J. Xu, *ACS Appl. Mater. Interfaces*, 2018, **10**, 44033-44040.
55. Z. Fan, P. Li, D. Du and J. Ouyang, *Adv. Energy Mater.*, 2017, **7**, 1602116.
56. J.-Y. Kim, W. Lee, Y. H. Kang, S. Y. Cho and K.-S. Jang, *Carbon*, 2018, **133**, 293-299.
57. D. Wang, Y. Su, D. Chen, L. Wang, X. Xiang and D. Zhu, *Compos. Part B-eng.*, 2015, **69**, 467-471.
58. N. Dalton, R. P. Lynch, M. N. Collins and M. Culebras, *Int. J. Biol. Macromol.*, 2019, **121**, 472-479.
59. G. Karalis, L. Tzounis, E. Lambrou, L. N. Gergidis and A. S. Paipetis, *Appl. Energy*, 2019, **253**, 113512.
60. Q. Meng, K. Cai, Y. Du and L. Chen, *J. Alloys Compd.*, 2019, **778**, 163-169.
61. Q. Wu and J. Hu, *Compos. Part B-eng.*, 2016, **107**, 59-66.
62. Y. Lin, J. Liu, X. Wang, J. Xu, P. Liu, G. Nie, C. Liu and F. Jiang, *Compos. Commun.*, 2019, **16**, 79-83.
63. Y. Zheng, Q. Zhang, W. Jin, Y. Jing, X. Chen, X. Han, Q. Bao, Y. Liu, X. Wang and S. Wang, *arXiv preprint arXiv:1907.04883*, 2019.
64. H. Xu, Y. Guo, B. Wu, C. Hou, Q. Zhang, Y. Li and H. Wang, *ACS Appl. Mater. Interfaces*, 2020, **12**, 33297-33304.
65. C. Zhou, C. Dun, Q. Wang, K. Wang, Z. Shi, D. L. Carroll, G. Liu and G. Qiao, *ACS Appl. Mater. Interfaces*, 2015, **7**, 21015-21020.
66. C. J. An, Y. H. Kang, A. Y. Lee, K.-S. Jang, Y. Jeong and S. Y. Cho, *ACS Appl. Mater. Interfaces*, 2016, **8**, 22142-22150.
67. M. Tonga, L. Wei, P. S. Taylor, E. Wilusz, L. Korugic-Karasz, F. E. Karasz and P. M. Lahti, *ACS Appl. Mater. Interfaces*, 2017, **9**, 8975-8984.
68. X. Wang, P. Liu, Q. Jiang, W. Zhou, J. Xu, J. Liu, Y. Jia, X. Duan, Y. Liu, Y. Du and F. Jiang, *ACS Appl. Mater. Interfaces*, 2019, **11**, 2408-2417.
69. J. A. Lee, A. E. Aliev, J. S. Bykova, M. J. de Andrade, D. Kim, H. J. Sim, X. Lepró, A. A. Zakhidov, J.-B. Lee, G. M. Spinks, S. Roth, S. J. Kim and R. H. Baughman, *Adv. Mater.*, 2016, **28**, 5038-5044.
70. Z. Zhang, G. Chen, H. Wang and X. Li, *Chem. Asian J.*, 2015, **10**, 149-153.
71. Q. Wang, Q. Yao, J. Chang and L. Chen, *J. Mater. Chem.*, 2012, **22**, 17612-17618.
72. J.-Y. Kim, J.-H. Mo, Y. H. Kang, S. Y. Cho and K.-S. Jang, *Nanoscale*, 2018, **10**, 19766-19773.
73. M. J. Chatterjee, D. Banerjee and K. Chatterjee, *Mater. Res. Express*, 2016, **3**, 085009.
74. V. H. Guerrero and D. D. L. Chung, *Compos. Interface.*, 2002, **9**, 395-401.
75. C. Yu, K. Choi, L. Yin and J. C. Grunlan, *ACS Nano*, 2011, **5**, 7885-7892.
76. Q. Yao, L. Chen, W. Zhang, S. Liufu and X. Chen, *ACS Nano*, 2010, **4**, 2445-2451.
77. K. Kirihaara, Q. Wei, M. Mukaida and T. Ishida, *Synthetic Met.*, 2017, **225**, 41-48.
78. A. Dey, A. Maity, M. A. Shafeeuulla Khan, A. K. Sikder and S. Chattopadhyay, *RSC Adv.*, 2016, **6**, 22453-22460.
79. J. Gao, L. Miao, C. Liu, X. Wang, Y. Peng, X. Wei, J. Zhou, Y. Chen, R. Hashimoto, T. Asaka and K. Koumoto, *J. Mater. Chem. A*, 2017, **5**, 24740-24748.
80. Y. Du, J. Xu, Y. Wang and T. Lin, *J. Mater. Sci. Mater. El.*, 2017, **28**, 5796-5801.
81. X. Chen, G. Tang, J. Pan and H. Wang, *J. Miner. Mater. Char. Eng.*, 2018, **6**, 448-463.
82. Y. Ding, Y. Qiu, K. Cai, Q. Yao, S. Chen, L. Chen and J. He, *Nat. Commun.*, 2019, **10**, 841. DOI: 10.1039/D0EE03520C
83. S. Shin, R. Kumar, J. W. Roh, D.-S. Ko, H.-S. Kim, S. I. Kim, L. Yin, S. M. Schlossberg, S. Cui, J.-M. You, S. Kwon, J. Zheng, J. Wang and R. Chen, *Sci. Rep.*, 2017, **7**, 7317.
84. F. Ren, P. Menchhofer, J. Kiggans and H. Wang, *J. Electron. Mater.*, 2016, **45**, 1412-1418.
85. N. Wen, Z. Fan, S. Yang, Y. Zhao, T. Cong, S. Xu, H. Zhang, J. Wang, H. Huang, C. Li and L. Pan, *Nano Energy*, 2020, **78**, 105361.
86. J. Wu, Y. Sun, W.-B. Pei, L. Huang, W. Xu and Q. Zhang, *Synthetic Met.*, 2014, **196**, 173-177.
87. J. Zhang, K. Zhang, F. Xu, S. Wang and Y. Qiu, *Compos. Part B-eng.*, 2018, **136**, 234-240.
88. S. Qu, Q. Yao, L. Wang, Z. Chen, K. Xu, H. Zeng, W. Shi, T. Zhang, C. Uher and L. Chen, *NPG Asia Mater.*, 2016, **8**, e292-e292.
89. B. Endrődi, J. Mellár, Z. Gingl, C. Visy and C. Janáky, *RSC Adv.*, 2014, **4**, 55328-55333.
90. S. Hiura, N. Okada, J. Wakui, H. Narita, S. Kanehashi and T. Shimomura, *Materials*, 2017, **10**, 468.
91. C. J. An, Y. C. Lee, Y. H. Kang and S. Y. Cho, *Carbon*, 2017, **124**, 662-668.
92. R. Chan Yu King, F. Roussel, J.-F. Brun and C. Gors, *Synthetic Met.*, 2012, **162**, 1348-1356.
93. L. Liang, G. Chen and C.-Y. Guo, *Compos. Sci. Technol.*, 2016, **129**, 130-136.
94. L. Liang, C. Gao, G. Chen and C.-Y. Guo, *J. Mater. Chem. C*, 2016, **4**, 526-532.
95. S. Xin, N. Yang, F. Gao, J. Zhao, L. Li and C. Teng, *Mater. Chem. Phys.*, 2018, **212**, 440-445.
96. X. Hu, K. Zhang, J. Zhang, S. Wang and Y. Qiu, *ACS Appl. Energy Mater.*, 2018, **1**, 4883-4890.
97. X. Lan, T. Wang, C. Liu, P. Liu, J. Xu, X. Liu, Y. Du and F. Jiang, *Compos. Sci. Technol.*, 2019, **182**, 107767.
98. M. Piao, M.-K. Joo, J. H. Choi, J. M. Shin, Y. S. Moon, G. T. Kim and U. Dettlaff-Weglikowska, *RSC Adv.*, 2015, **5**, 78099-78103.
99. Q. Jin, W. Shi, Y. Zhao, J. Qiao, J. Qiu, C. Sun, H. Lei, K. Tai and X. Jiang, *ACS Appl. Mater. Interfaces*, 2018, **10**, 1743-1751.
100. Q. Jiang, C. Liu, J. Xu, B. Lu, H. Song, H. Shi, Y. Yao and L. Zhang, *J. Polym. Sci. Pol. Phys.*, 2014, **52**, 737-742.
101. Y. Du, K. Cai, S. Chen, H. Wang, S. Z. Shen, R. Donelson and T. Lin, *Sci. Rep.*, 2015, **5**, 6411.
102. B. Hamdou, J. Gooth, T. Böhnert, A. Dorn, L. Akinsinde, E. Pippel, R. Zierold and K. Nielsch, *Adv. Energy Mater.*, 2015, **5**, 1500280.
103. H. S. Shin, B. Hamdou, H. Reith, H. Osterhage, J. Gooth, C. Damm, B. Rellinghaus, E. Pippel and K. Nielsch, *Nanoscale*, 2016, **8**, 13552-13557.
104. Q. Zhang, W. Wang, J. Li, J. Zhu, L. Wang, M. Zhu and W. Jiang, *J. Mater. Chem. A*, 2013, **1**, 12109-12114.
105. D. K. Taggart, Y. Yang, S.-C. Kung, T. M. McIntire and R. M. Penner, *Nano Lett.*, 2011, **11**, 125-131.
106. X. Hu, G. Chen, X. Wang and H. Wang, *J. Mater. Chem. A*, 2015, **3**, 20896-20902.
107. K. Zhang, J. Qiu and S. Wang, *Nanoscale*, 2016, **8**, 8033-8041.
108. Y. Du, H. Niu, J. Li, Y. Dou, S. Z. Shen, R. Jia and J. Xu, *Polymers*, 2018, **10**, 1143.

109. G. Lu, L. Bu, S. Li and X. Yang, *Adv. Mater.*, 2014, **26**, 2359-2364.
110. W. Lee, Y. H. Kang, J. Y. Lee, K.-S. Jang and S. Y. Cho, *RSC Adv.*, 2016, **6**, 53339-53344.
111. W. S. Kim, G. Anoop, I.-S. Jeong, H. J. Lee, H. B. Kim, S. H. Kim, G. W. Goo, H. Lee, H. J. Lee, C. Kim, J.-H. Lee, B. S. Mun, J.-W. Park, E. Lee and J. Y. Jo, *Nano Energy*, 2020, **67**, 104207.
112. Y. Xue, Z. Zhang, Y. Zhang, X. Wang, L. Li, H. Wang and G. Chen, *Carbon*, 2020, **157**, 324-329.
113. Q. Xu, S. Qu, C. Ming, P. Qiu, q. yao, C. Zhu, T.-R. Wei, J. He, X. Shi and L. Chen, *Energy Environ. Sci.*, 2020, **13**, 511-518.
114. S. V. N. Pammi, V. Jella, J.-S. Choi and S.-G. Yoon, *J. Mater. Chem. C*, 2017, **5**, 763-769.
115. Y. Lu, Y. Ding, Y. Qiu, K. Cai, Q. Yao, H. Song, L. Tong, J. He and L. Chen, *ACS Appl. Mater. Interfaces*, 2019, **11**, 12819-12829.
116. H. Ju, D. Park and J. Kim, *J. Mater. Chem. A*, 2018, **6**, 5627-5634.
117. E. W. Zaia, A. Sahu, P. Zhou, M. P. Gordon, J. D. Forster, S. Aloni, Y.-S. Liu, J. Guo and J. J. Urban, *Nano Lett.*, 2016, **16**, 3352-3359.
118. S. Ma, K. Anderson, L. Guo, A. Yousuf, E. C. Ellingsworth, C. Vajner, H. T. Wang and G. Szulczewski, *Appl. Phys. Lett.*, 2014, **105**, 073905.
119. C. Li, F. Jiang, C. Liu, W. Wang, X. Li, T. Wang and J. Xu, *Chem. Eng. J.*, 2017, **320**, 201-210.
120. N. E. Coates, S. K. Yee, B. McCulloch, K. C. See, A. Majumdar, R. A. Segalman and J. J. Urban, *Adv. Mater.*, 2013, **25**, 1629-1633.
121. K. C. See, J. P. Feser, C. E. Chen, A. Majumdar, J. J. Urban and R. A. Segalman, *Nano Lett.*, 2010, **10**, 4664-4667.
122. E. J. Bae, Y. H. Kang, K.-S. Jang and S. Y. Cho, *Sci. Rep.*, 2016, **6**, 18805.
123. Y. Wang, S. M. Zhang and Y. Deng, *J. Mater. Chem. A*, 2016, **4**, 3554-3559.
124. W. Thongkham, C. Lertsatitthanakorn, K. Jiramitmongkon, K. Tantisantisom, T. Boonkoom, M. Jitpukdee, K. Sinthiptharakoon, A. Klamchuen, M. Liangruksa and P. Khanchaitit, *ACS Appl. Mater. Interfaces*, 2019, **11**, 6624-6633.
125. M. He, J. Ge, Z. Lin, X. Feng, X. Wang, H. Lu, Y. Yang and F. Qiu, *Energy Environ. Sci.*, 2012, **5**, 8351-8358.
126. J. Choi, J. Y. Lee, S.-S. Lee, C. R. Park and H. Kim, *Adv. Energy Mater.*, 2016, **6**, 1502181.
127. C. Cho, S. Qin, K. Choi and J. C. Grunlan, *ACS Appl. Polym. Mater.*, 2019, **1**, 1942-1947.
128. C. Cho, B. Stevens, J.-H. Hsu, R. Bureau, D. A. Hagen, O. Regev, C. Yu and J. C. Grunlan, *Adv. Mater.*, 2015, **27**, 2996-3001.
129. C. Cho, K. L. Wallace, P. Tzeng, J. H. Hsu, C. Yu and J. C. Grunlan, *Adv. Energy Mater.*, 2016, **6**, 1502168.
130. H. Wang, S.-i. Yi, X. Pu and C. Yu, *ACS Appl. Mater. Interfaces*, 2015, **7**, 9589-9597.
131. L. Wang, Q. Yao, W. Shi, S. Qu and L. Chen, *Mater. Chem. Front.*, 2017, **1**, 741-748.
132. H. Song, Y. Qiu, Y. Wang, K. Cai, D. Li, Y. Deng and J. He, *Compos. Sci. Technol.*, 2017, **153**, 71-83.
133. C. T. Hong, W. Lee, Y. H. Kang, Y. Yoo, J. Ryu, S. Y. Cho and K.-S. Jang, *J. Mater. Chem. A*, 2015, **3**, 12314-12319.
134. P. Li, Y. Zhao, H. Li, S. Liu, Y. Liang, X. Cheng and C. He, *Compos. Sci. Technol.*, 2020, **189**, 108023.
135. L. Wang, Q. Yao, J. Xiao, K. Zeng, S. Qu, W. Shi, Q. Wang and L. Chen, *Chem. Asian J.*, 2016, **11**, 1804-1810. View Article Online
DOI:10.1039/C5CY01810A
136. L. Liang, J. Fan, M. Wang, G. Chen and G. Sun, *Compos. Sci. Technol.*, 2020, **187**, 107948.
137. K. Suemori, Y. Watanabe and S. Hoshino, *Appl. Phys. Lett.*, 2015, **106**, 113902.
138. K. Yusupov, S. Stumpf, S. You, A. Bogach, P. M. Martinez, A. Zakhidov, U. S. Schubert, V. Khovaylo and A. Vomiero, *Adv. Funct. Mater.*, 2018, **28**, 1801246.
139. R. Prabhakar, M. S. Hossain, W. Zheng, P. K. Athikam, Y. Zhang, Y.-Y. Hsieh, E. Skafidas, Y. Wu, V. Shanov and J.-H. Bahk, *ACS Appl. Energy Mater.*, 2019, **2**, 2419-2426.
140. D. Kim, Y. Kim, K. Choi, J. C. Grunlan and C. Yu, *ACS Nano*, 2010, **4**, 513-523.
141. H. Wang, J. H. Hsu, S. I. Yi, S. L. Kim, K. Choi, G. Yang and C. Yu, *Adv. Mater.*, 2015, **27**, 6855-6861.
142. X. Zeng, L. Ren, J. Xie, D. Mao, M. Wang, X. Zeng, G. Du, R. Sun, J.-B. Xu and C.-P. Wong, *ACS Appl. Mater. Interfaces*, 2019, **11**, 37892-37900.
143. B. Wu, Y. Guo, C. Hou, Q. Zhang, Y. Li and H. Wang, *Adv. Funct. Mater.*, 2019, **29**, 1900304.
144. J. Choi, Y. Jung, C. Dun, K. T. Park, M. P. Gordon, K. Haas, P. Yuan, H. Kim, C. R. Park and J. J. Urban, *ACS Appl. Energy Mater.*, 2020, **3**, 1199-1206.
145. W. Ma, Y. Liu, S. Yan, T. Miao, S. Shi, M. Yang, X. Zhang and C. Gao, *Nano Res.*, 2016, **9**, 3536-3546.
146. L. Zhao, X. Sun, Z. Lei, J. Zhao, J. Wu, Q. Li and A. Zhang, *Compos. Part B-eng.*, 2015, **83**, 317-322.
147. D. H. Sung, G.-H. Kang, K. Kong, M. Kim, H. W. Park and Y.-B. Park, *Compos. Part B-eng.*, 2016, **92**, 202-209.
148. E. K. Lee, L. Yin, Y. Lee, J. W. Lee, S. J. Lee, J. Lee, S. N. Cha, D. Whang, G. S. Hwang and K. Hippalgaonkar, *Nano Lett.*, 2012, **12**, 2918-2923.
149. C.-H. Chien, P.-C. Lee, W.-H. Tsai, C.-H. Lin, C.-H. Lee and Y.-Y. Chen, *Sci. Rep.*, 2016, **6**, 23672.
150. J. A. Hernandez, A. Ruiz, L. F. Fonseca, M. T. Pettes, M. Jose-Yacamán and A. Benitez, *Sci. Rep.*, 2018, **8**, 11966.
151. J. Wu, Y. Sun, W. Xu and Q. Zhang, *Synthetic. Met.*, 2014, **189**, 177-182.
152. N. Somdock, S. Kianwimol, A. Harnwunggmoung, A. Sakulkalavek and R. Sakdanuphab, *J. Alloys Compd.*, 2019, **773**, 78-85.
153. L. Hu, F. Meng, Y. Zhou, J. Li, A. Benton, J. Li, F. Liu, C. Zhang, H. Xie and J. He, *Adv. Funct. Mater.*, 2020, **30**, 2005202.
154. Q. Jin, S. Jiang, Y. Zhao, D. Wang, J. Qiu, D.-M. Tang, J. Tan, D.-M. Sun, P.-X. Hou and X.-Q. Chen, *Nat. Mater.*, 2019, **18**, 62-68.
155. Y. Wang, W.-D. Liu, X.-L. Shi, M. Hong, L.-J. Wang, M. Li, H. Wang, J. Zou and Z.-G. Chen, *Chem. Eng. J.*, 2019, **391**, 123513.
156. Y. Liu, Y. Zhang, K. H. Lim, M. Ibáñez, S. Ortega, M. Li, J. David, S. Martí-Sánchez, K. M. Ng and J. Arbiol, *ACS Nano*, 2018, **12**, 7174-7184.
157. Y. Wang, W. Liu, H. Gao, L. Wang, M. Li, X.-L. Shi, M. Hong, H. Wang, J. Zou and Z.-G. Chen, *ACS Appl. Mater. Interfaces*, 2019, **11**, 31237-31244.
158. H. Choi, K. Jeong, J. Chae, H. Park, J. Baeck, T. H. Kim, J. Y. Song, J. Park, K.-H. Jeong and M.-H. Cho, *Nano Energy*, 2018, **47**, 374-384.
159. Q. Zhang, J. Liao, Y. Tang, M. Gu, C. Ming, P. Qiu, S. Bai, X. Shi, C. Uher and L. Chen, *Energy Environ. Sci.*, 2017, **10**, 956-963.

160. F. Hao, P. Qiu, Y. Tang, S. Bai, T. Xing, H.-S. Chu, Q. Zhang, P. Lu, T. Zhang and D. Ren, *Energy Environ. Sci.*, 2016, **9**, 3120-3127.
161. Y. Min, G. Park, B. Kim, A. Giri, J. Zeng, J. W. Roh, S. I. Kim, K. H. Lee and U. Jeong, *ACS Nano*, 2015, **9**, 6843-6853.
162. M. Tan, W. D. Liu, X. L. Shi, H. Gao, H. Li, C. Li, X. B. Liu, Y. Deng and Z. G. Chen, *Small Methods*, 2019, **3**, 1900582.
163. B. Cai, H.-L. Zhuang, Q. Cao, H. Hu, J. Dong, Asfandiyar and J.-F. Li, *ACS Appl. Mater. Interfaces*, 2020, **12**, 16426-16435.
164. G. Yang, R. Niu, L. Sang, X. Liao, D. R. G. Mitchell, N. Ye, J. Pei, J.-F. Li and X. Wang, *Adv. Energy Mater.*, 2020, **10**, 2000757.
165. T. Mao, P. Qiu, X. Du, P. Hu, K. Zhao, J. Xiao, X. Shi and L. Chen, *Adv. Funct. Mater.*, 2020, **30**, 1908315.
166. D. Yang, X. Su, J. Li, H. Bai, S. Wang, Z. Li, H. Tang, K. Tang, T. Luo, Y. Yan, J. Wu, J. Yang, Q. Zhang, C. Uher, M. G. Kanatzidis and X. Tang, *Adv. Mater.*, 2020, **32**, 2003730.
167. J. Lei, Z. Ma, D. Zhang, Y. Chen, C. Wang, X. Yang, Z. Cheng and Y. Wang, *J. Mater. Chem. A*, 2019, **7**, 7006-7014.
168. M. Li, D. L. Cortie, J. Liu, D. Yu, S. M. K. N. Islam, L. Zhao, D. R. Mitchell, R. A. Mole, M. B. Cortie and S. Dou, *Nano Energy*, 2018, **53**, 993-1002.
169. K. Zhao, A. B. Blichfeld, H. Chen, Q. Song, T. Zhang, C. Zhu, D. Ren, R. Hanus, P. Qiu and B. B. Iversen, *Chem. Mater.*, 2017, **29**, 6367-6377.
170. P. Lu, H. Liu, X. Yuan, F. Xu, X. Shi, K. Zhao, W. Qiu, W. Zhang and L. Chen, *J. Mater. Chem. A*, 2015, **3**, 6901-6908.
171. W.-D. Liu, X.-L. Shi, R. Moshwan, L. Yang, Z.-G. Chen and J. Zou, *Chem. Eng. J.*, 2019, **375**, 121996.
172. X. Zhang, Z. Bu, S. Lin, Z. Chen, W. Li and Y. Pei, *Joule*, 2020, **4**, 986-1003.
173. W.-D. Liu, D.-Z. Wang, Q. Liu, W. Zhou, Z. Shao and Z.-G. Chen, *Adv. Energy Mater.*, 2020, **10**, 2000367.
174. L. Xie, Y. Chen, R. Liu, E. Song, T. Xing, T. Deng, Q. Song, J. Liu, R. Zheng, X. Gao, S. Bai and L. Chen, *Nano Energy*, 2020, **68**, 104347.
175. E. Nshimiyimana, S. Hao, X. Su, C. Zhang, W. Liu, Y. Yan, C. Uher, C. Wolverton, M. G. Kanatzidis and X. Tang, *J. Mater. Chem. A*, 2020, **8**, 1193-1204.
176. K. s. Bayikadi, S. Raman, C. T. Wu, L.-C. Chen, K. H. Chen and F.-C. Chou, *J. Mater. Chem. A*, 2020, **8**, 5332-5341.
177. G. Xie, Z. Li, T. Luo, H. Bai, J. Sun, Y. Xiao, L.-D. Zhao, J. Wu, G. Tan and X. Tang, *Nano Energy*, 2020, **69**, 104395.
178. P. Li, T. Ding, J. Li, C. Zhang, Y. Dou, Y. Li, L. Hu, F. Liu and C. Zhang, *Adv. Funct. Mater.*, 2020, **30**, 1910059.
179. M. Hong, K. Zheng, W. Lyv, M. Li, X. Qu, Q. Sun, S. Xu, J. Zou and Z.-G. Chen, *Energy Environ. Sci.*, 2020, **13**, 1856-1864.
180. J. Dong, F.-H. Sun, H. Tang, J. Pei, H.-L. Zhuang, H.-H. Hu, B.-P. Zhang, Y. Pan and J.-F. Li, *Energy Environ. Sci.*, 2019, **12**, 1396-1403.
181. J. Wei, L. Yang, Z. Ma, P. Song, M. Zhang, J. Ma, F. Yang and X. Wang, *J. Mater. Sci.*, 2020, **55**, 12642-12704.
182. B. Xiang, J. Liu, J. Yan, M. Xia, Q. Zhang, L. Chen, J. Li, X. Y. Tan, Q. Yan and Y. Wu, *J. Mater. Chem. A*, 2019, **7**, 18458-18467.
183. M. H. Lee, J. H. Yun, G. Kim, J. E. Lee, S.-D. Park, H. Reith, G. Schierning, K. Nielsch, W. Ko, A.-P. Li and J.-S. Rhyee, *ACS Nano*, 2019, **13**, 3806-3815.
184. P. Jood, M. Ohta, A. Yamamoto and M. G. Kanatzidis, *Joule*, 2018, **2**, 1339-1355.
185. L. Yang, Z.-G. Chen, M. Hong, L. Wang, D. Kong, L. Huang, G. Han, Y. Zou, M. Dargusch and J. Zou, *Nano Energy*, 2017, **31**, 105-112.
186. Y. Pei, G. Tan, D. Feng, L. Zheng, Q. Tan, X. Xie, S. Gong, Y. Chen, J. F. Li and J. He, *Adv. Energy Mater.*, 2017, **7**, 1601450.
187. Z. Chen, Z. Jian, W. Li, Y. Chang, B. Ge, R. Hanus, J. Yang, Y. Chen, M. Huang and G. J. Snyder, *Adv. Mater.*, 2017, **29**, 1606768.
188. T. Fu, X. Yue, H. Wu, C. Fu, T. Zhu, X. Liu, L. Hu, P. Ying, J. He and X. Zhao, *J. Materiomics*, 2016, **2**, 141-149.
189. C. F. Wu, T. R. Wei and J. F. Li, *Phys. Chem. Chem. Phys.*, 2015, **17**, 13006-13012.
190. C. Chang, G. Tan, J. He, M. G. Kanatzidis and L.-D. Zhao, *Chem. Mater.*, 2018, **30**, 7355-7367.
191. Z.-G. Chen, X. Shi, L.-D. Zhao and J. Zou, *Prog. Mater. Sci.*, 2018, **97**, 283-346.
192. X.-L. Shi, W.-Y. Chen, X. Tao, J. Zou and Z.-G. Chen, *Mater. Horiz.*, 2020, DOI: 10.1039/D0MH00954G.
193. L. Huang, J. Lu, D. Ma, C. Ma, B. Zhang, H. Wang, G. Wang, D. Gregory, X. Zhou and G. Han, *J. Mater. Chem. A*, 2020, **8**, 1394-1402.
194. X.-L. Shi, X. Tao, J. Zou and Z.-G. Chen, *Adv. Sci.*, 2020, **7**, 1902923.
195. Y.-X. Chen, X.-L. Shi, Z.-H. Zheng, F. Li, W.-D. Liu, W.-Y. Chen, X.-R. Li, G.-X. Liang, J.-T. Luo, P. Fan and Z.-G. Chen, *Mater. Today Phys.*, 2020, **16**, 100306.
196. Y. Zheng, X.-L. Shi, H. Yuan, S. Lu, X. Qu, W. Liu, L. Wang, K. Zheng, J. Zou and Z.-G. Chen, *Mater. Today Phys.*, 2020, **13**, 100198.
197. X. Shi, A. Wu, T. Feng, K. Zheng, W. Liu, Q. Sun, M. Hong, S. T. Pantelides, Z. G. Chen and J. Zou, *Adv. Energy Mater.*, 2019, **9**, 1803242.
198. M. Dargusch, X.-L. Shi, X. Q. Tran, T. Feng, F. Somidin, X. Tan, W. Liu, K. Jack, J. Venezuela, H. Maeno, T. Toriyama, S. Matsumura, S. T. Pantelides and Z.-G. Chen, *J. Phys. Chem. Lett.*, 2019, **10**, 6512-6517.
199. X.-L. Shi, W.-D. Liu, A.-Y. Wu, V. T. Nguyen, H. Gao, Q. Sun, R. Moshwan, J. Zou and Z.-G. Chen, *InfoMat*, 2020, **2**, 1201-1215.
200. Asfandiyar, B. Cai, H.-L. Zhuang, H. Tang and J.-F. Li, *Nano Energy*, 2020, **69**, 104393.
201. T. R. Wei, G. Tan, X. Zhang, C. F. Wu, J. F. Li, V. P. Dravid, G. J. Snyder and M. G. Kanatzidis, *J. Am. Chem. Soc.*, 2016, **138**, 8875-8882.
202. R. Moshwan, L. Yang, J. Zou and Z.-G. Chen, *Adv. Funct. Mater.*, 2017, **27**, 1703278.
203. R. Moshwan, W.-D. Liu, X.-L. Shi, Q. Sun, H. Gao, Y.-P. Wang, J. Zou and Z.-G. Chen, *J. Mater. Chem. A*, 2020, **8**, 3978-3987.
204. R. Moshwan, W.-D. Liu, X.-L. Shi, Y.-P. Wang, J. Zou and Z.-G. Chen, *Nano Energy*, 2019, **65**, 104056.
205. D. Sarkar, T. Ghosh, A. Banik, S. Roychowdhury, D. Sanyal and K. Biswas, *Angew. Chem. Int. Ed.*, 2020, **59**, 2-10.
206. S. Li, J. Xin, A. Basit, Q. Long, S. Li, Q. Jiang, Y. Luo and J. Yang, *Adv. Sci.*, 2020, DOI: 10.1002/adv.201903493, 1903493.
207. S. Roychowdhury, R. K. Biswas, M. Dutta, S. K. Pati and K. Biswas, *ACS Energy Lett.*, 2019, **4**, 1658-1662.
208. M. Ibáñez, R. Hasler, A. Genç, Y. Liu, B. Kuster, M. Schuster, O. Dobrozhan, D. Cadavid, J. Arbiol, A. Cabot and M. V. Kovalenko, *J. Am. Chem. Soc.*, 2019, **141**, 8025-8029.

209. W. Wei, C. Chang, T. Yang, J. Liu, H. Tang, J. Zhang, Y. Li, F. Xu, Z. Zhang and J.-F. Li, *J. Am. Chem. Soc.*, 2018, **140**, 499-505.
210. F. Zhuge, T. Yanagida, N. Fukata, K. Uchida, M. Kanai, K. Nagashima, G. Meng, Y. He, S. Rahong and X. Li, *J. Am. Chem. Soc.*, 2014, **136**, 14100-14106.
211. W. Zhao, S. Fan, N. Xiao, D. Liu, Y. Y. Tay, C. Yu, D. Sim, H. H. Hng, Q. Zhang and F. Boey, *Energy Environ. Sci.*, 2012, **5**, 5364-5369.
212. G. H. Carey, A. L. Abdelhady, Z. Ning, S. M. Thon, O. M. Bakr and E. H. Sargent, *Chem. Rev.*, 2015, **115**, 12732-12763.
213. L. D. Hicks and M. S. Dresselhaus, *Phys. Rev. B*, 1993, **47**, 12727-12731.
214. L. Hicks and M. Dresselhaus, *Phys. Rev. B*, 1993, **47**, 16631.
215. F. T. Rabouw and C. de Mello Donega, in *Photoactive Semiconductor Nanocrystal Quantum Dots*, Springer, 2017, pp. 1-30.
216. Z. Lu, M. Layani, X. Zhao, L. P. Tan, T. Sun, S. Fan, Q. Yan, S. Magdassi and H. H. Hng, *Small*, 2014, **10**, 3551-3554.
217. R. Mohammad and Ş. Katircioğlu, *Int. J. Mod. Phys. C*, 2016, **27**, 1650035.
218. C. Liu and J. Li, *Phys. Lett. A*, 2011, **375**, 2878-2881.
219. G. Chen, *Phys. Rev. B*, 1998, **57**, 14958-14973.
220. Y. Wu, S. W. Finerock and H. Yang, *Nano Energy*, 2012, **1**, 651-653.
221. G. Loke, W. Yan, T. Khudiyev, G. Noel and Y. Fink, *Adv. Mater.*, 2020, **32**, 1904911.
222. M. S. Dresselhaus, G. Chen, M. Y. Tang, R. G. Yang, H. Lee, D. Z. Wang, Z. F. Ren, J. P. Fleurial and P. Gogna, *Adv. Mater.*, 2007, **19**, 1043-1053.
223. Y. Qi, Z. Wang, M. Zhang, F. Yang and X. Wang, *J. Mater. Chem. A*, 2013, **1**, 6110-6124.
224. Y. Zhang, Y.-J. Heo, M. Park and S.-J. Park, *Polymers*, 2019, **11**, 167.
225. A. D. Avery, B. H. Zhou, J. Lee, E.-S. Lee, E. M. Miller, R. Ihly, D. Wesenberg, K. S. Mistry, S. L. Guillot, B. L. Zink, Y.-H. Kim, J. L. Blackburn and A. J. Ferguson, *Nat. Energy*, 2016, **1**, 16033.
226. T. Miao, W. Ma, X. Zhang, J. Wei and J. Sun, *Appl. Phys. Lett.*, 2013, **102**, 053105.
227. L. Shi, D. Li, C. Yu, W. Jang, D. Kim, Z. Yao, P. Kim and A. Majumdar, *J. Heat Trans.*, 2003, **125**, 881-888.
228. J. Hone, M. C. Llaguno, N. M. Nemes, A. T. Johnson, J. E. Fischer, D. A. Walters, M. J. Casavant, J. Schmidt and R. E. Smalley, *Appl. Phys. Lett.*, 2000, **77**, 666-668.
229. R. Jin, Z. X. Zhou, D. Mandrus, I. N. Ivanov, G. Eres, J. Y. Howe, A. A. Puretzky and D. B. Geohegan, *Physica. B*, 2007, **388**, 326-330.
230. H.-L. Zhang, J.-F. Li, B.-P. Zhang, K.-F. Yao, W.-S. Liu and H. Wang, *Phys. Rev. B*, 2007, **75**, 205407.
231. C. A. Hewitt, A. B. Kaiser, M. Craps, R. Czerw and D. L. Carroll, *J. Appl. Phys.*, 2013, **114**, 083701.
232. C. A. Hewitt, M. Craps, R. Czerw and D. L. Carroll, *Synthetic. Met.*, 2013, **184**, 68-72.
233. S. L. Kim, K. Choi, A. Tazebay and C. Yu, *ACS Nano*, 2014, **8**, 2377-2386.
234. Y. Nakai, K. Honda, K. Yanagi, H. Kataura, T. Kato, T. Yamamoto and Y. Maniwa, *Appl. Phys. Express*, 2014, **7**, 025103.
235. M. Piao, M.-K. Joo, J. Na, Y.-J. Kim, M. Mouis, G. Ghibaudo, S. Roth, W.-Y. Kim, H.-K. Jang, G. P. Kennedy, U. Dettlaff-Weglikowska and G.-T. Kim, *J. Phys. Chem. C*, 2014, **118**, 26454-26461. DOI: 10.1039/D0EE03520C
236. T. Miao, S. Shi, S. Yan, W. Ma, X. Zhang, K. Takahashi and T. Ikuta, *J. Appl. Phys.*, 2016, **120**, 124302.
237. G. Wu, C. Gao, G. Chen, X. Wang and H. Wang, *J. Mater. Chem. A*, 2016, **4**, 14187-14193.
238. J. H. Seol, I. Jo, A. L. Moore, L. Lindsay, Z. H. Aitken, M. T. Pettes, X. Li, Z. Yao, R. Huang, D. Broido, N. Mingo, R. S. Ruoff and L. Shi, *Science*, 2010, **328**, 213.
239. N. Xiao, X. Dong, L. Song, D. Liu, Y. Tay, S. Wu, L.-J. Li, Y. Zhao, T. Yu, H. Zhang, W. Huang, H. H. Hng, P. M. Ajayan and Q. Yan, *ACS Nano*, 2011, **5**, 2749-2755.
240. D. Sim, D. Liu, X. Dong, N. Xiao, S. Li, Y. Zhao, L.-J. Li, Q. Yan and H. H. Hng, *J. Phys. Chem. C*, 2011, **115**, 1780-1785.
241. Z. Wang, R. Xie, C. T. Bui, D. Liu, X. Ni, B. Li and J. T. L. Thong, *Nano Lett.*, 2011, **11**, 113-118.
242. A. V. Babichev, V. E. Gasumyants and V. Y. Butko, *J. Appl. Phys.*, 2013, **113**, 076101.
243. Y. Guo, J. Mu, C. Hou, H. Wang, Q. Zhang and Y. Li, *Carbon*, 2016, **107**, 146-153.
244. J. L. Blackburn, A. J. Ferguson, C. Cho and J. C. Grunlan, *Adv. Mater.*, 2018, **30**, 1704386.
245. N. Li, M. Cao and C. Hu, *Nanoscale*, 2012, **4**, 6205-6218.
246. V.-T. Tran, J. Saint-Martin, P. Dollfus and S. Volz, *Nanoscale*, 2018, **10**, 3784-3791.
247. W. Liu, L. Yang, Z.-G. Chen and J. Zou, *Adv. Mater.*, 2020, **32**, 1905703.
248. P.-a. Zong, J. Liang, P. Zhang, C. Wan, Y. Wang and K. Koumoto, *ACS Appl. Energy Mater.*, 2020, **3**, 2224-2239.
249. P. R. Jagadish, L. Phei Li, E. Cheah Su Fern, L. Ca Tou, N. Shi Pei, Y. Beng Soon, A. Chan, M. Khalid and D. Chandran, *IOP Conf. Ser.: Earth Environ. Sci.*, 2019, **268**, 012161.
250. B. Zhong, Y. Zhang, W. Li, Z. Chen, J. Cui, W. Li, Y. Xie, Q. Hao and Q. He, *Appl. Phys. Lett.*, 2014, **105**, 123902.
251. A. Olvera, N. Moroz, P. Sahoo, P. Ren, T. Bailey, A. Page, C. Uher and P. Poudeu, *Energy Environ. Sci.*, 2017, **10**, 1668-1676.
252. Y. Wu, Z. Chen, P. Nan, F. Xiong, S. Lin, X. Zhang, Y. Chen, L. Chen, B. Ge and Y. Pei, *Joule*, 2019, **3**, 1276-1288.
253. G. Tan, F. Shi, S. Hao, L.-D. Zhao, H. Chi, X. Zhang, C. Uher, C. Wolverton, V. P. Dravid and M. G. Kanatzidis, *Nat. Commun.*, 2016, **7**, 12167.
254. C. Chang, M. Wu, D. He, Y. Pei, C.-F. Wu, X. Wu, H. Yu, F. Zhu, K. Wang and Y. Chen, *Science*, 2018, **360**, 778-783.
255. L. D. Zhao, S. H. Lo, Y. Zhang, H. Sun, G. Tan, C. Uher, C. Wolverton, V. P. Dravid and M. G. Kanatzidis, *Nature*, 2014, **508**, 373-377.
256. J. Li, X. Zhang, Z. Chen, S. Lin, W. Li, J. Shen, I. T. Witting, A. Faghaninia, Y. Chen and A. Jain, *Joule*, 2018, **2**, 976-987.
257. D. Wu, L. Xie, X. Xu and J. He, *Adv. Funct. Mater.*, 2019, **29**, 1806613.
258. X. Xu, L. Xie, Q. Lou, D. Wu and J. He, *Adv. Sci.*, 2018, **5**, 1801514.
259. R. Chen, J. Lee, W. Lee and D. Li, *Chem. Rev.*, 2019, **119**, 9260-9302.
260. G. Zhang, Q. Yu, W. Wang and X. Li, *Adv. Mater.*, 2010, **22**, 1959-1962.
261. S. W. Finerock, Y. Wang, J. B. Ferguson, J. V. Ward, H. Fang, J. E. Pfluger, D. S. Dudis, X. Ruan and Y. Wu, *Nano Lett.*, 2013, **13**, 5006-5012.
262. A. Yadav, K. P. Pipe and M. Shtein, *J. Power Sources*, 2008, **175**, 909-913.

263. M. Sun, G. Tang, G. Qian, W. Liu, Z. Shi, D. Chen, Q. Qian and Z. Yang, *Mater. Lett.*, 2018, **217**, 13-15.
264. X.-L. Shi, H. Wu, Q. Liu, W. Zhou, S. Lu, Z. Shao, M. Dargusch and Z.-G. Chen, *Nano Energy*, 2020, **78**, 105195.
265. Y. Du, M. S. Zhang, J. Wu, L. Kang, S. Yang, P. Wu and Z. Yin, *Applied Physics A*, 2003, **76**, 1105-1108.
266. J. Wang, B.-Y. Zhang, H.-J. Kang, Y. Li, X. Yaer, J.-F. Li, Q. Tan, S. Zhang, G.-H. Fan, C.-Y. Liu, L. Miao, D. Nan, T.-M. Wang and L.-D. Zhao, *Nano Energy*, 2017, **35**, 387-395.
267. S. Ohta, T. Nomura, H. Ohta, M. Hirano, H. Hosono and K. Koumoto, *Appl. Phys. Lett.*, 2005, **87**, 092108.
268. J. Han, Y. Zeng, Y. Song and H. Liu, *Electron. Mater. Lett.*, 2019, **15**, 278-286.
269. S. Maensiri and W. Nuansing, *Mater. Chem. Phys.*, 2006, **99**, 104-108.
270. C. Gayner and Y. Amouyal, *Adv. Funct. Mater.*, 2019, **30**, 1901789.
271. L. Yang, Z.-G. Chen, M. S. Dargusch and J. Zou, *Adv. Energy Mater.*, 2017, **8**, 1701797.
272. F. Ren, H. Wang, P. A. Menchhofer and J. O. Kiggans, *Appl. Phys. Lett.*, 2013, **103**, 221907.
273. S. Wan, X. Huang, P. Qiu, S. Bai and L. Chen, *Mater. Design.*, 2015, **67**, 379-384.
274. K. Yin, X. Su, Y. Yan, H. Tang, M. G. Kanatzidis, C. Uher and X. Tang, *Scripta Mater.*, 2017, **126**, 1-5.
275. S. Wen and D. D. L. Chung, *Cement Concrete Res.*, 2000, **30**, 1295-1298.
276. M. Sun, Z. Li, Q. Mao and D. Shen, *Cement Concrete Res.*, 1998, **28**, 549-554.
277. M. Sun, Z. Li, Q. Mao and D. Shen, *Cement Concrete Res.*, 1998, **28**, 1707-1712.
278. S. Wen and D. D. L. Chung, *Cement Concrete Res.*, 2000, **30**, 661-664.
279. S. Wen and D. D. L. Chung, *Cement Concrete Res.*, 2002, **32**, 821-823.
280. D. D. L. Chung, *Compos. Part B-eng.*, 2000, **31**, 511-526.
281. S. Wen and D. D. L. Chung, *J. Mater. Res.*, 2000, **15**, 2844-2848.
282. S. Wen and D. D. L. Chung, *Cement Concrete Res.*, 1999, **29**, 1989-1993.
283. D. Bahar and Y. Salih, *New Carbon Mater.*, 2008, **23**, 21-24.
284. J. Wei, L. Hao, G. He and C. Yang, *Ceram. Int.*, 2014, **40**, 8261-8263.
285. J. Zuo, W. Yao and K. Wu, *Fuller. Nanotub. Car. N.*, 2015, **23**, 383-391.
286. S. Wen and D. D. L. Chung, *J. Mater. Sci.*, 2004, **39**, 4103-4106.
287. Y. Wang, L. Yang, X. Shi, X. Shi, L. Chen, M. Dargusch, J. Zou and Z.-G. Chen, *Adv. Mater.*, 2019, **31**, 1807916.
288. T. Varghese, C. Hollar, J. Richardson, N. Kempf, C. Han, P. Gamarachchi, D. Estrada, R. J. Mehta and Y. Zhang, *Sci. Rep.*, 2016, **6**, 33135.
289. Y. Li, K. Buddharaju, B. C. Tinh, N. Singh and S. J. Lee, *IEEE. Electr. Device. L.*, 2012, **33**, 715-717.
290. D. Kong, W. Zhu, Z. Guo and Y. Deng, *Energy*, 2019, **175**, 292-299.
291. W. Zhao, J. Ding, Y. Zou, C.-a. Di and D. Zhu, *Chem. Soc. Rev.*, 2020, **49**, 7210-7228.
292. Y. Zhang and S.-J. Park, *Polymers*, 2019, **11**, 909.
293. H. K. a. T. I. Yoshio Nogami, *Solid State Commun.*, 1990, **76**, 583-586.
294. H. Ju and J. Kim, *ACS Nano*, 2016, **10**, 5730-5739.
295. N. Mateeva, H. Niculescu, J. Schlenoff and L. Testardi, *J. Appl. Phys.*, 1998, **83**, 3111-3117. DOI: 10.1039/D0EE03520C
296. P. Pingel and D. Neher, *Phys. Rev. B*, 2013, **87**, 115209.
297. Z. Fan and J. Ouyang, *Adv. Electron. Mater.*, 2019, **5**, 1800769.
298. T. Masuda, *J. Polym. Sci. Pol. Chem.*, 2007, **45**, 165-180.
299. S. Peng, D. Wang, J. Lu, M. He, C. Xu, Y. Li and S. Zhu, *J. Polym. Environ.*, 2016, **25**, 1208-1218.
300. Z. Fan, D. Du, X. Guan and J. Ouyang, *Nano Energy*, 2018, **51**, 481-488.
301. K. W. Shah, S.-X. Wang, D. X. Y. Soo and J. Xu, *Appl. Sci.*, 2019, **9**, 1422.
302. C. Luo, A. K. K. Kyaw, L. A. Perez, S. Patel, M. Wang, B. Grimm, G. C. Bazan, E. J. Kramer and A. J. Heeger, *Nano Lett.*, 2014, **14**, 2764-2771.
303. H.-R. Tseng, H. Phan, C. Luo, M. Wang, L. A. Perez, S. N. Patel, L. Ying, E. J. Kramer, T.-Q. Nguyen, G. C. Bazan and A. J. Heeger, *Adv. Mater.*, 2014, **26**, 2993-2998.
304. O. Bubnova, Z. U. Khan, H. Wang, S. Braun, D. R. Evans, M. Fabretto, P. Hojati-Talemi, D. Dagnelund, J.-B. Arlin, Y. H. Geerts, S. Desbief, D. W. Breiby, J. W. Andreasen, R. Lazzaroni, W. M. Chen, I. Zozoulenko, M. Fahlman, P. J. Murphy, M. Berggren and X. Crispin, *Nat. Mater.*, 2014, **13**, 190-194.
305. S. Shen, A. Henry, J. Tong, R. Zheng and G. Chen, *Nat. Nano.*, 2010, **5**, 251-255.
306. W. Shi, Z. Shuai and D. Wang, *Adv. Funct. Mater.*, 2017, **27**, 1702847.
307. M. G. Culebras, C. M. Cantarero, A., *J. Mater. Chem. A*, 2014, **2**, 10109-10115.
308. F. Jiang, L. Wang, C. Li, X. Wang, Y. Hu, H. Liu, H. Yang, F. Zhao and J. Xu, *J. Polym. Res.*, 2017, **24**, 1-7.
309. Q. Yao, L. Chen, X. Xu and C. Wang, *Chem. Lett.*, 2005, **34**, 522-523.
310. Y. Sun, Z. Wei, W. Xu and D. Zhu, *Synthetic. Met.*, 2010, **160**, 2371-2376.
311. X. Shi, Z.-G. Chen, W. Liu, L. Yang, M. Hong, R. Moshwan, L. Huang and J. Zou, *Energy Storage Mater.*, 2018, **10**, 130-138.
312. X. L. Shi, K. Zheng, M. Hong, W. D. Liu, R. Moshwan, Y. Wang, X.-L. Qu, Z. G. Chen and J. Zou, *Chem. Sci.*, 2018, **9**, 7376-7389.
313. X. L. Shi, K. Zheng, W. D. Liu, Y. Wang, Y. Z. Yang, Z. G. Chen and J. Zou, *Adv. Energy Mater.*, 2018, **8**, 1800775.
314. X. Shi, A. Wu, W. Liu, R. Moshwan, Y. Wang, Z.-G. Chen and J. Zou, *ACS Nano*, 2018, **12**, 11417-11425.
315. W. Liu, X. Shi, M. Hong, L. Yang, R. Moshwan, Z.-G. Chen and J. Zou, *J. Mater. Chem. C*, 2018, **6**, 13225-13231.
316. W. Liu, X. Shi, R. Moshwan, M. Hong, L. Yang, Z.-G. Chen and J. Zou, *Sustain. Mater. Technol.*, 2018, **17**, e00076.
317. K. M. Coakley, B. S. Srinivasan, J. M. Ziebarth, C. Goh, Y. Liu and M. D. McGehee, *Adv. Funct. Mater.*, 2005, **15**, 1927-1932.
318. S. Samitsu, T. Shimomura, S. Heike, T. Hashizume and K. Ito, *Macromolecules.*, 2008, **41**, 8000-8010.
319. P. Kumar, E. W. Zaia, E. Yildirim, D. V. M. Repaka, S.-W. Yang, J. J. Urban and K. Hippalgaonkar, *Nat. Commun.*, 2018, **9**, 5347.
320. A. Dey, O. P. Bajpai, A. K. Sikder, S. Chattopadhyay and M. A. Shafeeuulla Khan, *Renew. Sust. Energ. Rev.*, 2016, **53**, 653-671.

321. Y. Lin, M. Gigliotti, M. C. Lafarie-Frenot and J. Bai, *J. Reinf. Plast. Comp.*, 2014, **34**, 173-184.
322. M. O. Ansari, M. M. Khan, S. A. Ansari, I. Amal, J. Lee and M. H. Cho, *Chem. Eng. J.*, 2014, **242**, 155-161.
323. T. Dongyan, Q. Liangsheng, J. Zheng and C. Weimin, *J. Appl. Polym. Sci.*, 2002, **84**, 709-715.
324. T. Dongyan, L. Hong and C. Weimin, *Ferroelectrics*, 2002, **265**, 259-264.
325. S. Han and D. D. L. Chung, *Carbon*, 2013, **52**, 30-39.
326. M. Kim, D. H. Sung, K. Kong, N. Kim, B.-J. Kim, H. W. Park, Y.-B. Park, M. Jung, S. H. Lee and S. G. Kim, *Compos. Part B-eng.*, 2016, **90**, 37-44.
327. S. Saq'an, A. M. Zihlif, S. R. Al-Ani and G. Ragosta, *J. Mater. Sci. Mater. El.*, 2008, **19**, 1079-1085.
328. L. Allison, S. Hoxie and T. L. Andrew, *Chem. Commun.*, 2017, **53**, 7182-7193.
329. Y. Jia, L. Shen, J. Liu, W. Zhou, Y. Du, J. Xu, C. Liu, G. Zhang, Z. Zhang and F. Jiang, *J. Mater. Chem. C*, 2019, **7**, 3496-3502.
330. M.-K. Kim, M.-S. Kim, S. Lee, C. Kim and Y.-J. Kim, *Smart Mater. Struct.*, 2014, **23**, 105002.
331. C. A. Hewitt, A. B. Kaiser, S. Roth, M. Craps, R. Czerw and D. L. Carroll, *Nano Lett.*, 2012, **12**, 1307-1310.
332. M. K. Kim, M. S. Kim, S. E. Jo, H. L. Kim, S. M. Lee and Y. J. Kim, 2013.
333. Z. Lu, H. Zhang, C. Mao and C. M. Li, *Appl. Energ.*, 2016, **164**, 57-63.
334. S. W. Finefrock, X. Zhu, Y. Sun and Y. Wu, *Nanoscale*, 2015, **7**, 5598-5602.
335. G. Tan, L. D. Zhao and M. G. Kanatzidis, *Chem. Rev.*, 2016, **116**, 12123-12149.
336. W.-D. Liu, L. Yang and Z.-G. Chen, *Nano Today*, 2020, **35**, 100938.
337. W. Liu, Q. Jie, H. S. Kim and Z. Ren, *Acta Mater.*, 2015, **87**, 357-376.
338. K. Zhao, P. Qiu, X. Shi and L. Chen, *Adv. Funct. Mater.*, 2019, **30**, 1903867.
339. M. Hong, W. Lyv, M. Li, S. Xu, Q. Sun, J. Zou and Z.-G. Chen, *Joule*, 2020, **4**, 2030-2043.
340. C. Bounioux, P. Díaz-Chao, M. Campoy-Quiles, M. S. Martín-González, A. R. Goñi, R. Yerushalmi-Rozen and C. Müller, *Energy Environ. Sci.*, 2013, **6**, 918-925.
341. M. Ito, T. Koizumi, H. Kojima, T. Saito and M. Nakamura, *J. Mater. Chem. A*, 2017, **5**, 12068-12072.
342. Q. Yao, Q. Wang, L. Wang and L. Chen, *Energy Environ. Sci.*, 2014, **7**, 3801-3807.
343. S. Qu, Y. Chen, W. Shi, M. Wang, Q. Yao and L. Chen, *Thin Solid Films*, 2018, **667**, 59-63.
344. Y. Peng and Y. Cui, *Joule*, 2020, **4**, 724-742.
345. S. Hong, Y. Gu, J. K. Seo, J. Wang, P. Liu, Y. S. Meng, S. Xu and R. Chen, *Sci. Adv.*, 2019, **5**, eaaw0536.
346. R. Hu, Y. Liu, S. Shin, S. Huang, X. Ren, W. Shu, J. Cheng, G. Tao, W. Xu, R. Chen and X. Luo, *Adv. Energy Mater.*, 2020, **10**, 1903921.
347. E. Steven, J. G. Park, A. Paravastu, E. B. Lopes, J. S. Brooks, O. Englander, T. Siegrist, P. Kaner and R. G. Alamo, *Sci. Technol. Adv. Mat.*, 2011, **12**, 055002.
348. M. Li, M. Hong, M. Dargusch, J. Zou and Z.-G. Chen, *Trends in Chemistry*, 2020, DOI: <https://doi.org/10.1016/j.trechm.2020.11.001>.
349. A. Yang, L. Cai, R. Zhang, J. Wang, P.-C. Hsu, H. Wang, G. Zhou, J. Xu and Y. Cui, *Nano Lett.*, 2017, **17**, 3506-3510.
350. J. Ripp, O. T. Eldakar, A. C. Gallup and P. T. Arena, *J. Urban Ecol.*, 2018, **4**, juy005. DOI: 10.1039/D0EE03520C
351. P. Bandara, T. Chandler, R. Kelly, J. McCredden, M. May, S. Weller, D. Maisch, S. Pockett, V. Leach and R. Cullen, *J. Australas. Coll. Nutr. Environ. Med.*, 2020, **39**, 27.